The Endocannabinoid System Regulates Synaptogenesis in a Cortical Spheroid Model of Fetal Neurodevelopment

by

Alexis Rose Papariello

July, 2021

Director of Dissertation: Dr. David Taylor, Dr. Ken Soderstrom, and Dr. Karen Litwa

Department of Pharmacology & Toxicology at the Brody School of Medicine, ECU

The endocannabinoid system plays a complex role in synaptogenesis and the subsequent development of neural circuitry during fetal brain development. The cannabinoid receptor type 1 controls synaptic strength at both excitatory and inhibitory synapses and thus contributes to the balance of excitatory and inhibitory signaling. Imbalances in the ratio of excitatory to inhibitory synapses have been implicated in various neuropsychiatric disorders associated with dysregulated central nervous system development including autism spectrum disorder, epilepsy, and schizophrenia. The role of the endocannabinoid system in human brain development has been difficult to study but advances in induced pluripotent stem cell technology have allowed us to model the fetal brain environment. Our cortical spheroid model resembles the cortex of the dorsal telencephalon during mid-fetal gestation and possesses functional synapses and spontaneous activity. Using SR141716A, we observed an increase in excitatory, and to a lesser extent, inhibitory synaptogenesis as measured by confocal image analysis. We also observed increased variability of neural activity and decreased GTPase RhoA activity. Overall, we have established that cortical spheroids express ECS components and are thus a useful model for exploring endocannabinoid mediation of childhood neuropsychiatric disease.

THE ENDOCANNABINOID SYSTEM REGULATES SYNAPTOGENESIS IN A CORTICAL SPHEROID MODEL OF FETAL NEURODEVELOPMENT

A Dissertation

Presented to the faculty of the Department of Pharmacology & Toxicology

Brody School of Medicine at East Carolina University

In partial fulfillment of the requirements for the degree of

Doctor of Philosophy in Pharmacology & Toxicology

By

Alexis Rose Papariello

July, 2021

THE ENDOCANNABINOID SYSTEM REGULATES SYNAPTOGENESIS IN A CORTICAL SPHEROID MODEL OF FETAL NEURODEVELOPMENT

by

Alexis Papariello

APPROVED BY:

DIRECTOR OF DISSERTATION: _____
(David Taylor, PhD)

CO-DIRECTOR OF RESEARCH:_____
(Karen Litwa, PhD)

CO-DIRECTOR OF RESEARCH:_____
(Ken Soderstrom, PhD)

COMMITTEE MEMBER:_____
(Lisa Domico, PhD)

COMMITTEE MEMBER:_____
(Stefan Clemens, PhD)

CHAIR OF THE DEPARTMENT OF
PHARMACOLOGY AND TOXICOLOGY:_____
(David Taylor, PhD)

DEAN OF THE GRADUATE SCHOOL:_____
(Paul Gemperline, PhD)

DEDICATIONS

This dissertation is dedicated to Dr. Gerald J. Papariello.

ACKNOWLEDGEMENTS

First and foremost, I would like to sincerely thank my research mentors, Dr. Soderstrom and Dr Litwa, for their invaluable advice, constant support, perpetual patience, and genuine interest in this project. I believe I've exited this program as a better scientist and a better person. Next, I would like to thank Dr Taylor and Dr Van Dross, as well as my committee members, Dr Domico and Dr Clemens, for supporting my project since the start. I thank my lab mates, particularly Emily Wilson, who selflessly shared her mini brains with me and never expected anything in return other than a laugh and beer. I thank all of my lab managers (Brenna, Michelle, and Jackie) as well as our local histology wiz Joani, for making my job easier on a daily basis. I thank all of my colleagues in the Pharmacology and Toxicology Department whom I didn't see often, but when I did, I always felt like I was with the right people. Last but not least, I'd like to thank my family and friends: Michael, for taking a leap of faith with me on my adventure to Greenville, my parents, for instilling a sense of scientific curiosity in me, and Hanzo, for being the cutest dog on the planet.

Table of Contents

List of Tables

List of Figures

List of Abbreviations and Symbols

2-AG	2-arachidonoyl glycerol
Aβ	amyloid-β
AArG	sn-1-acyl-2-arachidonoylglycerols
AD	Alzheimer's disease
AEA	arachidonoyl ethanolamide (anandamide)
AMPA	α-amino-3-hydroxy-5-methyl-4-isoxazolepropionic acid receptor
APP	amyloid precursor protein
ASD	autism spectrum disorder
BBB	blood-brain barrier
CB_1	cannabinoid receptor type 1
CB_2	cannabinoid receptor type 2
CCK	cholecystokinin
CNR1	cannabinoid receptor type 1 gene
CHD8	chromodomain helicase DNA-binding protein 8
DAGLα/β	diacylglycerol lipase α and β
DMSO	dimethylsulfoxide
EC50	effective dose in 50% of population
ECS	endocannabinoid system
E/I	ratio of excitatory to inhibitory synapses
FAAH	fatty acid amide hydrolase
FAD	familial Alzheimer's disease

FDA	Food and Drug Administration (U.S.)
FMRP	fragile X mental retardation protein
FXS	fragile X syndrome
GABA	gamma aminobutyric acid
GFP	green fluorescent protein
GPCR	G-protein coupled receptor
GSI	γ-secretase inhibitors
hIPSC	human induced pluripotent stem cells
IGF1	insulin-like growth factor 1
IPSC	induced pluripotent stem cells
IQR	interquartile range
MAGL	monoacylglycerol lipase
LOPAC	Library of Pharmaceutically Active Compounds
LTD	long-term depression
LTP	long-term potentiation
MEA	micro-electrode array
MeCP2	methyl-CpG-binding protein 2
NArPE	N-arachidonoylphosphatidylethanolamines
NDMA	N-methyl-D-aspartate receptor
NPR-19	neuropeptide receptor family 19
NAPE-PLD	N-acylphosphatidylethanolamine-specific phospholipase D
PSD-95	post-synaptic density protein 95

ROCK	RhoA kinase
RT-PCR	real time polymerase chain reaction
RTT	Rett syndrome
SAD	sporadic Alzheimer's disease
SEM	standard error of the mean
SNAP25	synaptosomal-associated protein (25 kDa)
SR	SR141716A (CB_1 antagonist)
STORM	Stochastic Optical Reconstruction Microscopy
THC	Δ^9-tetrahydrocannabinol
TRPV	vanilloid-type transient receptor potential cation channel
VEH	vehicle
VGAT	vesicular GABA transporter
VGLUT	vesicular glutamate transporter
WMFR	weighted mean firing rate

CHAPTER ONE: An introduction to cannabinoids

1.1 A brief history of *Cannabis*

The therapeutic effects of *Cannabis* and cannabinoids have been well documented for thousands of years [1], [2]. Taking into consideration the expansive and multicultural history of *Cannabis,* there has been relatively little clinical research on cannabinoids in the United States over the past century[1]. Hesitancy over biochemical consistency, abuse liability, safety, efficacy, and natural product law has mired cannabinoid research for decades [3]. However, this is changing rapidly as state governments in the United States legalize the possession and distribution of *Cannabis*. Cannabinoid research appears to be rapidly expanding with these easing restrictions. The elucidation of cannabinoid pharmacology is intimately tied to the history of *Cannabis* regulation, and because of this, any introduction to cannabinoid pharmacology seems woefully incomplete without some cultural and historical context. Consequently, a brief history of medical *Cannabis* will be covered here.

The *Cannabis* plant first evolved during the Pleistocene era in central Asia and propagated around the world due to a high degree of adaptability during human domestication [1], [4]. *Cannabis* derives it's meaning from a combination of two words: "*kan*" meaning a long, wooden cane with branches, and "*bis*" meaning perfumed and scented in a pleasing way [5]. A combination of written records and archaeobotanical evidence suggests that *Cannabis* was first

used medicinally by shamans in ancient China to treat rheumatic pain among other ailments associated with diminished "yin" [1]. Ancient Vedic texts from India also describe the analgesic, anxiolytic, and anesthetic properties of a preparation of *Cannabis* called "bhanga" [1], [4]. In addition to its medical properties, *Cannabis* was used as a source of clothing fiber and food in almost every ancient civilization, from the Greeks to the Egyptians [1]. Thus, *Cannabis* appears to have had utilitarian, shamanistic, and healing properties in ancient civilization before the Middle Ages, when *Cannabis* was demonized as an "unholy sacrament of the satanic mass." [6].

The scientific method was first applied to *Cannabis* by Irish physician Dr. William Brooke O'Shaughnessy, who worked in India during the 19th century and observed the use of *Cannabis* by local populations [1], [4]. Using a contemporary approach, O'Shaughnessy evaluated the potential toxicity of *Cannabis* extracts in animals before using locally-sourced tinctures to treat human populations [1]. Interestingly, after observing the effect of muscle relaxation in a tetanus patient, O'Shaughnessy tried his *Cannabis* extract on a baby who was suffering from increasingly severe seizures [7]. O'Shaughnessy not only observed complete remission of convulsive activity after treatment with the *Cannabis* extract, but he also observed the return of convulsions when the patient was given water as a placebo [7]. Thus, by using a method which resembles current pharmacological practice (preclinical determination of safety followed by clinical trials) O'Shaughnessy and his *Cannabis* extract experiments paved the way for a modern approach to *Cannabis* pharmacology.

1.2 The modern history of phytocannabinoids and the discovery of the endocannabinoid system

Following O'Shaughnessy's clinical work, doctors began prescribing *Cannabis* preparations in Italy [1]. Attempts were made to extract the active components of *Cannabis*, however, extraction techniques at the time were not well-suited for the lipophilic nature of cannabinoids [1]. In fact, it was the lipophilic nature of cannabinoids that caused the 150-year gap between the identification of morphine and Δ^9-tetrahydrocannabinol (**THC**) [3]. Despite this, the use of *Cannabis* preparations spread across Europe and the United States during the late 19th and early 20th century, where they were prescribed for their analgesic, anti-inflammatory, and antispastic properties [1], [4]. While cannabidiol and cannabinol had been isolated in the early 1940s, these isolations did not produce the characteristic psychoactive effect of *Cannabis* and thus, a search for the "active" component of *Cannabis* was still in motion [4], [8]. Much advancement in the cannabinoid field occurred during the 1960s and 1970s, when novel chromatographic and spectrometric techniques allowed scientists to isolate and characterize lipid compounds [9]. Of note, Mechoulam and Gaoni discovered the major psychoactive constituent of *Cannabis*, THC, in 1964 [10]. Over 100 cannabinoids have been isolated from the *Cannabis* plant since then [4], [11].

The discovery of THC prompted renewed interest in determining the neuropharmacology of cannabinoids in animal models [9]. Several bioassays were created to measure effects such as the "mouse tetrad assay," which measured cannabinoid-induced hypokinesia, hypothermia, and antinociception [2], [9]. Early observations regarding the stereoselectivity and potency, or "structure-activity relationship", of THC's psychoactive effects prompted researchers to investigate brain receptors which bound THC [2], [12]. Allyn Howlett, facilitated by advancements in the field of G-protein coupled receptors (**GPCR**), discovered that cannabinoids act through a GPCR because they inhibit adenylate cyclase through $G_{i/o}$ proteins [13]. Further,

Howlett used the high affinity, tritium-labelled, cannabinoid agonist CP55940 to probe recognition sites and prove that cannabinoid compounds selectively bound to receptors in the brain [13]. Confirming the finding of cannabinoid receptors in the brain, the cannabinoid-1 receptor (**CB_1**) was cloned in 1990 followed by the cannabinoid-2 receptor (**CB_2**) in 1993 [14], [15].

Scientists at the time of discovery believed these receptors were likely modulated by endogenous molecules which were chemically similar to THC, thus, the search for a lipid-based signaling system called the "endocannabinoid system" (**ECS**) followed the discovery of CB_1 [2], [9]. The first endocannabinoid discovered, arachidonoyl ethanolamide, or anandamide (**AEA**), was named after the Sanskrit word "ananda" meaning "bliss" [2], [16]. The eicosanoid anandamide displaced the high affinity agonist CP55940 from the CB_1 receptor and after its isolation, its cannabimimetic effects were confirmed on smooth tissue [2], [16]. The discovery of fatty acid derivatives serving as signaling molecules in mammals prompted further research into compounds similar to AEA, and 2-arachidonoyl glycerol (**2-AG**) was discovered next [2], [17]. Based upon its ability to elicit relatively more intrinsic efficacy than AEA, 2-AG is considered a full agonist of CB_1 while AEA is considered a partial agonist [18]. Endocannabinoids have been found to act on a wide variety of tissues types in the body, with the highest abundance of CB_1 occurring in nervous system and immune system tissue [19]. While 2-AG and AEA are both metabolized into arachidonic acid, they utilize separate paths with 2-AG metabolism occurring via monoacylglycerol lipase (**MAGL**) and AEA metabolism occurring via the serine hydrolase fatty acid amide hydrolase (**FAAH**) [9], [20]. 2-AG and AEA are synthesized on demand by diacylglycerol lipase α and β (**DAGLα/β**) and N-acylphosphatidylethanolamine-specific

phospholipase D (**NAPE-PLD**), respectively [9], [20]. A diagram of endocannabinoid enzymatic pathways can be found in Figure 1.1.

Prior to the 1980s, cannabinoids were defined as the diterpene compounds which are secreted from the glandular trichomes of the *Cannabis* plant [11]. Currently, cannabinoids define a broad class of natural, synthetic, and semi-synthetic compounds [8], [21]. Thus, there has been much advancement in the field of cannabinoid and endocannabinoid science in the past thirty years. Additionally, states are rapidly transforming *Cannabis* policy. While it may appear that current policy is trying to catch up with the science, it may actually be the opposite. With expanding legalization comes questions about the safety and efficacy of *Cannabis* in special populations, such as pregnant women or those predisposed to mental illness. There is a looming body of evidence that indicates disruption to the ECS during neurodevelopment may have lasting effects on neural circuit development [22]–[25]. However, before one can determine whether or not this disruption is occurring, one must determine what the function of the ECS is in the fetal brain.

1.3 Elucidating the function of the ECS through conserved evolutionary processes

The ECS is one of the most primitive cell-signaling complexes in the nervous system. Expression of ECS enzymes and CB_1/CB_1-like receptors occurs in both vertebrates and invertebrates, indicating ECS evolution occurred prior to the development of chordates [26], [27]. In fact, human isoforms of DAGL were only discovered after a BLAST search was performed using DAGL first identified in the prokaryotic bacterium *Penicillium* [28]. While

DAGL and MAGL orthologues can be found in many invertebrate phyla [27], CB_1 and CB_1-like receptors have been scarcely reported [26]. A previous 2004 study using algorithm-based phylogenetic tree analysis and phylogenomic comparisons suggested that cannabinoid receptors had a heterogenous distribution, with CB_1 and DAGLα limited to bilaterian animals, CB_2 and DAGLβ limited to vertebrates, and MAGL limited to chordates [29]. Thus far, CB_1-like receptors have been identified in a few invertebrate model systems, including the functional ortholog NPR-19 in *C. elegans* and the CB_1-like receptor in the medical leech *H. medicinalis* [26]. It is likely that the canonical role of synaptic plasticity predates CB_1 receptor expression in vertebrates, as leeches demonstrate 2-AG mediated long-term depression (**LTD**) through the vanilloid-type transient receptor potential cation channel (**TRPV**) [27]. In light of the incredibly diverse and sometimes contradictory character of our own ECS, much can be elucidated from conserved roles across phylogenetic groups. This section will cover the effects of endocannabinoids on feeding behavior, metabolic homeostasis, and learning/memory, all of which are highly conserved across vertebrate and invertebrate phyla.

Appetite stimulation is a well-known effect of *Cannabis* that has important therapeutic applications. As such, researchers are currently investigating how the ECS mediates hunger, satiety, and metabolism. It is believed that endocannabinoids modulate feeding behavior, which is a broad term applied to adaptations which allow an organism to acquire food [27], [30]. For example, endocannabinoids inhibit feeding behavior in the *Hydra vulgaris*, from the aquatic phylum Cnidaria [30]. The *Hydra* is the most phylogenetically primitive organism with both a putative endocannabinoid system and nervous system [30]. This “nervous system”, composed of homogenously dispersed unipolar and bipolar neurons in the epithelia, controls the “feeding response” of the *Hydra*, which opens and closes its mouth in the presence of prey/glutathione

[30]. Interestingly, while DAGL was not investigated in this study, mammalian DAGLs are activated by glutathione, suggesting 2-AG production may initiate the *Hydra* feeding response [20]. However, bath application of AEA inhibited, rather than stimulated, the *Hydra* feeding response, an effect that was reversed by 50 nM and 100 nM of CB_1 antagonist SR141716A [30]. While CB_1 receptors were not found in the Hydra, these data suggest that a functional CB_1 ortholog which binds AEA and SR is present [30]. In addition to *Hydra*, the invertebrate *C. elegans* has also been investigated. Using a cholesterol depletion paradigm of developmental arrest, the addition of AEA and 2-AG prevented arrested development through enhanced mobilization of cholesterol reserves and increased trafficking efficiency [31]. Notably, the addition of 2-AG and AEA did not simply "replace" the missing cholesterol but rather activated metabolic pathways which produced cholesterol [31]. This suggests endocannabinoids promote metabolic homeostasis in invertebrates through the dynamic modulation of lipid pathways in the context of food/nutrient availability. Vertebrate studies, which show increased endocannabinoid levels during reduced food availability, further confirm a dynamic role for the ECS in feeding behavior and metabolic homeostasis [32]–[34]. For example, in the goldfish, *C. auratus*, food deprivation caused an increase in AEA but not 2-AG [32] while food deprivation in the zebra finch, *T. guttata*, causes elevations in 2-AG but not AEA [35]. Additionally, 2-AG injection into the rat nucleus accumbens dose dependently increases food intake in a biphasic manner [34]. It is possible that reductions in food availability may drive increased endocannabinoid tone as a way of stimulating appetite and increasing feeding behavior. Seemingly contradictory to this, exogenous CB_1 agonist administration reliably decreases motor activity in mammals, which would presumably decrease feeding behavior [2], [34]. This divergence of endogenous and exogenous cannabinoid effect can be explained by the ligand-specific and dose-dependent nature

of CB_1 effect [34]. In addition to pharmacological investigations, CB_1 KO models are useful for determining the role of CB_1 in feeding behavior. As such, *CNR1* KO mice demonstrate decreased neonatal survival stemming from decreased milk suckling [36]. Those that survive struggle to gain significant weight [36]. This implies CB_1 is necessary for both the initiation of feeding behavior and the maintenance of healthy weight during neonatal development. Together, these studies highlight the centrality of the ECS in maintaining whole-body, metabolic homeostasis through dynamic feeding behavior changes.

Learning and memory are core nervous system functions possessed by both vertebrate and invertebrate organisms [27]. Evolutionarily, the ability to consolidate memories and act upon learned knowledge improves adaptability and survivability in unpredictable environments [37]. The endocannabinoid system plays a critical role in learning and memory, first gleaned from the deleterious effect of exogenous cannabinoids on short-term memory formation [38]. Endocannabinoid-mediated LTD and long-term potentiation (**LTP**) are considered central mechanisms in the regulation of synaptic plasticity, which is necessary for learning and memory [19], [23], [39]. Interestingly, the "machinery" required for synaptic plasticity, such as **NDMA** (N-methyl-D-aspartate receptor), **AMPA** (α-amino-3-hydroxy-5-methyl-4-isoxazolepropionic acid receptor), and kainite receptors, emerged in the cnidarian phylum and can be found in the starlet sea anemone, *N. vectensis* [40]. In the medical leech, NMDA-mediated LTP and endocannabinoid-mediated LTD have been observed [41]. In the pond snail (*L. stagnalis*), WIN55 a full CB_1 agonist, has a deleterious effect on learning and memory consolidation during a tactile stress paradigm [42]. Additionally, while the sea-hare, *Aplysia,* demonstrated decreased neuronal excitability in response to THC, researchers failed to later investigate endocannabinoid-mediated synaptic plasticity [43]. This is particularly disappointing considering the robustness of

the Aplysia as a model for invertebrate learning. While invertebrate model systems are beneficial due to their simplicity, vertebrate model systems better recapitulate the complexity of human learning and memory. The zebra finch is a particularly important model of vocal sensorimotor learning due to similarities with our own language acquisition [44]. Juvenile birds must be able to hear a song, remember the song, and practice the song in order to reproduce the song later [44]. Importantly, there are specific periods of sensorimotor development during which juvenile birds are particularly vulnerable to exogenous cannabinoid insult and fail to reproduce previously learned songs [33], [44]. This indicates that exogenous cannabinoids are disruptive to the process of memory retrieval during motor production. Notably, adult birds given cannabinoid treatment have no alterations to their song [44]. This suggests that the ECS plays a long-lasting role in juvenile sensorimotor development.

The ECS plays a vast role in regulating brain and body homeostasis. This is evidenced by the seemingly endless list of ECS-mediated processes in humans which includes memory, cognition, social behavior, emotional liability, hunger, satiety, and circadian rhythms [19], [34], [45], [46]. This expansive role, while impressive, can often be confusing and contradictory. To further compound this confusion, the fetal ECS possesses unique cellular and subcellular localizations [47], which suggests differential adult and fetal ECS function. Despite the progress made in endocannabinoid science over the past 30 years, the function of the fetal ECS remains elusive. Abundant, global expression of CB_1 in the mammalian brain can make it difficult to extract specific functions. However, the illumination of conserved ECS functions across diverse phyla can help put our own ECS functions in perspective. Thus, while the list of ECS-mediated processes in humans grows, the contextualization of results with conserved ECS processes will help improve our understanding of the ECS.

Figure 1.1 Diagram depicting the major biosynthetic and degradative enzymatic pathways of the endocannabinoids anandamide (AEA) and 2-arachidonoyl glycerol (2-AG). Biosynthesis of AEA starts with a small family of membrane phospholipids precursors, the N-arachidonoylphosphatidylethanolamines (NArPE). NArPE is directly converted into AEA by N-acylphosphatidylethanolamine-specific phospholipase D (NAPE- PLD). AEA is metabolized into arachidonic acid and ethanolamine by fatty acid amide hydrolase (FAAH). Precursors of 2-AG are derived from membrane phosphatidylinositols. Diacylglycerol lipase α and β hydrolyze sn-1-acyl-2-arachidonoylglycerols (AArG) to directly produce 2-AG. 2-AG is metabolized into arachidonic acid and glycerol by monoacylglycerol lipase (MAGL). Adapted from Di Marzo [20] and Scotchie et al. [48]

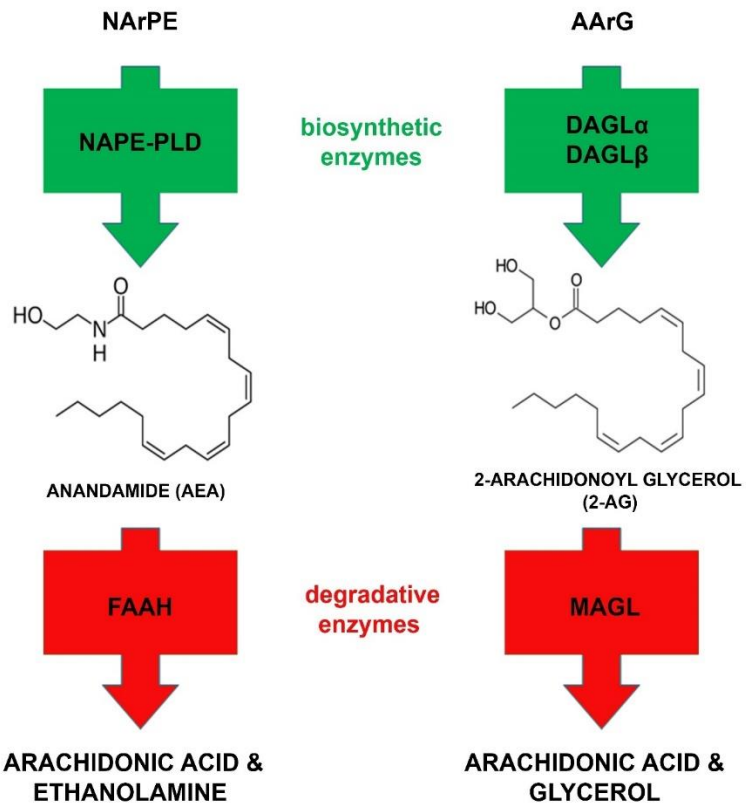

CHAPTER TWO: The role of the endocannabinoid system in fetal neurodevelopment

2.1 An overview of CB_1 in the adult brain

CB_1 is the most abundant GPCR in the vertebrate brain [19]. The highest expression of CB_1 in the adult human occurs in the cortex, hippocampus, basal ganglia, and cerebellum [19]. Within these regions, the canonical role of CB_1 is the activity-dependent inhibition of presynaptic neurotransmitter release at excitatory and inhibitory synapses [23], [39]. Activation of presynaptic CB_1 by endogenous or exogenous agonists elicits $G_{i/o}$ events, such as decreased adenylate cyclase, decreased cAMP production, and decreased protein kinase A activity [19]. CB_1 activation also inhibits N-type Ca^{2+} channels and activates inward rectifying K^+ channels [19]. Together, these cellular events hyperpolarize the presynapse and prevent vesicular exocytosis of neurotransmitters. The presynaptic control of neurotransmitter release by the endocannabinoid system is central to activity-dependent synaptic plasticity [23]. This process, defined as the dynamic regulation of synaptic strength in response to the level of activity it receives, critically maintains homeostasis within neural circuits and controls important aspects of memory and learning [23]. It is currently unknown if activity-dependent synaptic plasticity takes place in the fetal brain, however, current literature suggests activity-dependent plasticity is acquired during childhood [49]. Thus, with the current lack of evidence supporting fetal synaptic

plasticity, we suggest a non-canonical role for the developmental ECS where CB_1 directs axonal motility and synapse generation. This hypothesis is supported by multiple observations, including the differential localization of endocannabinoid constituents at both the cellular and synaptic level in mature versus immature neurons [23], [47].

2.2 Gross expression profile of CB_1 in the fetal brain

The endocannabinoid system plays a multifaceted role in neurodevelopment. It participates in the proliferation and differentiation of neural progenitor cells, the migration of neurons, and the establishment of neural circuits via synaptogenesis. Unsurprisingly, much of what we know about the endocannabinoid system's role in the immature brain stems from animal model work. CB_1 is highly conserved across chordate species, exhibiting a 97–99% sequence homology across rat, mouse, and human species [19]. CB_1 also has high conservation in birds [50] and amphibians [51]. In the human fetal brain, CB_1 receptor binding occurs as early as week 14 of gestation [52]. Similarly, CB_1 is expressed in the mouse brain starting at embryonic day 12.5 (**E12.5**), coinciding with the development of major neurotransmitters [24]. By 20 weeks of gestation, human CB_1 mRNA is expressed in all layers of the cerebral cortex, as well as in the hippocampus and amygdala [53], [54]. This regional pattern is mirrored in the rat brain (**E16**), with CB_1 expression occurring in the hippocampus, cerebellum, caudate-putamen, and cortex [24]. One notable difference between human and murine CB_1 expression is that CB_1 expression in the murine brain peaks after birth [55], while CB_1 expression in the human fetal brain peaks during mid fetal gestation (Figure 2.1). The increased CB_1 expression in the murine brain coincides with the post-natal development of the cortical layers, which highlights a major difference in cortical layer generation between human and murine models of neurodevelopment

[56]. Additionally, CB_1 expression is very low in the human fetal cerebellum, but exhibits high, regional expression levels in the fetal murine cerebellum [24], [54], [57]. This difference is also attributed to the protracted development of the human cerebellum compared to the mouse cerebellum during gestation [57]. Thus, while CB_1 exhibits conserved regional expression between fetal and adult brains, there are differences in the temporal regulation of fetal CB_1 expression between murine and human species.

2.3 Functional insights from the cellular and subcellar profile of fetal CB_1

Temporal differences in CB_1 expression also occur at a cellular level. The cell-specific expression of adult and fetal CB_1 in cortical neurons is differentially regulated in immature and mature neurons. Specifically, fetal CB_1 abundantly localizes to cortical, glutamatergic projection axons, while adult CB_1 localizes more so to GABAergic interneurons [24], [47]. Coinciding with the postnatal switch from glutamatergic to GABAergic CB_1 expression, 49% of pyramidal cells, 63% of somatostatin expressing interneurons, and 69% of vasoactive intestinal polypeptide expressing interneurons express CB_1 in the neocortex of the infantile rat (14 – 21 days old) [58]. Current literature suggests that CB_1 during development modulates the targeting and structure of axonal tracts in the developing brain by negatively affecting cortical neurite growth [22], [24]. CB_1 also plays a role in axon fasciculation, which is the bundling of multiple axonal projections along the same, long-distance trajectory [22], [59], [60]. This process of fasciculation is necessary for macro-scale neural circuitry building, as neuronal tracts (sometimes called fascicles) connect different regions of the brain [61]. It is presumed that correct axon

fasciculation is necessary for complete integration of neural circuits. The role of CB_1 as a mediator of axon guidance is supported by studies which observe faulty fasciculation and mistargeting of axonal tracts in rodents which have undergone genetic or pharmacological CB_1 inactivation [59], [60]. Misrouted corticothalamic/thalamocortical projections were observed in CB_1 KO mice, where the misrouted bundles of projection axons were larger and more scattered than those observed in control littermates [59]. These defects persisted postnatally. Unfortunately, no behavioral assays of the mice were completed. In other studies, CB_1 KO mice displayed increased social anxiety and decreased social interaction [45], [62]. These results are intriguing in the context of neurodevelopmental disease and the role CB_1 plays in coordinating regional connectivity. Thus, the changing expression pattern of CB_1 at the cellular level during postnatal development and the role this plays in cortical development highlights the uniqueness of the fetal brain environment.

At the subcellular level, differences between the adult and fetal endocannabinoid system are also apparent. For example, at the distal tip of the elongating axon, growth cones use autocrine endocannabinoid signaling rather than canonical paracrine signaling [47]. This is a result of differential DAGLα expression during development, where DAGLα localizes to the presynapse rather than the postsynapse [47], [63]. In the adult brain, DAGLα is postsynaptic and produces 2-AG which binds to CB_1 in a paracrine manner across the synaptic cleft [20]. However, in the fetal brain, 2-AG signaling is autocrine because DAGLα is localized next to CB_1 at the presynapse [47], [60]. Current literature suggests that autocrine 2-AG and CB_1 signaling prevents premature synaptogenesis [24], [47]. Interestingly, CB_1 expression in the fetal brain is greatest during weeks 19 – 24 of gestation (Figure 2.1). This window of mid-fetal gestation coincides with the initiation of synaptogenesis and suggests that CB_1 is heavily involved in

regulating establishment of cortical synapses [64]. Increased populations of perisomatic vesicular GABA transporter (**VGAT)** and vesicular glutamate transporter-3 (**VGLUT3)** boutons have been observed in the neocortex of adult mice with CB_1 KO in GABAergic interneurons [65]. Additionally, in cultured cortical neurons, DAGLα inhibition, which suppresses 2-AG release, increases synaptosomal-associated protein (25 kDa) (**SNAP25**) expression. [60]. SNAP25 is a protein which is involved in the exocytosis of neurotransmitters, as it regulates the fusion of vesicular and cellular membranes [66]. Increased SNAP25 due to DAGLα inhibition suggests the lack of CB_1 activation by 2-AG induces greater neurotransmitter release which likely initiates synapse creation. The inhibition of synaptogenesis by CB_1 activation is particularly important for glutamatergic projection neurons, which must acquire correct radial and tangential orientation prior to synaptogenesis [64]. As such, CB_1 KO mice have cortical layer malformations and increased seizure susceptibility [25]. Thus, endocannabinoid-mediated inhibition of synaptogenesis is likely necessary for correct cortical layering.

2.4 Challenges, objectives, and research hypothesis

The role of the endocannabinoid system in human synaptogenesis has been difficult to study for multiple reasons. First, while there is some conservation of CB_1 function in brain development between murine models and humans, there are discrepancies. These discrepancies include increased cortical region specificity, increased cortical map complexity, and protracted cortical layer development in humans [64]. Thus, human tissue models are particularly important for human synaptogenesis because murine models do not capture the protracted development of the human cerebral cortex [67]. Secondly, components of the endocannabinoid system are differentially localized in the fetal and adult brain, implying that the canonical roles of CB_1 in the

adult brain do not always match the roles in the developing brain. Luckily, many of these challenges are being addressed by the use of human-specific brain organoid models which mirror human neurodevelopment more closely than animal models [68]–[70].

Our research objectives included characterizing the endocannabinoid system in neurotypical patient-derived cortical spheroids, determining how disruptions to the endocannabinoid system impact establishment of neural circuitry, and evaluating the differential regulation of the ECS in cortical spheroids derived from patients with autism spectrum disorder (**ASD**). ASD is a heterogeneous neurodevelopmental disorder that is characterized by a complex behavioral phenotype including deficits in social communication and restricted, repetitive behavior [71]. ASD does not have a defining cellular pathology and research is currently focused on discovering convergent mechanisms **that** govern synaptic pathologies. Postmortem brain samples from idiopathic ASD cases exhibit synaptic alterations, including changes to the density of dendritic spines and imbalances in the ratio of excitatory and inhibitory synapses [72], [73]. Direct and indirect changes to the ECS likely play a role in the manifestation of ASD, as evidenced by the high overlap between ECS function and ASD symptoms/comorbidities [74]. Specifically, the ECS regulates social reward, emotional reactivity, and anxiety/fear responses, as well as learning/memory, circadian rhythm, and seizure susceptibility [25], [74]–[76]. Studies have found lower peripheral endocannabinoid tone in ASD patients [77], as well as a correlations between *CNR1* polymorphisms and social reward response [78], [79]. Additionally, since the ECS is globally expressed in the brain, it plays an outsized role in synapse maintenance compared to other GPCRs [80]. There is currently a small, but growing, body of evidence linking genetic and environmental ASD models to ECS dysfunction [74]. Further investigation of the link between ASD and the ECS will be important for the development of targeted pharmaceutical

therapies as there are only 2 FDA-approved drugs for ASD-associated irritability and no approved treatments for the core symptoms of ASD [81].

Overall, our global hypothesis is that disruptions to the fetal ECS contribute to the etiology of neurodevelopmental disease, specifically ASD. We hypothesized that a decrease in CB_1 activation during the initiation of synaptogenesis would propagate the ASD phenotype of excitatory/inhibitory synapse imbalance. We sought to test our hypothesis through confocal microscopy, **STORM** (Stochastic Optical Reconstruction Microscopy), and micro-electrode array (**MEA**). Our results, detailed below, make it apparent that the endocannabinoid system is functionally unique in the fetal brain. Because of this uniqueness, organoids which recapitulate the fetal brain during development are an excellent model for capturing the endocannabinoid-mediated regulation of synaptogenesis. Thus, we will discuss organoids and their utility in modeling brain disorders next.

Figure 2.1 *CNR1* expression is greatest during mid-fetal gestation, specifically during post-conception weeks 19-24. This period of gestation aligns with the initiation of both synaptogenesis and astrogliogenesis [64]. Data compiled by Dr Karen Litwa using data from the Allen Brain Institute.

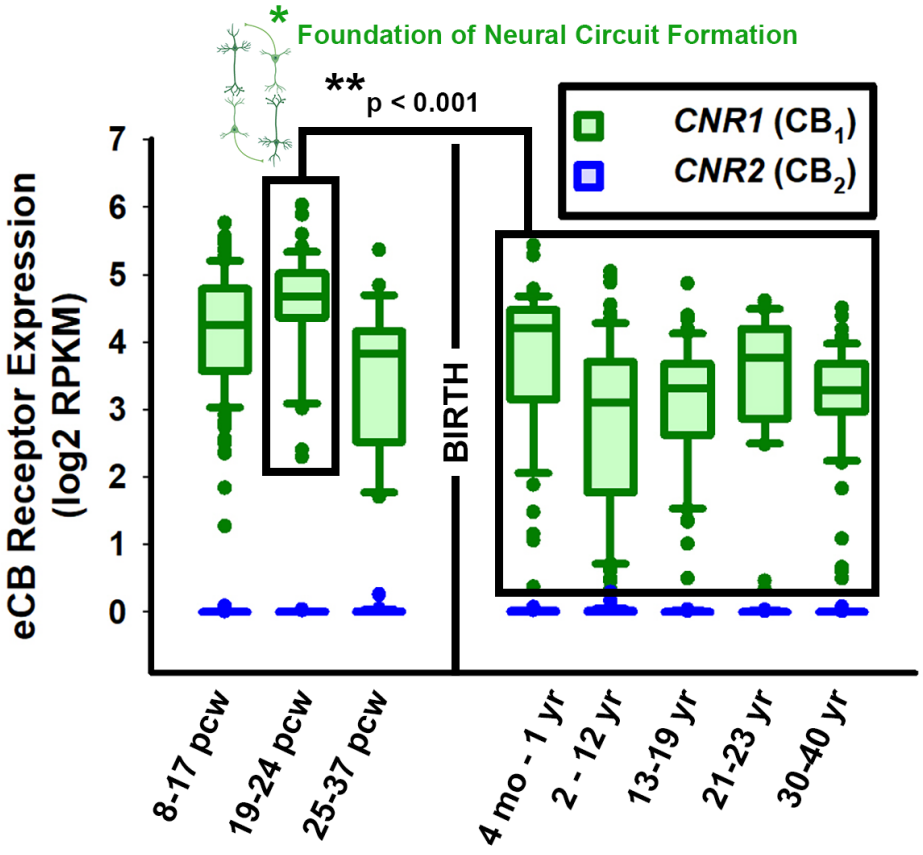

CHAPTER THREE: Human-Derived Brain Models: Windows into Neuropsychiatric Disorders and Drug Therapies

Alexis Papariello[a] and Karen Newell-Litwa[b]

[a] Department of Pharmacology and Toxicology, Brody School of Medicine at East Carolina University, Greenville, NC.

[b] Department of Anatomy and Cell Biology, Brody School of Medicine at East Carolina University, Greenville, NC.

Publication Citation: Alexis Papariello and Karen Newell-Litwa. ASSAY and Drug Development Technologies.Mar 2020.79-88.http://doi.org/10.1089/adt.2019.922

Published in Volume: 18 Issue 2: February 14, 2020

Online Ahead of Print:May 15, 2019

3.1 Abstract

Human-derived neurons and brain organoids have revolutionized our ability to model brain development in a dish. In this review, we discuss the potential for human brain models to advance drug discovery for complex neuropsychiatric disorders. First, we address the advantages of human brain models to screen for new drugs capable of altering CNS activity. Next, we propose an experimental pipeline for using human-derived neurons and brain organoids to rapidly assess drug impact on key events in brain development, including neurite extension, synapse formation, and neural activity. The experimental pipeline begins with automated high content imaging for analysis of neurites, synapses, and neuronal viability. Following morphological examination, multi-well microelectrode array technology examines neural activity in response to drug treatment. These techniques can be combined with high throughput sequencing and mass spectrometry to assess associated transcriptional and proteomic changes. These combined technologies provide a foundation for neuropsychiatric drug discovery and future clinical assessment of patient-specific drug responses.

3.2 Introduction

As the incidences of chronic neurological diseases continue to increase, new methods are needed to screen therapeutic compounds more effectively [82]. Current estimates for the economic burden of neurological diseases are astoundingly high, totaling nearly 800 billion dollars in 2014, of which Alzheimer's Disease (AD) accounts for at least 243 billion [82]. This cost is only expected to increase as the country's elderly population will nearly double, from 43.1 million to 83.7 million, by 2050 [83]. To reduce disease and economic burden, better therapies are needed to prevent and treat debilitating neuropsychiatric disorders.

However, drug development also faces economic challenges, with a single new drug costing upward of 800 million dollars [84]. Major hurdles affecting the development of new neuropsychiatric drug therapies include the lack of suitable animal disease models, unknown etiologies, patient-specific differences, especially in spectrum disorders such as autism, and unanticipated drug toxicity in humans [85]. Positive preclinical results observed in animal models may not be recapitulated in humans due to discrepancies in brain physiology or genetic disease modeling [86]. All these factors can lead to unexpected failures, with ~90% failure rate of drugs that enter the clinical pipeline [87].

Thus, we propose a model that is an ideal alternative to *in situ* brain tissue and can serve as an important tool in preclinical research and development: neurons and brain organoids developed from human induced pluripotent stem cells (hIPSCs). This review details a proposed pipeline for the use of hIPSC neuronal models in therapeutic drug discovery. We will begin with an introduction to how hIPSC neuronal models are currently used to model complex neuropsychiatric disorders and therapeutic responses. We will then address how hIPSCs can be

combined with recent technologies to enable rapid and effective screening of drug therapies (Figure 3.1).

3.3 hIPSC Models of Neuropsychiatric Disorders

Since the discovery of hIPSCs, a wide array of neurological diseases has been modeled, including neurodegenerative diseases, such as AD, and neurodevelopment disorders, such as Autism Spectrum Disorders (ASDs) [88]. hIPSCs have also provided a unique tool to gain insights in rare neurologic disorders, such as Kleefstra Syndrome [89], Dravet Syndrome [90], and Smith Lemli Opitz Syndrome [91]. These hIPSC models mimic brain development and pathology more closely than human immortal cancer cell lines and primary animal cell culture; this will likely allow for more accurate predictions of patient responses [92].

In addition to drug discovery, hIPSCs can be used clinically to evaluate patient-specific drug responses, for example, drug-induced changes in neural activity. These hIPSC-derived models can be combined with high throughput RNA sequencing technologies to define transcriptomes associated with specific patient populations, eventually leading to personalized therapeutic intervention [93]. Furthermore, proteomic, metabolomic, and lipidomic signatures can be used for patient classification and analysis of drug efficacy[93]. In neurodegenerative disorders, biomarkers will allow for diagnosis before disease onset, and aid in developing therapies that prevent neuronal loss, rather than inhibit further loss after disease onset.

The following sections describe how hIPSCs have been used to model pathology and therapeutic responses in AD and ASDs as representative neurodegenerative and neurodevelopmental disorders, respectively. We will then use these two examples to demonstrate

how our proposed experimental strategies can advance drug discovery for complex neuropsychiatric conditions.

3.3.1 Alzheimer's Disease

AD is the most common cause of dementia, accounting for up to 80% of all dementia cases [94]. In humans, AD results in extracellular amyloid plaques, intracellular neurofibrillary hyperphosphorylated tau tangles, and synapse loss preceding neurodegeneration [95]. There is difficulty recapitulating these key pathological features in mouse models, which require expression of human amyloid precursor protein (**APP**) and human tau for formation of disease-associated amyloid plaques and neurofibrillary tangles [96]–[98]. Thus, a human model has the potential to greatly advance therapeutic drug discovery for AD.

Several hIPSC models have been developed to model both sporadic and familial forms of AD (**sAD and fAD**) [99]. Beginning in 2011, hIPSC-derived neurons were used to model early onset fAD in patients with presenilin mutations. Presenilin-1 and -2 are the major components of γ-secretase, which cleaves APP into amyloid-β (**Aβ**) peptides [100]. fAD-associated presenilin mutations increase the ratio of the amyloidogenic Aβ-42 peptide to the shorter Aβ-40 peptide [101]. This study demonstrated that hIPSC-derived neurons from fAD patients secrete more Aβ-42, and that γ-secretase inhibitors (**GSIs**) decreased the levels of secreted Aβ-42 [102].

In 2011, another study similarly demonstrated the ability of γ- and β-secretase inhibitors to lower Aβ production in control hIPSC-derived neurons [103]. β-secretase functions in the first step of APP processing, preceding γ-secretase, in the production of amyloidogenic Aβ peptides [104]. These findings were extended to hIPSC-derived neurons from a sAD patient and fAD patients with *APP* duplications, all of which exhibited disease-associated increases in Aβ

peptide, active GSK-3β, and phosphorylated tau [105]. While both β- and γ-secretase inhibitors decreased secreted Aβ, only β-secretase inhibitors decreased GSK-3β and phosphorylated tau [105]. Notably, hIPSC-derived neurons from another sAD patient did not exhibit disease-associated phenotypes, highlighting the benefit of hIPSCs to reveal patient-specific differences and identify patients likely to benefit from a given therapy [105].

In addition to confirming the ability of secretase inhibitors to reverse AD phenotypes, hIPSC-derived neurons have also been used to overcome the limitations of cell lines for secretase inhibitor optimization. For example, GSIs decrease Aβ peptide production in APP-overexpressing cell lines, but have failed in human clinical trials [106]. This failure prompted researchers to pursue more physiologically relevant AD models, fibroblasts and hIPSC-derived neural progenitor cells and neurons from FAD patients with presenilin-1 mutations [85]. This study revealed differential drug efficacy in specific cell types, with the greatest Aβ reduction observed in hIPSC-derived neurons [85]. Importantly, this study also revealed that the IC_{50} of the GSI, semagacestat, was five times higher in hIPSC-derived neurons than APP-overexpressing cell lines, perhaps contributing to its clinical failure [85].

Additionally, hIPSC-derived neurons have been used to identify new Aβ lowering compounds through a pharmaceutical library screen and chemiluminescent measurement of the resulting Aβ levels [107]. This study led to the development of an Aβ lowering cocktail that significantly reduced Aβ levels in hIPSC-derived neurons from fAD patients with presenilin mutations and to a lesser extent, fAD patients with *APP* mutations and sAD patients [107]. This study used a rapid neuronal induction protocol to screen for Aβ levels within 10 days of neuronal differentiation, thus accelerating drug screening and identification of promising therapies [107].They also ensured that reduced Aβ levels did not result from increased neuronal cell death

[107]. However, the authors note that this cocktail still cannot move to clinical trials as IPSC-derived neurons alone do not address whether the drugs cross the blood-brain barrier (BBB) [107]. Thus, cultures that more closely mimic the brain environment, for example, by incorporating vascular endothelium, have the potential to advance therapies from drug discovery to clinical trials [108]–[110].

hIPSC-derived neurons have also been used to validate protherapeutic effects of alternative AD treatments in a human model, such as nobiletin and apigenin. Nobiletin is a compound found in citrus peel that exhibits antidementia effects in mice [111], [112]. Nobiletin reduced intracellular and secreted Aβ in hIPSC-derived neurons with an fAD-associated presenilin-1 mutation [113]. The observed protherapeutic effect is due to increased expression of the Aβ-degrading enzyme, neprilysin [113]. Similarly, apigenin, the polyphenolic compound found in celery, parsley, and artichoke, exhibited neuroprotective effects in hIPSC-derived sAD and fAD neurons [114]. Apigenin's anti-inflammatory properties reduced nitric oxide production, increased neurite length, and rescued cell viability [114]. Together, these studies highlight the use of hIPSC-derived neurons to validate and optimize AD therapies in a human model.

3.3.2 Brain Organoids in AD Research

While hIPSC-derived neurons show promise for drug discovery, brain organoids capture key pathological features that can only be observed in a three-dimensional (3D) matrix that mimics the complex tissue microenvironment. For example, AD-derived neurons exhibit increased secretion of insoluble Aβ, but fail to form amyloid plaques [115], [116]. Amyloid plaques reside in the extracellular matrix, thus requiring a 3D model for retention. Additionally, Aβ plaques are hypothesized to initiate the formation of tau neurofibrillary tangles, eventually

leading to cell death [117]. This is consistent with observations in AD-derived neurons, which fail to retain Aβ plaques. These AD-derived neurons exhibit increased tau phosphorylation, but they do not form intracellular tau neurofibrillary tangles [116]. Furthermore, cell death has not been documented in 2D AD-derived neurons.

To test the Aβ hypothesis of AD pathogenesis, 3D brain models are needed to capture Aβ plagues. The first 3D human AD model used hydrogels, which promoted Aβ retention and intracellular tau neurofibrillary tangle formation, although cell death was not reported [116]. Using this model, both γ- and β-secretase inhibitors reduced Aβ plague formation and tau phosphorylation [81]. However, the GSK-3β inhibitor, 1-Azakenpaullone, specifically decreased tau phosphorylation, but did not affect Aβ production [81]. These results support a disease model in which GSK-3β phosphorylates tau, but does not phosphorylate APP to increase Aβ production [118]. By contrast, cerebral organoid models of AD exhibit amyloid plaques, intracellular tau neurofibrillary tangles, and increased cell death[119].

By capturing Aβ plaque formation, tau neurofibrillary tangles, and neurodegeneration, 3D brain organoid models provide unique opportunities for neurodegenerative disease research and drug discovery. For example, recent data indicate that mutant tau exhibits prion-like properties, leading to stereotyped propagation of tau neurofibrillary tangles with disease progression [120]. Similarly, in mice, mutant APP results in the spread of amyloid plaques to distal brain regions [85]. Brain organoids have the unique ability to monitor the spread of insoluble plaques and tangles, and test for drugs that prevent spreading.

To monitor protein aggregation in brain organoids, they can be injected with toxic Aβ or tau mutants. Alternatively, chimeras of unaffected and AD-derived brain organoids can be created. For example, a recent study used the propensity for brain spheroids to fuse with one

another to monitor interneuron migration between brain spheroids [121]. By similarly allowing for fusion of AD and unaffected brain organoids, one could monitor the propagation of pathological features and the resulting cell death. This method can also be used to fuse brain region-specific organoids and assay for drugs that block the spread of protein aggregates between brain regions [122]. Thus, brain organoids recapitulate key pathological features missing in hIPSC-derived neurons. By more accurately modeling the disease state, brain organoids have the potential to further advance drug discovery.

3.3.3 Autism Spectrum Disorders

ASD is a heterogeneous, neurodevelopmental condition that is characterized by a complex behavioral phenotype. Key features of the disorder include deficits in social communication and restricted, repetitive patterns of behavior that exist on a continuum of severity[71]. ASD is one of the most common developmental disorders in the United States, affecting 1 in 59 children, with a male to female diagnosis ratio of 4:1 [123]. Due to the disabling nature of the disorder, children often require special accommodations. Estimates for the lifetime cost of supporting a child who has ASD with an intellectual disability are over 2 million dollars per child, citing educational services, productivity loss from parents, and higher frequency of health care office visits and prescriptions [124], [125].

Unlike AD, ASD does not have a defining cellular pathology. Research is currently focused on discovering convergent mechanisms that govern synaptic changes seen in ASD. Postmortem brain samples from idiopathic ASD cases exhibit synaptic alterations, including changes to the density of dendritic spines, the primary sites of excitatory synaptogenesis [126], [127]. Much research focuses on syndromic, monogenetic ASD disorders, for example, fragile X

syndrome (**FXS**) and Rett Syndrome (**RTT**) [128]. FXS results in increased excitatory synapses, (Penzes 2011) while excitatory synapse formation in RTT depends on ***MeCP2*** (methyl-CpG-binding protein 2) gene dosage, with *MECP2* deletion reducing excitatory synapse formation and *MECP2* duplication increasing excitatory synapse formation [129].

Drug development for ASDs is particularly challenging due to this heterogenous nature and future research must be aimed at identifying the molecular pathways that cause different synaptic alterations [130]. A particular benefit of hIPSC brain models is the ability to classify patients based on phenotypic presentation and develop therapies for specific patient populations within the spectrum.

Using an hIPSC-FXS model of ASD, researchers screened over 5,000 drugs for compounds that increase *FMR1* gene expression [131]. In FXS patients, cognitive disability is caused by the loss of fragile X mental retardation protein (**FMRP**) via silencing of the *FMR1* gene [97]. In this study, an assay was developed that allowed for FMRP protein detection in hIPSCs derived from four patients who had a completely silenced *FMR1* allele; this factor is crucial because positive hits (increased FMRP) indicate FMR1 gene reactivation rather than increases in translation [97]. This study used a time-resolved FRET assay to measure FMRP levels of lysed cells in a 1,536-well plate [97]. Of the >5,000 compounds, only 4 compounds (Protoporphyrin IX, SB216763, Geliomycin, and Tibrofan) produced a dose-dependent increase in FMRP [97].

Future studies are needed to determine the mechanism by which these compounds reactivate *FMR1* gene expression, although SB216763 is a GSK3β inhibitor known to improve hippocampus-dependent learning and neurogenesis in the *FMR1* knockout mouse, where it is not possible to reactivate *FMR1* expression [131], [132]. Another GSK3β inhibitor, lithium chloride,

did not reactivate *FMR1* expression, suggesting that SB216763 reactivates FMR1 independent of GSK3β inhibition [97]. Two of these drugs, Geliomycin and Tibrofan, are FDA-approved as an antibiotic and disinfectant respectively, demonstrating the use of hIPSCs to identify novel and repurposed drugs for the treatment of neuropsychiatric disorders [97].

A similar study evaluated the effects of 50,000 compounds on hIPSC-derived neurons from FXS patients to assess *FMR1* gene reactivation [133]. Positive hits in the assay were defined as drugs that increased FMRP cytoplasmic protein levels three or more standard deviations above the negative control; this procedure was done via high throughput imaging and analysis techniques [99]. Since DNA hypermethylation silences *FMR1* gene expression, this study used 5-aza-2′-deoxycytidine, a known inhibitor of DNA methyltransferase DNMT1, as a positive control for evaluating FRMP increase [99]. After the primary exploration, 790 compounds were chosen to undergo dose–response curve experiments; only a few compounds showed increased FMRP expression before cytotoxicity, and all identified compounds were more toxic than the positive control [99]. While this study was not successful in finding a lead compound, it did establish a high content image-based assay for drug screening in a population of patients who do not yet have an FDA-approved treatment option.

In a proof-of-concept pharmacogenomic study, Darville *et al.* demonstrated how hIPSC-derived neurons can be used to find new treatment options for ASD patients using a *SHANK3* haploinsufficiency model [91]. Loss-of-function mutations of the *SHANK3* gene affect ∼2% of ASD patients who present with moderate to severe intellectual disability [134]. The SHANK3 protein is a scaffolding molecule localized to the postsynaptic density of excitatory synapses; it mediates the interaction between various glutamate receptors and the actin

cytoskeleton, indicating an important role for regulation of synaptic plasticity in disease pathogenesis [135].

Since *SHANK3* mutations in ASD patients only affect one allele, transcription of the second allele can be upregulated and *SHANK3* mRNA levels can be increased [56]. The authors screened 202 compounds in 4 patient-derived hIPSC neuron lines using automated high throughput mRNA quantification and then followed up with high content image analysis of 16 selected compounds that demonstrated a dose–response curve [56]. Lithium and valproic acid, two FDA-approved compounds, increased SHANK3 at both the mRNA and protein level in *SHANK3* haploinsufficient hIPSC-derived neurons [56]. The authors were also able to confirm the clinical efficacy of lithium in one of the ASD patients who donated their hIPSC line, demonstrating the feasibility of using hIPSC models for personalized therapeutics [56].

RTT is also used as a genetic model of ASD in hIPSC-derived neurons. This neurological disorder is caused by loss-of-function mutations in the X-linked gene that encodes the epigenetic regulator protein MeCP2 [136]. Neurons derived from RTT patients with an *MeCP2* deletion had fewer excitatory synapses and altered electrophysiological profiles, including decreased frequency and amplitude of excitatory postsynaptic currents [137]. Insulin-like growth factor 1 (**IGF1**) is currently being explored as a potential therapeutic for RTT patients; it has been shown to increase the number of glutamatergic synapses and increase neurite length back to baseline in RTT-hIPSC derived neurons [103]. Clinical studies support the safety and efficacy of recombinant human IFG1 treatment in RTT patients; treatment is associated with significant improvements in disease severity including improved social and cognitive measures [138]. IGF1 has also been explored in clinical trials for the treatment of other monogenetic neurodevelopmental disorders, including promising phase 2 trials in both FXS and Phelan-

McDermid Syndrome patients [139]. Thus, hIPSC models of ASD are already being used to develop therapies for specific patient subgroups.

3.3.4 Brain Organoids in Autism Research

Similar to AD, brain organoids are providing further insights into the temporal development of autism pathology and unique opportunities for drug discovery. Brain organoids develop on similar timescales to the fetal brain *in utero*, with synaptogenesis occurring during mid-fetal gestation [121]. Likewise, excitatory synapses shift to specialized dendritic spines after ~8 months of organoid culture, at stages that resemble perinatal brain development [86]. Transcriptional correspondence between brain organoids and the human fetal brain after similar developmental times make brain organoids an ideal system to study both transcriptional and cellular changes associated with specific periods of brain development [86].

For example, IPSC-derived telencephalic organoids from ASD patients with increased brain size have elevated RNA levels of the transcription factor, *FOXG1*, resulting in increased production of inhibitory neurons and synapses [140]. Increased GABAergic cell fate correlated with symptom severity, suggesting that *FOXG1* may be an early driver of altered neural circuitry associated with autism pathology [106]. Dysregulation of GABAergic interneurons has also been seen in other ASD brain organoid models, notably in the heterozygous knockout of chromodomain helicase DNA-binding protein 8 ***(CHD8)***, a gene commonly mutated in ASD patients [141]. Brain organoids with the *CHD8* heterozygous knockout displayed increased expression of two genes that regulate GABAergic interneuron development [107]. Intriguingly, patients with *CHD8* mutations exhibit macrocephaly, suggesting that increased GABAergic production may be a common feature of ASD patients with larger-than-average head size.

Furthermore, RTT brain organoids have enabled research into prenatal roles of MECP2, namely altered neural progenitor cell proliferation and neurogenesis, whereas previous research has primarily focused on postnatal roles of MECP2 [142]. Specifically, brain organoids allowed the researchers to visualize increased area of ventricles, which form in brain organoids, but not monolayer cultures [108]. These newly discovered transcriptional and cellular changes can be used in drug-screening applications, for example, to identify drugs that regulate interneuron differentiation or neural progenitor cell proliferation.

The following sections explore how high content imaging and multi-well microelectrode arrays (MEAs) can be used to assess drug-induced changes to neuronal morphology and function in both hIPSC-derived neurons and brain organoids. These drug screening assays will further therapeutic discovery for the treatment of neuropsychiatric disorders, such as AD and ASD.

3.4 Drug Screening for Neuroprotective Effects

3.4.1 Automated High Content Imaging and Analysis

Decreased neurite length is a common phenotype of ASD-derived and AD-derived neurons [143]. Thus, screening for drugs that promote neurite length could reveal potential therapeutic candidates for both neurodevelopmental and neurodegenerative disorders. High content imaging systems can be used to rapidly screen neurite length following drug treatment [144]. In this platform, fixed neurons are fluorescently immunostained with early neurite markers, such as β-III tubulin/TUJ1, together with a nuclei marker, such as Hoechst or DAPI [141], [145]. Following nuclei detection, the system performs neurite segmentation, providing readouts such as neurite length, number of neurites, and neurite branching [146]. Automated

analysis can be combined with the high content imaging system or performed by separate software/freeware, such as CellProfiler [147].

Using high content imaging and analysis, Sherman and Bang screened several bioactive compound libraries to identify positive and negative regulators of neurite outgrowth [112]. Compounds promoting neurite outgrowth included kinase inhibitors, such as inhibitors of the myosin kinases, ROCK and MLCK, and GSK3β inhibitors [146]. While ROCK inhibition increases neurite outgrowth, it does not affect electrophysiological maturation in hIPSC-derived neurons, demonstrating the need for a comprehensive therapeutic screen that includes both morphological and functional neuronal characterization through techniques such as MEA [148]. Other compounds that promote neurite outgrowth include regulators of steroid hormone receptors and neurotransmitter receptors [112].

This study also identified novel regulators of neurite outgrowth, including some fatty acids [112]. Importantly, some compounds had opposite effects on neurite outgrowth than those reported for immortalized rodent cell lines, including the mouse neuroblastoma Neuro-2A cell line and rat pheochromocytoma PC12 cell line, providing further evidence that a physiologically relevant human model is needed for neuropsychiatric drug screens [112].

Importantly, the neurite-promoting effects of these compounds also need to be validated in disease models. For example, GSK3β inhibitors might have an increased effect on neurite outgrowth in AD models, where there is increased GSK3β activation [94]. Alternatively, specific compounds may only have a therapeutic effect in disease models, as is illustrated by NC009-1-mediated increase in neurite outgrowth in hIPSC-derived neurons from fAD patients with *APP* mutations but not in control hIPSC-derived neurons [143]. Similarly, specific patients may exhibit different responses. In the case of ASD patients, a rapid screen of neurite length to

identify patients with defective neurite outgrowth may help to identify patients likely to benefit from neurite-promoting therapies.

In addition to neurite defects, AD and ASD also present with synaptic abnormalities that can be rapidly analyzed using a high content imaging platform, where co-localization of pre- and postsynaptic markers identifies synapses [147]. For example, co-localization of the presynaptic vesicle marker, synapsin-1, with the postsynaptic scaffold protein PSD-95 identifies excitatory synapses, whereas co-localization between synapsin-1 and gephyrin identifies inhibitory synapses [113].

Synapse loss is observed before neurodegeneration in AD, thus drugs that promote synapse formation and/or prevent synapse loss could be attractive therapies [149]. In contrast to synapse loss in neurodegeneration, synaptic alterations associated with neurodevelopment are more varied. Postmortem brain cortex from idiopathic ASD patients exhibits increased excitatory synapses [127]. However, other ASD-associated mutations, such as RTT *MeCP2* deletion, reduce excitatory synapse formation [129]. Decreased excitatory synapses and increased inhibitory synapses have also been observed in both hIPSC-derived neurons and brain organoids from ASD patients with larger-than-average brains [150]. This heterogeneity of synaptic abnormalities demonstrates how hIPSC-derived neurons can be used to assess patient-specific phenotypes and develop personalized therapies.

Finally, high content imaging systems can be catered for rapid analysis of a variety of fluorescent-based, and even brightfield, images. For example, a study aimed at identifying tau-lowering compounds as AD therapies, conducted high content imaging and analysis to detect tau levels relative to β-III tubulin [141]. After screening the 1,280 compounds in the Library of Pharmaceutically Active Compounds (**LOPAC**), they identified adrenergic receptor agonists as

the top tau-lowering compounds [107]. Thus, high content imaging and analysis can be catered to assess disease-specific phenotypes, such as tau levels for AD, FMRP levels in FXS, and SHANK3 levels in *SHANK3* haploinsufficient ASD patients [107], [91], [133].

When using high content imaging to analyze drug-induced changes to neurons, there are several important considerations. One primary consideration is to first determine whether the drug negatively impacts cell health and viability, in which case the observed effects to neurons may be caused by cellular stress responses rather than specific drug-induced changes to neuronal physiology. Multiple methods have been used for automated analysis of cell health, including abnormal nuclei, viability dyes, such as calcein-AM, and caspase assays for apoptosis [145], [146], [151]. Furthermore, 384-well cell culture plates can negatively impact cell viability and consistency across wells due to media loss through evaporation [152]. To overcome this limitation, researchers developed a ferromagnetic micro-raft array, where an array of 1,600 microrafts are cultured together and then magnetically transferred to a 384-well plate [118]. This technique improved neuronal viability, allowing for robust and reproducible drug screening [118]. Additionally, cell and organoid cultures are being optimized for 1,536-well glass-bottom plates, further increasing the throughput of high content imaging systems [153].

3.4.2 Multi-Well MEA Analysis of Neural Activity

In addition to high content imaging, MEA technology has emerged as a powerful tool to analyze basal and evoked neural activity in currently up to 96 samples. The MEA measures the extracellular field potential corresponding to action potential formation [154]. Notably, this technique requires longer maturation than is needed for assessment of neurite length, with

spontaneous action potentials occurring after ~1–2 months of monolayer hIPSC-derived neuronal culture and ~3 months or more in hIPSC-derived brain organoids [155]

However, techniques to rapidly induce physiological maturation can be used to accelerate drug screening. For example, in 2D, forced expression of neuronal transcription factors, NeuroD2 or neuroligin-2, can be used to accelerate neuronal maturation, with neural activity occurring after ~1 week of neuronal induction [156]. Furthermore, optogenetics can be used to increase neural activity and potentially accelerate maturation of hIPSC-derived neurons and brain organoids, allowing for more rapid assessment of drug-induced changes to neural activity [157].

Using MEA analysis, reduced spontaneous firing rate has been observed for several idiopathic cases of ASD [150]. However, ASD has also been associated with increased hyperactivation and epilepsy [158]. These differences are consistent with patient-specific synaptic differences in ASD, and emphasize the need to identify drug therapies catered to specific patient populations. MEAs provide a powerful tool to capture epileptiform neural activity and screen for antiseizure medications [159]. MEA recordings of control hIPSC-derived neurons revealed increased epileptiform activity in response to proconvulsant drugs and decreased activity in response to seizure medication [160]. Thus, using MEAs, hIPSC brain models can be used to monitor activity signatures associated with epilepsy and other neuropsychiatric disorders [126].

In the case of neurodegenerative disorders, hIPSC-derived neurons gene-edited to model triple tau mutations in AD exhibit increased activity, consistent with AD-associated neuronal hyperactivity [161]. Hyperactivation is an early indicator of AD, preceding amyloid plaque formation and neuronal silencing, and can surprisingly be treated with GABA receptor

antagonists in mice [127]. It will be necessary to confirm whether GABA receptor antagonists similarly rescue neuronal function in human brain models.

While there are currently no published large-scale MEA drug screens of hIPSC-derived neuronal function, this is partially due to optimization of control hIPSC-derived neurons for accelerated maturation and reduced variability in neuronal function between cultures [162]. However, given the ability to record temporal changes in neural activity, MEA technology can assess drug-induced changes in neural activity at specific stages of neurodevelopment and disease progression. This will be particularly useful for identifying therapies that function before synapse loss and those that restore normal activity following synapse loss and subsequent neurodegeneration.

3.5 Concluding Remarks and Important Considerations in hIPSC Drug Screens

While this review focused on neuronal morphology and function, other brain cells including glia, such as astrocytes, microglia, and oligodendrocytes, also contribute to neuropsychiatric disease pathology. A recent study using hIPSC-derived AD-associated astrocytes and microglia demonstrated defective Aβ clearance [163]. Furthermore, microglial activation and neuroinflammation contribute to neurodegenerative and neurodevelopmental pathogenesis [164]. A specific advantage of the hIPSC model is the ability to derive specific brain cell types (neurons, astrocytes, and microglia) from either controls or affected individuals to address the contribution to disease pathology. These different hIPSC-derived cells can also be used to address how specific drugs differentially affect specific cell types. Furthermore, whole

brain organoids can also be used to address drug impact in a complex tissue environment. For example, a recent study validated potential inhibitors of Zika virus infection in both human brain organoids and the adult mouse brain [165].

While hIPSC models provide an ideal opportunity to screen for on-target drug effects, they are currently limited in their ability to measure drug distribution and BBB penetrance. However, techniques, such as 3D bioprinting, allow for the introduction of blood vessels to organoid models, suggesting that we will soon be able to address BBB drug penetrance in hIPSC brain models [109]. Furthermore, hIPSC-animal chimeras can be used to evaluate drug effects in a complex brain environment that includes disease-associated neuroinflammation, and the BBB to limit drug availability [109]. These increasingly more accurate models of human brain development will enable a progression of drug screening techniques, beginning with rapid and high throughput screens to identify therapeutic candidates of interest and proceeding to evaluate their effects in engineered human tissues or hIPSC-animal chimeras [166].

Figure 3.1 Drug discovery in hIPSC-derived brain models. This figure highlights how high content imaging platforms and MEA technologies can be combined to analyze neuronal physiology, including neuronal morphology and neural activity. While this review focuses on high content imaging and MEA technologies in drug discovery, they can be combined with other high throughput technologies, including RNA sequencing and mass spectrometry.

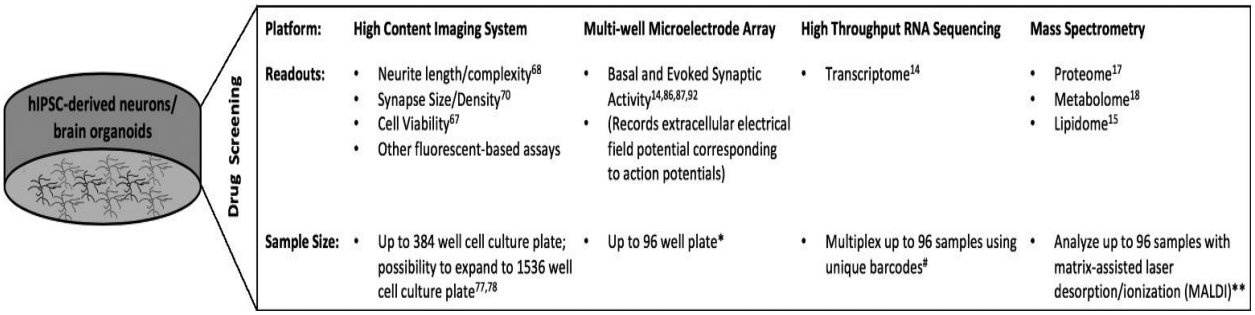

CHAPTER FOUR: CB_1 antagonism increases excitatory synaptogenesis in a cortical spheroid model of fetal neurodevelopment

Alexis Papariello[a], David Taylor[a], Ken Soderstrom[a], and Karen Newell-Litwa[b]

[a] Department of Pharmacology and Toxicology, Brody School of Medicine at East Carolina University, Greenville, NC.

[b] Department of Anatomy and Cell Biology, Brody School of Medicine at East Carolina University, Greenville, NC.

Publication citation:

Papariello, A., Taylor, D., Soderstrom, K. & Litwa, K. CB1 antagonism increases excitatory synaptogenesis in a cortical spheroid model of fetal brain development. *Sci. Rep.* **11**, (2021).

4.1 Abstract

The endocannabinoid system (ECS) plays a complex role in the development of neural circuitry during fetal brain development. The cannabinoid receptor type 1 (CB_1) controls synaptic strength at both excitatory and inhibitory synapses and thus contributes to the balance of excitatory and inhibitory signaling. Imbalances in the ratio of excitatory to inhibitory synapses have been implicated in various neuropsychiatric disorders associated with dysregulated central nervous system development including autism spectrum disorder, epilepsy, and schizophrenia. The role of CB_1 in human brain development has been difficult to study but advances in induced pluripotent stem cell technology have allowed us to model the fetal brain environment. Cortical spheroids resemble the cortex of the dorsal telencephalon during mid-fetal gestation and possess functional synapses, spontaneous activity, an astrocyte population, and pseudo-laminar organization. We first characterized the ECS using STORM microscopy and observed synaptic localization of components similar to that which is observed in the fetal brain. Next, using the CB_1-selective antagonist SR141716A, we observed an increase in excitatory, and to a lesser extent, inhibitory synaptogenesis as measured by confocal image analysis. Further, CB_1 antagonism increased the variability of spontaneous activity within developing neural networks, as measured by micro electrode array. Overall, we have established that cortical spheroids express ECS components and are thus a useful model for exploring endocannabinoid mediation of childhood neuropsychiatric disease.

4.2 Introduction

The endocannabinoid system (ECS) classically regulates synaptic plasticity via inhibitory presynaptic feedback in the adult brain[20]. Constituents of the ECS are also expressed in the human brain during fetal gestation[52], [54], where they direct numerous neurodevelopmental processes, including neural progenitor proliferation[167], differentiation[168], neuronal migration[25], and axonal growth cone directionality[22], [24], [63]. While the role of the ECS in the adult brain is well defined, the role of the ECS in the initial establishment of synapses during fetal brain development is not. In the following research, we investigate whether ECS disruption via CB_1 antagonism impacts synaptogenesis in a cortical spheroid model of fetal brain development.

Synaptogenesis begins when nascent pre- and post-synaptic surfaces contact and adhere to one another[169]. This process requires the coordinated activity of multiple subcellular systems including cell adhesion molecules[64], scaffold proteins and receptors,[64], [170] and cytoskeletal regulators[64], [171]. Disruption of these systems which govern synapse selection and maintenance can cause altered excitatory/inhibitory (E/I) synapse balance[73], [169], [172]. Effective information transfer in the brain relies on homeostatic balance between excitatory and inhibitory synapses, thus, changes to the E/I balance during critical periods of development may negatively impact behavior and cognition[73]. Altered E/I balance is a phenotype which has been implicated in neuropsychiatric ailments that lack clear etiologies including epilepsy[173], schizophrenia[73], [174] and autism spectrum disorder (ASD)[73]. Thus, while neural circuits are pliant during early development, they are also particularly vulnerable to genetic and environmental disruption.

Many features of neurodevelopmental disorders are difficult to adequately characterize in animal models. This stems from the heterogeneous genetic nature of many neurodevelopmental disorders, the timing of critical periods, and diagnostic criteria that is not easily translated into animal research (such as verbal and nonverbal communication)[175]. Recent advances in the use of induced pluripotent stem cells (IPSC) and the creation of organoid and spheroid model systems promise progress[69], [176]. These models, which replicate brain tissue structure better than two-dimensional cell culture,[70], [91] provide an avenue for drug testing in a genetically relevant paradigm[68], [92] and allow for the study of human disease processes without complicated *in vivo* work[69], [91]. Using IPSCs from neurotypical control patients, we are able to grow cortical spheroids which have functional synapses, spontaneous activity, an astrocyte population, and pseudo-laminar organization which resembles the dorsal telencephalon of the human fetus at 19-24 weeks post conception[88], [155], [177].

To address how the ECS impacts synapse formation, we focused on the role of endocannabinoid receptor CB_1. CB_1 is not only the predominant endocannabinoid receptor in the brain[19], it is also the most abundant G-protein coupled receptor in the vertebrate central nervous system[51]. Activation of presynaptic CB_1 by the endogenous, endocannabinoid agonist 2-arachidonoylglycerol (2-AG) elicits activity-dependent, G_i-linked effects[19], [178] that decrease presynaptic neurotransmitter release and weakens synaptic strength[19], [24]. The biosynthetic enzyme for 2-AG, diacylglycerol lipase (DAGLα, the principal CNS isoform), along with the metabolic enzyme monoacylglycerol lipase (MAGL), control the local distribution of 2-AG, which is the principal endocannabinoid during gestation[168], [179], [180]. In addition to the classic, paracrine signaling of 2-AG during CB_1-mediated presynaptic feedback inhibition, 2-AG also exhibits distinct, autocrine signaling during development[47],

[181]. DAGLα colocalization with CB_1 within the growth cone promotes neuronal polarization and subsequent radial migration by preventing premature synaptogenesis through autocrine, CB_1 mediated inhibition of presynaptic vesicle exocytosis [25], [47], [60], [65], [182]. Once synaptogenesis commences, DAGLα expression in the growth cone decreases while MAGL expression in the nascent presynapse increases[47]. Ultimately, DAGLα localization is redistributed to postsynaptic sites around the somatodendritic axis of mature neurons[47]. This change in enzyme localization is necessary for the switch from autocrine to paracrine 2-AG signaling and facilitates the ability of CB_1 to regulate synaptic strength. Other important effects mediated by the activation of CB_1 by 2-AG include neurite retraction[65], [183] and repulsive axonal head movement[184]. Global CB_1 knockouts in mice, as well as specific interneuron and pyramidal cell CB_1 knockouts, are viable but show axonal guidance errors and impaired postsynaptic target selection[25], [60], [65]. Interestingly, pharmacological treatment with both CB_1 agonists and antagonists creates axon fasciculation errors during development in mice[22], [60], [185], [186]. It is clear from this research that the ECS is necessary for correct axonal targeting and the subsequent establishment of synapses in the developing brain.

Due to the prominent role of the ECS in synapse establishment and maintenance, endogenous or exogenous disruptions to this system during fetal neurodevelopment can impact synaptogenesis and early circuit building. We have developed a model of altered ECS function in cortical spheroids to monitor the effects on synapse formation and the development of synaptic activity in neural circuits. Within our cortical spheroids, we found abundant expression of CB_1 and ECS-associated enzymes FAAH, MAGL, and DAGLα. Through acute SR141716A (SR) mediated CB_1 antagonism, we demonstrate that the ECS system regulates the initial establishment of neuronal connections and the resulting synaptic activity. Specifically, SR treatment resulted in a

selective and dose-dependent increase in excitatory synapses, and a biphasic response in inhibitory synapses. These complex changes in excitatory and inhibitory synapse formation significantly increased the variability of synaptic activity in developing neural networks. This work establishes cortical spheroids as a powerful model for addressing how endogenous and exogeneous ECS disruption can drive synaptogenesis in neurodevelopmental disorders.

4.3 Materials & methods

IPSC culture information and techniques Control WTC-11-ActBmeGFP IPSCs were obtained under MTA from the Coriell Institute. The parental WTC-11 IPSC line was developed by Bruce Conklin of the Gladstone Institute, and was further gene-edited by the Allen Institute for Cell Science using CRISPR/Cas9 to tag endogenous β-actin with monomeric Green Fluorescent Protein (GFP)[99]. Control 7545 19B IPSCs were generated by Dr. Mike McConnell (Lieber Institute for Brain Development) from fibroblasts obtained under MTA from the Coriell Institute. ASD patient IPSCs (UMB# : 5278, 5403, and 797) were obtained under MTA from the NICHD Brain and Tissue Bank for Developmental Disorders. IPSCs were cultured in Matrigel-coated plates and maintained at 37°C and 5% O_2 in mTeSR or Essential 8 media. ROCK inhibitor Y-27632 (10 μM) was added to the media during the first 24 hours of plating after thawing or splitting cells.

Cortical spheroid generation and feeding schedule This protocol is adapted from the Pasca protocol[155]. On day 0, IPSCs were enzymatically lifted off the plate and pelleted for 5 minutes at 300 rpm. The pellet was disrupted and transferred into 3 wells of a low attachment plate with

ESDMEM media (DMEM/F12, 1.5% HEPES, 1% GlutaMAX, 1% NEAA, 10% Knock-Out Serum, and 1% Pen/Strep). ROCK inhibitor Y-27632 (10 µM) and dual SMAD inhibitors SB431542 (10 µM) and Dorsomorphin (10 µM) were added to the media. On day 2, old ESDMEM was replaced with fresh ESDMEM and both SMAD inhibitors were replaced. This protocol continued for the next 3 days. On day 6, dual SMAD inhibitors were substituted with EGF (20 ng/mL) and FGF2 (20 ng/mL) in Neuronal Medium (Neurobasal-A, 2% Gibco B-27 serum substitute without vitamin A, 1% GlutaMax, 1% Pen/strep). Media was replaced every day with fresh FGF2 and EGF for the first 10 days and then every other day for the following 9 days. On day 25, BDNF (20 ng/mL) and NT3 (20 ng/mL) supplementation began and media was changed every other day until day 42. On day 43 all supplements were removed and the Neuronal Media was changed out every 4 days. All cultures underwent regular mycoplasma testing.

Quantitative real-time polymerase chain reaction Three independent sets of cortical spheroids from control- and autism derived-iPSCs were used to isolate RNA and synthesize cDNA. For total RNA extraction, spheroids were homogenized in guanidinium-acid-phenol reagent. RNA quality was confirmed by gel electrophoresis. Total RNA (200 ng) was used to synthesize cDNA using an iScript synthesis kit (Bio-Rad). Completed reactions were diluted to a total volume of 200 µL using nuclease-free water and 5 µL was used for each amplification. Each sample set was amplified in triplicate (for an overall total of n = 9 reactions per gene and spheroid type). PCR was done using a kit (SsoAdvanced Universal SYBR Green Supermix, Bio-Rad). Reactions began with a denaturation step for 30 sec at 95 C followed by 38 cycles of 95 C x 10 sec, 63 C x 30 sec. Melt curve analyses were done after reactions were completed to confirm selective

amplification. Data were obtained as C_T values using CFX Manager software (Bio-Rad), and the DDC_T method was used to compare expression in control- vs autism-derived spheroids. Primer sequences used can be found in Table 1.

Dosing with SR141716A (SR) for confocal imaging For confocal imaging, 90-day old cortical spheroids were treated with vehicle, 30 nM, or 300 nM of SR141716A. This CB_1-selective antagonist/inverse agonist was chosen due to experiments with it in prior work[187], [188]. Concentrations employed were determined following dose-response experiments measuring neurite length of IPSC-derived neuronal monolayers (Figure 4.7). The SR141716A was dissolved in DMSO which also served as the vehicle control. Our vehicle control group was bathed in a final concentration of 0.00001% DMSO, equal to the amount of DMSO added to our 300 nM SR141716A dose groups. Each treatment group consisted of 3-5 midsized (diameter > 1 mm) cortical spheroids. Treatment occurred for 24 hours and spheroids were kept in low-attachment plates at 37 C°. This experiment was repeated 3 times with independently grown sets of cortical spheroids. A treatment period of 24 hours was chosen to selectively perturb synaptogenesis (rather than migration or differentiation) and prior research from our lab has shown that this is an effective period of treatment for altering synaptogenesis[177].

Fixation and cryosection After 24 hours of treatment, spheroids were fixed in 4% paraformaldehyde and cryoprotected in 30% sucrose solution. Spheroids were then placed in OCT embedding medium overnight at 4 C° in a 24 well plate. Spheroids were transferred to a disposable base mold and frozen with dry ice and 2-methyl butane slush. Once frozen, spheroids

were sliced 10 µm thick on a cryostat with the objective temperature set at -7 C°. Mount sections were thawed and transferred on to slides treated with 2% 3-Aminopropyl Triethoxysilane.

Immunofluorescent staining A Sequenza rack system was used to stain sectioned cortical spheroids. Slides were blocked in 5% normal goat serum for 30 minutes. Primary antibodies were diluted in 2% normal goat serum and applied to the slides overnight at 4 C°. Secondary antibodies were diluted in 2% normal goat serum and applied to the slides for 1 hour at room temperature in the dark. Slides were removed from the Sequenza rack system and 1.5 mm coverslips were affixed to the slide using Fluorogel with or without DAPI. Slides were placed on a plate warmer for 15 minutes to ensure coverslip attachment. Cortical spheroids were kept in the dark during the immunofluorescent staining protocol. All antibodies used can be found in Table 2. Our CB_1 antibody was raised to target a 16-amino acid region within the intracellular tail portion of the receptor. The predicted epitope is FRSMFP, corresponding to amino acids 409 – 414 of human CB_1. This well-conserved sequence is identical across human, rat, mouse and zebra finch orthologs. Anti-CB_1 specificity was demonstrated previously by western blot labeling of appropriately sized proteins, expected histological CNS staining patterns and absence of both types of labeling following preincubation with 20 µM of the immunizing peptide[33].

Confocal imaging settings and equipment Imaging took place using ZEN Black Software on a Zeiss Laser Scanning Microscope 700 with a 40x objective (Plan-Apochromat/1.4 Oil DIC M27). Only cortical spheroids larger than 1 mm were imaged and analyzed. Nine total images per treatment group were taken. Each image consisted of a 4x4 tile scan (592.16 x 592.16 µm, 3789 x 3789 pixels) as well as a z-stack. The z-stack was compiled of 5 slices with 1 µm

between each slice, making a 4 µm thick stack. Confocal images in figures 4.1 and 4.2 were pseudocolored from their original, 8-bit, greyscale format. Brightness and contrast have been enhanced equally across controls and experimental groups. Figures were assembled in Adobe Photoshop version 21.2.

STORM staining and imaging The preparation of slides for the Nikon STORM microscope follows the same protocol as described above for the confocal with the addition of a 10-minute, formaldehyde (4%) and glutaraldehyde (0.1%) post-fix after application of the secondary antibody. Slides were mounted with Vectashield and put onto a plate warmer for 20 minutes then sealed with nail polish to ensure coverslips were anchored. Stained slides were used within two weeks of staining to ensure a robust signal. STORM images were acquired using Nikon NIS-Elements AR software and an Apo TIRF 100× objective (1.49 NA) on a Nikon Ti-E inverted microscope equipped with N-STORM. Period count was set to 20,000 and laser intensity was set to 100% for all channels.

Dissociation of cortical spheroids for micro-electrode array (MEA) recording Cytoview 24-well MEA plates with 16 electrodes per well (Axion Biosystems) were prepared with polyethylenimine which was incubated at 37 C° for 1 hour. Wells were then washed 4 times with sterile water and allowed to dry out overnight in a sterile hood. Wells were treated with laminin (5 µM) overnight at room temperature after which laminin was replaced with HBSS prior to plating. Cortical spheroids were dissociated onto 24-well MEA plates after 90 days of growth. Between 4-6 cortical spheroids were placed into a 1.5 mL tube and washed with ice cold HBSS. Neuronal Isolation Enzyme with papain (Pierce Primary Neuron Isolation Kit, ThermoFisher)

was added to the spheroids and incubated at 37 C° for 30 minutes. Spheroids were dissociated into a single-cell suspension via vigorous pipetting with a 1000 µL micropipette. A cell count was performed with trypan blue. Cells were plated at a density of 250,000 cells per well. The MEA plate was placed in a 37 C° incubator for an hour before MEA media (Neurobasal-A, 2% B27 Plus, 1% GlutaMAX, 1% Pen/Strep) was added to each well. Half of the media was replaced every 3 to 4 days with fresh media.

MEA recording and SR141716A dosing MEA recording was performed on day 40 after plating and 48 hours after the last feeding. Extracellular recordings were performed in AxIS Naviagtor software using an Axion Maestro Edge set at 37 C° and 5% CO_2. The recording stream was configured for spontaneous neural bursting activity with network burst detection. Data underwent DC offset filtering and Butterworth band-pass filtering with 0.1 Hz and 5 kHz cutoffs prior to spike detection. A "spike" was defined as a short, extracellular, electrical event with a peak voltage 6 times or greater than the standard deviation of the estimated "noise" signal. A "burst" was defined as 5 or more spikes with no more than 100 ms separating each spike. The MEA plate was placed into the Maestro Edge and activity was allowed to normalize for 5 minutes prior to a 10-minute basal recording. The plate was then removed from the instrument and dosed with vehicle (0.00001% DMSO), 3 nM, 30 nM, or 300 nM of SR141716A in a sterile hood (n=6 wells per treatment group per independent replicate). The plate was then returned to the instrument and one 10-minute recording was taken every hour for 24 hours. Recording took place 48 hours after the last feeding. Experiment repeated in triplicate with independently grown and plated spheroids.

Data analysis software and settings

Confocal imaging analysis**:** All. czi images were exported from the ZEN Black software as a greyscale .tiff files. Using ImageJ, individual channel z-stacks were consolidated into a max intensity z projection. Each channel had a threshold applied to it. Synapse masks were defined by the coloc_2 plugin using the thresholded presynaptic and postsynaptic images. For figure 4.2, synapse characteristics of area, size, and number were determined using the particle analysis function. For figure 4.3, we used ratiometric image analysis by using the image calculator function in Image J to divide the active RhoA area by the total RhoA area. This area was then overlayed with VGLUT1 area to determine the ratio of activated RhoA at excitatory presynapses. Synapse measurements were taken along the outer edge of the cortical spheroid using 10 x 100 µm diameter circles. Only the outer 100 µm was measured because this is the area of active synaptogenesis in our model at 90 DIV. Within each circle the pre-synaptic, post-synaptic, co-localized pre- and post-synaptic, and CB_1 staining area was measured. All area values were normalized to the internal GFP-tagged actin. Three images per dose group were analyzed and this process was independently repeated in triplicate. A total of 6-7 cortical spheroids were analyzed per treatment group.

MEA analysis: MEA video recording streams (.raw files) were batch processed in AxIS Navigator to detect spontaneous neural spiking activity (.spk). These files were further processed into .csv files by Axion Neural Metrics software. Active electrodes were defined by having 5 or more spikes per minute. The weighted mean firing rate is a measure of spikes per minute within a well and is weighted by the number of active electrodes within that well.

STORM analysis**:** In the NIS-Elements AR program, raw .nd2 files had a constant threshold applied corresponding to the lowest “blink” value in each channel. These files were batch

processed into .bin files. Molecular count was performed at this stage. After processing, synapses were located and a z-stack was captured. Subsequent analysis of processed. nd2 files was performed with ImageJ whereby the 3D projection was recreated. A line was drawn across the synaptic cleft and the intensity of CB_1 as well as pre- and post-synaptic markers was analyzed using the plot profile function of ImageJ.

Statistical analysis and reporting Statistical analysis was performed in GraphPad Prism 8. Differences in endocannabinoid gene expression levels in spheroids derived from control vs autism samples were assessed using unpaired two-tailed t-tests. Mann Whitney tests were utilized for STORM distance data. For confocal image analysis, a one-way ANOVA with multiple comparisons was performed across the vehicle control group and both SR dose groups. Stains were normalized to the internal standard of GFP-tagged β-actin. A Kolmogroff-Smirnoff test was performed for the cumulative distribution in Fig 4.2. One way ANOVA with multiple comparisons was used for RhoA data. One-way ANOVA with multiple comparisons was utilized for MEA data across time. Dunnett's T3 multiple comparisons test was used for comparison of MEA interquartile ranges. A p-value of less than 0.05 was considered statistically significant. All values are reported as mean ± SEM.

4.4 Results

4.4.1 Cortical spheroids derived from human IPSCs express CB_1, DAGL*α*, MAGL, and FAAH.

The ECS plays a dual role in the developing brain by modulating both growth cone directionality[22], [60], [184] (Fig 4.1a) and presynaptic feedback inhibition at mature synapses[19], [189] (Fig 4.1b). Disruptions to this system during critical periods of development may have lasting impacts on neural circuitry building. We first examined ECS gene expression levels in cortical spheroids derived from control iPSCs and iPSCs from 3 children with the neurodevelopmental disorder ASD (Fig 4.1c). Using quantitative RT-PCR, we found that DAGLα and MAGL, the principal synthetic and metabolic enzymes for 2-AG respectively, were expressed at significantly higher levels in cortical spheroids derived from autistic patients relative to controls (DAGLα: $p = 0.007$, MAGL: $p = 0.012$) (Fig 4.1c). Across 3 independent cortical spheroid experiments, DAGLα expression increased from 0.102 ± 0.02 to 0.258 ± 0.05 -fold mRNA expression relative to TATA-BP. Even more dramatically, MAGL expression increased from 0.056 ± 0.01 to 0.351 ± 0.11 -fold mRNA expression relative to TATA-BP. Additionally, the enzyme responsible for anandamide metabolism, FAAH, had significantly higher expression ($p = 0.014$) in ASD spheroids relative to controls and increased from 0.050 ± 0.01 to 0.159 ± 0.04-fold mRNA expression relative to TATA-BP. Significant expression differences were not observed for CB_1, DAGLβ or NAPE-PLD. We attempted to amplify CB_2 receptor cDNA but no amplification was observed, leading us to conclude that this receptor is not expressed at detectable levels in our model. The lack of CB_2 serves as an internal control for our model system because the use of dual-SMAD inhibition blocks mesodermal and endodermal differentiation and therefore the cortical spheroids do not generate microglia, the cell type which primarily expresses CB_2 in the brain[18], [190].

Using immunofluorescent staining and imaging, we observed abundant cytosolic, synaptic, and neurite expression of CB_1 in our 90-day old, control patient-derived cortical

spheroids (Fig 4.1d). We also observed the 2-AG enzymatic regulators, MAGL and DAGLα, in our 90-day old cortical spheroids, as well as FAAH. Interestingly, in concordance with our qRT-PCR results, we found that the area of DAGLα and MAGL was increased in cortical spheroids derived from 2 out of 3 of our ASD patient lines (Figure 4.5). DAGLα area significantly increased ($p > 0.001$) from 0.109 ± 0.01% in our control patient cell line to 0.795 ± 0.06% and 0.469 ± 0.05% in cortical spheroids derived from ASD patient 1 and 2, respectively. MAGL area was also significantly increased ($p > 0.001$), from 0.636 ± 0.06% in the control patient cell line to 1.34 ± 0.14% and 1.45 ± 0.05% in cortical spheroids from ASD patient 1 and 2, respectively. In the third patient, DAGLα was significantly increased (mean: 0.216 ± 0.02%, control patient vs ASD patient 3: $p > 0.001$) but MAGL was not significantly different from cortical spheroids derived from the control patient IPSCs (mean: 0.462 ± 0.04%) (Figure 4.5). These findings confirm the presence of the ECS in our cortical spheroid model and suggest increased expression of 2-AG enzymes MAGL and DAGLα may occur in concordance with previous observations of ECS alterations associated with ASD[74], [191].

We wanted to further analyze whether ECS components exhibit synaptic localization characteristic of fetal autocrine signaling. However, confocal microscopy is limited by resolution and prevents us from determining whether ECS components such as CB_1 correctly localizes to the presynaptic compartment in our system. To overcome this limitation, we used stochastic optical reconstruction microscopy (STORM) which has a resolution of up to ~20 nm in x,y, allowing us to resolve individual synapses which have a synaptic cleft distance of ~20 nm[88], [192]. Examples of excitatory and inhibitory synapses can be found in Fig 4.1e and Fig 4.1f, respectively. Using STORM, we analyzed 126 excitatory synapses and confirmed presynaptic localization of CB_1 in our cortical spheroid model, consistent with previous findings in other

models[22], [193], [194]. The median distance between CB_1 and presynaptic marker VGLUT-1 was 0.060 μm, which is significantly smaller ($p < 0.0001$) than the median distance between CB_1 and postsynaptic marker PSD-95 (0.141 μm) (Fig 4.1g). This indicates that CB_1 is closer to the presynaptic marker than the postsynaptic marker and preferentially localizes to the presynapse. The median distance between VGLUT-1 and PSD-95 (0.131 μm) was similar to distance between CB_1 and PSD-95 and is consistent with our previous STORM measurements of synaptic cleft size[88], [177]. Additionally, we investigated CB_1 localization at inhibitory synapses (n = 47) and observed a significantly shorter (p = 0.014) median distance between CB_1/presynaptic marker VGAT (0.046 μm) compared to CB_1/postsynaptic marker gephyrin (0.062 μm) (Fig 4.1h). Further, we observed presynaptic localization of DAGLα (Fig 4.1i) and postsynaptic localization of MAGL (Fig 4.1j) at excitatory synapses. The median distance between DAGLα and VGLUT1 (0.052 μm) was significantly shorter (p = 0.006, n = 77 synapses) than the distance between DAGLα and PSD95 (0.086 μm). MAGL was postsynaptic, with a significantly shorter (p > 0.001, n = 105 synapses) median distance between MAGL and PSD95 (0.045 μm) compared to the distance between MAGL and VGLUT1 (0.072 μm). These localizations are consistent with a developmental autocrine CB_1 signaling paradigm[47], [182].

Since the number of CB_1 molecules at inhibitory versus excitatory synapses could impact the effect of pharmacological treatment, we used STORM microscopy to analyze the distribution of CB_1 receptor count at excitatory and inhibitory synapses. We found that CB_1 receptors are more abundant at excitatory synapses (530 ± 25 CB_1 molecules/synapse) than at inhibitory synapses (262 ± 14 CB_1 molecules/synapse) in the outer, 100 μm of the cortical spheroid (p > 0.001, unpaired t-test) (Figure 4.6). Association of the presynaptic terminal with a postsynaptic process is indicative of synapse formation, and increased postsynaptic area is indicative of

synaptic strengthening[195]. Our model recapitulates synaptic scaling at both excitatory and inhibitory synapses as demonstrated by the positive relationship between the molecular count of pre- and postsynaptic markers at a given synapse (Figure 4.6). We therefore sought to determine whether the number of CB_1 molecules scaled with increased postsynaptic association. We observed a positive relationship between CB_1 receptor count and postsynaptic marker count at both excitatory (PSD95) and inhibitory (gephyrin) synapses (Fig 4.6), suggesting that CB_1 receptors exhibit synaptic scaling.

Thus, we have determined that human cortical spheroids express ECS machinery, and that CB_1, the predominant ECS receptor type in the brain, localizes to presynaptic compartments at both excitatory and inhibitory synapses. We also observed DAGLα localization to the presynapse and MAGL localization to the postsynapse in excitatory synapses using STORM microscopy. Our data supports cortical spheroids as a model of the fetal ECS system.

4.4.2 Treatment with CB_1 antagonist SR141716A increases the number and total area of excitatory synapses

Having established the expression and presynaptic localization of CB_1 within our system, we sought to determine how ECS disruption impacts synaptogenesis. In order to selectively perturb CB_1 during synaptogenesis, we allowed cortical spheroids to develop for 90 days, so as to not disrupt neural differentiation and migration preceding synaptogenesis. At 90 days old, our cortical spheroids model the mid-gestational fetal brain[155], a critical window of development during which the brain undergoes rapid synaptic proliferation[64]. Disruptions to the spatial and temporal regulation of synaptogenesis during this critical window is thought to drive

developmental disorders such as ASD[69], [196]. At 90 days of development, we have previously demonstrated that our cortical spheroids exhibit both excitatory and inhibitory synapses[88], [177]. Furthermore, these synaptic connections exhibit a high level of plasticity, and are readily altered by acute perturbations to either the intracellular cytoskeleton or extracellular matrix[88], [177]. Thus, we have established a window to selectively observe how CB_1 signaling contributes to the initial formation of synaptic connections and subsequent development of synaptic activity. In order to selectively disrupt the process of synaptogenesis, we acutely treated 90-day old cortical spheroids with selective CB_1 antagonist SR141716A (SR) for 24 hours and observed the resulting effects on excitatory and inhibitory synapses.

Using confocal image analysis (Fig 4.2a), we determined the effects of SR treatment on excitatory and inhibitory synaptogenesis by independently measuring pre- and post-synaptic marker area. Cortical spheroids were stained with antibodies against excitatory synaptic markers [vesicular glutamate transporter 1 (VGLUT-1) and postsynaptic density protein 95 (PSD-95)] or inhibitory synaptic markers [vesicular GABA transporter (VGAT) and gephyrin (GEPHRYIN)]. We defined the area of overlap between presynaptic marker (VGLUT-1 or VGAT) and their respective postsynaptic marker (PSD-95 and GEPHRYIN) as a "synapse". We determined the effect of SR on the number of synapses and size of synapses in the outer 100 µm of the spheroid using this method. Example confocal images used for analysis are given in Fig 4.2b and Fig 4.2c. Under basal conditions, our cortical spheroids have more excitatory synapses than inhibitory synapses[177]. However, we found that SR treatment impacts both excitatory and inhibitory synapses. SR treatment increased expression of excitatory synapses markers in a dose-dependent fashion, whereas increased inhibitory synapses were only observed at the lower dose of 30nM

SR. To compare the area of synaptic markers across treatment groups, we normalized the area of the synaptic marker to the endogenous β-actin-GFP expression in our cortical spheroids.

The area of excitatory presynaptic marker VGLUT-1 significantly increased from 32.4 ± 4.6% in the vehicle control to 76.7 ± 6.7% and 74.0 ± 7.8% in the 30 nM and 300 nM SR dose groups, respectively (0 vs 30: $p < 0.001$, 0 vs 300: $p = 0.001$) (Fig 4.2d). The area of the excitatory postsynaptic scaffold PSD-95 also significantly increased from 14.9 ± 1.4% in the vehicle control to 27.8 ± 2.4% and 49.5 ± 3.0% in the 30 nM and 300 nM SR dose groups, respectively (0 vs 30: $p < 0.001$, 0 vs 300: $p < 0.001$) (Fig 4.2d). Additionally, there was a significant, dose dependent relationship between the low and high doses of SR on PSD-95 expression (30 vs 300: $p < 0.001$) (Fig 4.2d). Using the colocalization of excitatory presynaptic marker VGLUT-1 and postsynaptic marker PSD-95, we determined that SR treatment significantly increased both the total area (30 vs 300: $p < 0.001$) (Fig 4.2f) and number (30 vs 300: $p = 0.003$) (Fig 4.2g) of excitatory synapses in a dose dependent manner. Excitatory synapse area significantly increased from 1.6 ± 0.3% in the vehicle control to 5.7 ± 0.6% and 10.7 ± 1.2% in the 30 nM and 300 nM SR dose groups, respectively (0 vs 30: $p < 0.001$, 0 vs 300: $p < 0.001$) (Fig 4.2f). Additionally, the number of excitatory synapses per area of actin significantly increased from 0.03 ± 0.005 synapses/μm2 in the vehicle control group to 0.05 ± 0.005 synapses/μm2 and 0.09 ± 0.007 synapses/μm2 in the 30 nM and 300 nM SR dose groups, respectively (0 vs 30: $p = 0.009$, 0 vs 300: $p < 0.001$) (Fig 4.2g). The size of individual excitatory synapses trended towards an increase but was found not significant by Kolmogorov-Smirnov test, despite a rightward shift in the cumulative distribution plot (Fig 4.2i). Having observed that CB_1 antagonism increases excitatory synaptogenesis, we also sought to determine whether synaptic CB_1 distribution was altered in response to SR treatment. We therefore examined CB_1

localization to excitatory and inhibitory synapses. CB_1 area as a percent of total excitatory synapse area significantly increased from 25.6 ± 1.5% of total excitatory synapses to 37.5 ± 1.6% percent of total excitatory synapses after application of 30 nM SR (0 vs 30: $p < 0.001$) (Fig 4.2h). Surprisingly, the percent of CB_1-positive excitatory synapses returned to a value similar to the vehicle control after application of 300 nM SR (28.4 ± 2.6% of total excitatory synapses) (0 vs 300: $p = 0.719$, 30 vs 300: $p = 0.014$) (Fig 4.2h). Thus, the 30 nM SR treatment captures a window of dynamic ECS alterations at excitatory synapses.

Interestingly, the effect of SR on inhibitory synapses was greatest at the lower, 30 nM dose of SR. The area of presynaptic inhibitory marker VGAT significantly increased from 23.2 ± 2.3% in the vehicle control to 38.5 ± 3.8% in the 30 nM SR dose group (0 vs 30: $p = 0.003$) (Fig 4.2e). A decrease in VGAT was observed in the high dose group (19.4 ± 1.5%) when compared to the low dose group (30 vs 300: $p < 0.001$) (Fig 4.2e). When compared to the controls, the area of the postsynaptic inhibitory scaffold, gephyrin, was not significantly altered, however, there was a decrease between low and high doses (30 vs 300: $p = 0.011$) (Fig 4.2e). There was a significant increase in the area (0 vs 30: $p = 0.012$) (Fig 4.2f) and number (0 vs 30: $p = 0.001$) (Fig 4.2g) of inhibitory synapses in the low dose SR group compared to the control group. The area of inhibitory synapses increased from 1.02 ± 0.1% in the control group to 1.63 ± 0.2% and 2.41 ± 0.5% in the 30 nM and 300 nM dose groups, respectively (0 vs 30: $p = 0.012$, 0 vs 300: $p = 0.030$) (Fig 4.2f). The number of inhibitory synapses per area of actin changed from 0.015 ± 0.002 synapses/μm^2 in the control group to 0.035 ± 0.005 synapses/μm^2 and 0.021 ± 0.003 synapses/μm^2 in the low and high dose groups, respectively (0 vs 30: $p = 0.001$, 30 vs 300: $p = 0.047$) (Fig 4.2g). Unlike the results we observed earlier where there was a redistribution of synaptic CB_1 at excitatory synapses, we did not observe significant differences in CB_1

localization to inhibitory synapses and the percent of CB_1-positive inhibitory synapses remained steady at approximately 40% (Fig 4.2h).

In order to investigate mechanisms of increased synaptogenesis by CB_1 antagonism, we used image analysis to measure the ratio of active RhoA to total RhoA (Fig 4.3a). CB_1 activation is associated with rapid growth cone retraction through the GTPase RhoA system[184]; additionally, antagonizing RhoA through ROCK inhibition increases excitatory synapse formation[88]. We therefore sought to determine if CB_1 antagonism changed RhoA activation through radiometric image analysis at VGLUT1-positive synapses. Activated RhoA was distinguished from total RhoA by an antibody targeting the GTP-bound form of RhoA compared to an antibody that distinguished total RhoA levels. Treatment of cortical spheroids with 30 nM and 300 nM SR141716A decreased the relative intensity of RhoA activation at excitatory synapses (0 nM vs 30 nM: $p > 0.001$, 0 nM vs 300 nM: $p > 0.001$) (Fig 4.3b), consistent with the observed increase in excitatory synapses at these doses.

Thus, using the CB_1 selective antagonist SR141716A, we successfully manipulated the cortical spheroid system, resulting in increased excitatory synaptogenesis. This increased excitatory synaptogenesis corresponded with increased inhibitory synaptogenesis and CB_1 expression at excitatory synapses selectively at the lower, 30 nM SR treatment. These results demonstrate the functionality of the ECS in our cortical spheroids and suggest that 30 nM SR treatment could restore excitatory and inhibitory synaptic balance in disrupted systems.

4.4.3 SR141716A increased variability of synaptic activity as measured by micro electrode array (MEA)

The effects of cannabinoid modulation on neural activity are complex due to CB_1 localization at both glutamatergic and GABAergic synapses[178].To address whether the complex changes in synaptogenesis altered the development of spontaneous activity in neural circuits, we used MEA to measure the extracellular field potential which corresponds to action potential. After 90 days of development, we dissociated cortical spheroids directly onto micro electrodes (Fig 4.4a and 4.4b). In order to observe consistent activity in our control spheroids, we allow neurons to re-establish connections for an additional month after dissociation, resulting in reproducible activity measurements. We then measure spontaneous neural activity with or without SR treatment. Spontaneous extracellular activity caused by multiple, local action potentials is measured by the electrodes in units called "spikes" (Fig 4.4c). Thus, a spike represents an increase in activity across a small area of multiple cells. Multiple spikes of 5 or more in quick succession (< 100 ms between spikes) are defined as "bursts" and represent rapid communication between populations of cells. Synchronous bursting between multiple electrodes is characteristic of mature communication patterns.

We determined that our vehicle decreased the weighted mean firing rate (WMFR) of dissociated cortical spheroids over a period of 24 hours. Immediately after dosing, the mean WMFR was 7.64 ± 7.0% above the pre-treatment average, however, after 3 hours of treatment the WMFR started to decrease (-9.11 ± 6.95% of pre-treatment) and continued to decrease. The WMFR of the vehicle control group significantly decreased from the initial recording after 15 hours of vehicle treatment (0 hr vs 15 hr: $p = 0.0423$, 0 hr vs 18 hr: $p = 0.0131$, 0 hr vs 21 hr $p = 0.0094$, 0 hr vs 24 hr $p = 0.0099$) (Fig 4.4d). We believe that this decrease is attributable to nutrient depletion over time. Interestingly, SR treatment prevented this decrease in WMFR. More strikingly, we observed highly variable activity in response to SR treatment which was not

observed in the DMSO vehicle treatment group. WMFR means of the 30 nM and 300 nM group over time were approximately 50% greater than their respective pre-treatment values but there was no significant effect found over time.

The bursting frequency data showed the same trends as the WMFR data. Bursting frequency of the vehicle control group was initially 48.31 ± 10.7% greater than pre-treatment bursting frequency at hour 0, but later decreased to 50% of pre-treatment values after 12 hours. Specifically, the vehicle treated wells had significantly decreased bursting frequency continuing after 6 hours of treatment (0 hr vs 6 hr: $p = 0.0442$, 0 hr vs 9 hr: $p = 0.0062$, 0 hr vs 12 hr $p < 0.0001$, 0 hr vs 15 hr: $p < 0.0001$, 0 hr vs 18 hr: $p = 0.0010$, 0 hr vs 21 hr: $p < 0.000$, 0 hr vs 24 hr: $p = 0.0001$)(Fig 4.4e). While the low dose of SR showed a significant decrease in bursting frequency after 18 hours (0 hr vs 18 hr: $p = 0.0440$, 0 hr vs 21 hr: $p = 0.0308$), this decrease took a longer time to manifest when compared to the vehicle treated group (Fig 4.4e). Treatment with 30 nM of SR increased bursting frequency by over 200% for every timepoint, but this increase did not vary significantly across time. The high dose of 300 nM SR also increased overall bursting frequency by about 75% but there was no significant effect over time.

While we did not observe significant increases in WMFR and bursting frequency, we did observe a high degree of variability across our SR dose groups. We measured the effects of variability by utilizing the interquartile ranges (IQR) of each timepoint within dose groups and then compared dose groups. The average WMFR IQR of the control group over 24 hours was 39.3 ± 4.7 compared to 61± 4.6 in the 3 nM group, 124 ± 7.3 in the 30 nM group, and 87 ± 7.7 in the 300 nM group. SR treatment significantly increased the WMFR IQR when compared to vehicle treated controls (VEH vs 3 nM: $p = 0.026$, VEH vs 30 nM: $p < 0.001$, VEH vs 300 nM: $p = 0.001$) (Fig 4.4f). The variability of the 30 nM group was significantly higher than the 3 nM

group (3 nM vs 30 nM: $p < 0.0001$) but the variability of the 300 nM group was significantly lower than the 30 nM group (30 nM vs 300 nM: $p = 0.0166$) (Fig 4.4f). Our bursting frequency results parallel the results of the WMFR, where SR caused significantly more variability compared to the vehicle control (VEH vs 3 nM: $p = 0.0221$, VEH vs 30 nM: $p = 0.0005$, VEH vs 300 nM: $p = 0.0267$) (Fig 4.4g). Bursting frequency IQR within the control group over 24 hours was 32.5 ± 3.5. SR increased the mean IQR to 110 ± 20 in the 3 nM group, 647 ± 88 in the 30 nM group, and 137 ± 27 in the 300 nM group. Similar to WMFR measurements, we observed a biphasic dose response that displayed significantly more IQR variability in our 30 nM group than in our 3 nM group (3 nM vs 30 nM: $p = 0.001$) and less variability in our 300 nM group when compared to the 30 nM group (30 nM vs 300 nM: $p = 0.001$) (Fig 4.4g). Increased variability of synaptic activity, particularly at the 30 nM dose of SR, parallels the complex and differential changes to excitatory and inhibitory synapse formation we observed in our confocal analysis of synaptic area.

4.5 Discussion

Human IPSC-derived cortical spheroids represent a powerful model to explore the effects of genetic and pharmacological manipulation on developing neural circuits which resemble human fetal brain development. The ECS is expressed in human IPSC-derived neurons[183], mouse IPSC-derived brain organoids[197], and human IPSC-derived forebrain organoids[198]. Concordantly, we observed ECS expression in both IPSC-derived neurons (Fig 4.7) and cortical spheroids (Fig 4.1). Our IPSC-derived neurons displayed a biphasic response to CB_1 antagonism, where CB_1 antagonist treatment with 3 – 300 nM SR abolished WIN-induced neurite length

reduction (Figure 4.8). This indicates that CB_1 receptors located on neurons which have been differentiated for only 24 hours are functional through their response to exogenous cannabinoid modulation. Similarly, recent studies have demonstrated the mutability of the ECS in human-derived brain organoids, specifically showing that 1 μM THC treatment reduces neuronal activity as measured by mean firing rate[199]. Additionally, chronic treatment of dissociated brain organoids with cannabinoid modulators has been shown to produce profound impacts on the process of neuronal differentiation and maturation[198]. With expanding legalization and resultant increased recreational use of cannabis by pregnant women[200], it is necessary to evaluate the effects of cannabis on fetal neurodevelopment. Importantly, distinctions must be made between acute and chronic maternal use as well as acute and chronic effects of cannabis on the fetal brain. In this research, we sought to characterize the expression and synaptic localization of ECS components in developing neural circuits and to analyze the functional consequences of acute CB_1 antagonism on synaptic development.

We first wanted to determine if constituents of the ECS were present in our cortical spheroid model and consequently found that CB_1 mRNA is expressed in our cortical spheroids. Notably, CB_1 is the predominant cannabinoid receptor in the CNS and one of the most abundant G-protein coupled receptors in the brain[19], [51]. CB_2 mRNA was not detected in the cortical spheroids, however, this differential expression of cannabinoid receptors is in line with our model which does not express microglial cells[155], the main host of CB_2 in the brain[190]. We additionally observed differential regulation of DAGLα and MAGL mRNA expression in our cortical spheroids derived from autistic patient IPSCs. Specifically, there was a significant increase in both DAGLα and MAGL mRNA expression. Interestingly, these changes mirror those observed in the mouse model of Fragile X syndrome, where *FMR1* knockout increased

striatal DAGLα and MAGL expression[201]. The expression of DAGLα, MAGL, and FAAH dramatically increase in post-natal development, coinciding with a period of synaptic refinement and maturity[202], [203]. Thus, increased ECS enzyme levels earlier in development could represent accelerated maturation of neural circuit development, a phenotype which has been observed in neurons derived from autism patients[204]. Pharmaceuticals which alter CB_1 activation and 2-AG metabolism may be useful treatment options for specific ASD symptoms linked to stress and anxiety, however, the consequences of endocannabinoid manipulation during brain development are unclear and may have unintended consequences. For example, while the inhibition of DAGL in patients with Fragile X syndrome appears reasonable due to increased DAGL expression in mouse models[201], reduced 2-AG synthesis is associated with increases in stress[205], impaired neuroinflammation, and disrupted synaptogenesis[206]. Additionally, MAGL inhibition, while linked to anxiolytic and nociceptive effects[207], is also associated with impaired learning and memory[208]. Thus, an evaluation of the endocannabinoid system as a primary cause of synaptic dysfunction or as a compensatory mechanism in response to other synaptic changes at the patient level is warranted. We suggest that ECS disruptions may drive the pathophysiology of neurodevelopmental disorders, which would likely disturb the spatial and temporal regulation of homeostatic synapse selection in the developing brain[47]. Additionally, while we believe neurodevelopmental disorders such as ASD are caused by a constellation of deficits that culminate at the synaptic level[73], we also believe that the disruption of the ECS greatly impacts synaptogenesis and perpetuates synaptic deficits during development.

To determine how antagonism of ECS signaling impacts neural circuity development, we used SR141716A to acutely and selectively disrupt CB_1 activity during the period of cortical spheroid development coinciding with synaptogenesis. At 30 nM SR, CB_1 antagonism increased

both glutamatergic and GABAergic synaptogenesis. However, at 300 nM, SR continued to increase glutamatergic synaptogenesis but GABAergic synaptogenesis did not significantly differ from the controls. This biphasic effect observed at inhibitory synapses, but not excitatory synapses, is interesting and may be explained by a combination of variables. Firstly, we observe distinct basal expression of CB_1 at inhibitory and excitatory synapses, with CB_1 favoring inhibitory synapses (excitatory synapses with CB_1 = 25%, inhibitory synapses with CB_1 = 39%, Fig 4.2h). This ratio of excitatory to inhibitory CB_1 expression is comparable to fetal murine models[58], [65], but is notably different from adult CB_1 expression in the neocortex, where CB_1 primarily localizes to interneurons[58]. Secondly, we found that CB_1 receptor count scaled up with both excitatory and inhibitory postsynaptic marker count (Fig 4.6), indicating that the number of CB_1 receptors at the presynapse was a function of synapse size, regardless of type. Our observation of dynamic CB_1 expression at excitatory synapses during fetal synaptogenesis is consistent with previous literature which describes CB_1 regulation of glutamatergic neurons from the start of their migration[209], [210] Thirdly, our model system does not have a 1:1 ratio of excitatory to inhibitory synapses in the zone of active synaptogenesis, but rather expresses significantly less inhibitory synapses[177]. Thus, the biphasic effect only observed at inhibitory synapses may due to extraordinarily sensitive CB_1-positive inhibitory synapses. However, while CB_1 expressing inhibitory synapses may be more sensitive to the antagonist treatment, we did not observe a decrease in overall activity which would be predicted if CB_1 antagonism at inhibitory synapses was dominant over CB_1 antagonism at excitatory synapses. Due to cell-specific and synaptic location-specific effects, it is not fully reliable to characterize ECS regulatory strength based upon the count or density of CB_1 at excitatory and inhibitory synapses[211]. For example, sparsely expressed CB_1 on glutamatergic neurons of adult mice

plays an outsized role in controlling neural activity in the hippocampus[193]. The disparity between excitatory and inhibitory synapse response to SR141716A in our system may also be explained by the differential expression of glutamatergic and GABAergic neurons across time during development, whereby glutamatergic projection neuron generation and migration occurs prior to interneuron generation[64].

Complex changes in synaptogenesis mediated by SR141716A were reflected in the variability of neural activity. Under basal culture conditions, spiking and bursting variability decreases across time, mirroring the emergence of synchronized neural networks in the developing brain[70]. Synchronization is a large-scale network process observed in maturing neurons, whereby neuronal spiking activity becomes less variable and larger groups of neurons participate in simultaneous action potentials[212]. In contrast, SR141716A increased the variability of firing activity, indicative of disruption to developing neural networks. Notably, asynchronous activity is observed in neuropsychological disorders such as ASD[213] and schizophrenia[212]. The disruption of neural synchronicity (i.e. increased variability) was most prominent at 30 nM SR141716A, the dose at which we observed significant increases in both inhibitory and excitatory synapses (Fig 4.2f and Fig 4.2g). This increase, along with the greater expression of CB_1-positive excitatory synapses at 30 nM (Fig 4.2h) may explain the greater variability of activity. Interestingly, GABA receptor agonists in organoid models decrease synchronicity[70]. Additionally, CCK+ interneurons play a role in determining the firing threshold of pyramidal cells in the hippocampus[214] and may have a similar effect in the cortex. This fact may help to explain why our model experienced greater variability, as CB_1 antagonism at GABAergic synapses would likely increase GABAergic signaling through the disruption of endocannabinoid-mediated presynaptic inhibition. However, not all inhibitory synapses are the

same, and these results are further complicated by the differential impact of CB_1 at GABAergic perisomatic synapses versus axodendritic synapses[211]. Thus, we report that 30 nM SR141716A results in dynamic ECS alterations that impact synaptogenesis and the resulting neural activity. These complex changes are consistent with the variable and state-dependent response of rat cortical neurons to CB_1 antagonism[178]. Together, these results demonstrate that ECS signaling critically modulates developing neural circuits by coordinating the proper development and synchronization of excitatory and inhibitory synapses.

The ECS impacts synaptogenesis not only by modulating synaptic strength at mature synapses, but also by influencing axon targeting through autocrine 2-AG release around the growth cone. Prior to synaptogenesis, autocrine 2-AG signaling prevents premature synapse creation by thwarting presynaptic vesicular exocytosis and inducing repulsive, cytoskeletal motility[47], [184]. In the presence of SR141716A, this inhibitory process is released and we observed significant increases to excitatory synapse area and count (Fig 4.2), indicating an increase in excitatory synaptogenesis. Above average increases in synaptic density during early childhood are a common finding in ASD[69] and increased glutamatergic synaptic spine density has been observed in post-mortem brains of non-syndromic ASD patients[127]. Excitatory synapse proliferation is physically governed by the cytoskeletal system, which provides the structure of both the pre- and post-synapse. Interestingly, CB_1 mediated bidirectional modulation of RhoGTPase Rac1 activity has been observed within the growth cone,[215] and CB_1 agonism induces RhoA kinase (ROCK) dependent growth cone repulsion[65]. The modulation of RhoGTPase activity by CB_1 provides a direct link between the ECS, the cytoskeletal system, and the regulation of synaptogenesis in neurodevelopmental disorders. Our lab has previously demonstrated that the inhibition of ROCK in cortical spheroids increases excitatory

synaptogenesis[88], mirroring the effects we observed using SR141716A. Thus, CB_1 antagonism likely prevents CB_1 mediated, ROCK-dependent repulsion and allows for attractive cues surrounding the growth cone to dominate, ultimately leading to an increase in synaptogenesis.

We have shown that the ECS is present in a cortical spheroid model of fetal brain development and can be antagonized to create a phenotype which displays increased excitatory synaptogenesis and increased variability of neural activity. If the CB_1 receptor has been likened to a circuit breaker[216], SR141716A can be likened to a short in the circuit, which interrupts the ability of the breaker to trip and causes the faulty activity to propagate. In this sense, disrupted ECS signaling allows for disrupted synaptic signaling to continue. While synaptic pathologies in neurodevelopmental disorders tend to be propagated by deficits in multiple synaptic regulatory pathways, the ECS plays an outsized role due to the global expression of CB_1[73]. In this research, we have established that cortical spheroids are an appropriate model for exploring the ECS in the context of fetal brain development and childhood neuropsychiatric disorders. Additionally, we have demonstrated that CB_1 antagonism produces disruptions to excitatory and inhibitory synaptic balance in cortical spheroids. Our results further confirm the role of the ECS in synaptic pathology and we propose the utilization of CB_1 as a targetable receptor for therapeutics in neurodevelopmental disorders.

FIGURE 4.1 ECS constituents are expressed in 90-day old cortical spheroids. CB_1, MAGL, DAGLα, and FAAH have increased transcription in cortical spheroids derived from patients with the neurodevelopmental disorder ASD. (a) Primary developmental endocannabinoid 2-AG is produced by DAGLα within the growth cone and activates CB_1 in an autocrine manner during fetal neurodevelopment[47], [181]. **(b)** Paracrine signaling mediated by 2-AG at mature synapses regulates both excitatory and inhibitory synaptic plasticity. **(c)** Expression levels of DAGLα, FAAH, and MAGL are elevated in cortical spheroids derived from patients with ASD compared to controls (DAGLα: $p = 0.007$, FAAH: $p = 0.014$, MAGL: $p = 0.012$)**.** Expression levels were assessed by qRT-PCR and are expressed as fold differences from TATA-BP. No significant gene expression differences were observed between control- and ASD-derived samples for CB_1. Error bars = SEM, compared using student's t-test. **(d)** Confocal images of 10 µm thick cryosections of 90-day old control cortical spheroids expressing ECS constituents CB_1, DAGLα, MAGL, and FAAH. All cortical spheroids express endogenous GFP-linked β-actin (actin-GFP)**. (e)** Example of an excitatory synapse captured using STORM microscopy. Dashed line represents the synaptic cleft, with CB_1 (blue) and VGLUT1 (green) on the presynaptic side and PSD95 (red) on the postsynaptic side. **(f)** Example of inhibitory synapse captured via STORM microscopy with CB_1 (green) located at the presynapse with VGAT (cyan), opposite of gephyrin (red). **(g)** The median distance between CB_1 and presynaptic marker VGLUT-1 (0.060 µm) is significantly less ($p < 0.0001$, n = 126 synapses) than the distance between CB_1 and postsynaptic marker PSD-95 (0.141 µm), indicating presynaptic localization. **(h)** The median distance between VGAT and CB_1 (0.046 µm) was significantly shorter ($p = 0.014$, n = 47 synapses) than the distance between gephyrin and CB_1 (0.062 µm), indicating presynaptic localization of CB_1 at inhibitory synapses. **(i)** DAGLα was presynaptic, with a

median distance between DAGLα and VGLUT1 (0.052 µm) that was significantly shorter ($p = 0.006$, $n = 77$ synapses) than the distance between DAGLα and PSD95 (0.086 µm). **(j)** MAGL was postsynaptic, with a significantly shorter ($p > 0.001$, $n = 105$ synapses) median distance between MAGL and PSD95 (0.045 µm) compared to the distance between MAGL and VGLUT1 (0.072 µm). Distances were compared using the Mann Whitney test, significance was defined as $p < 0.05$. Illustrations in panel a and b were created by Alexis Papariello.

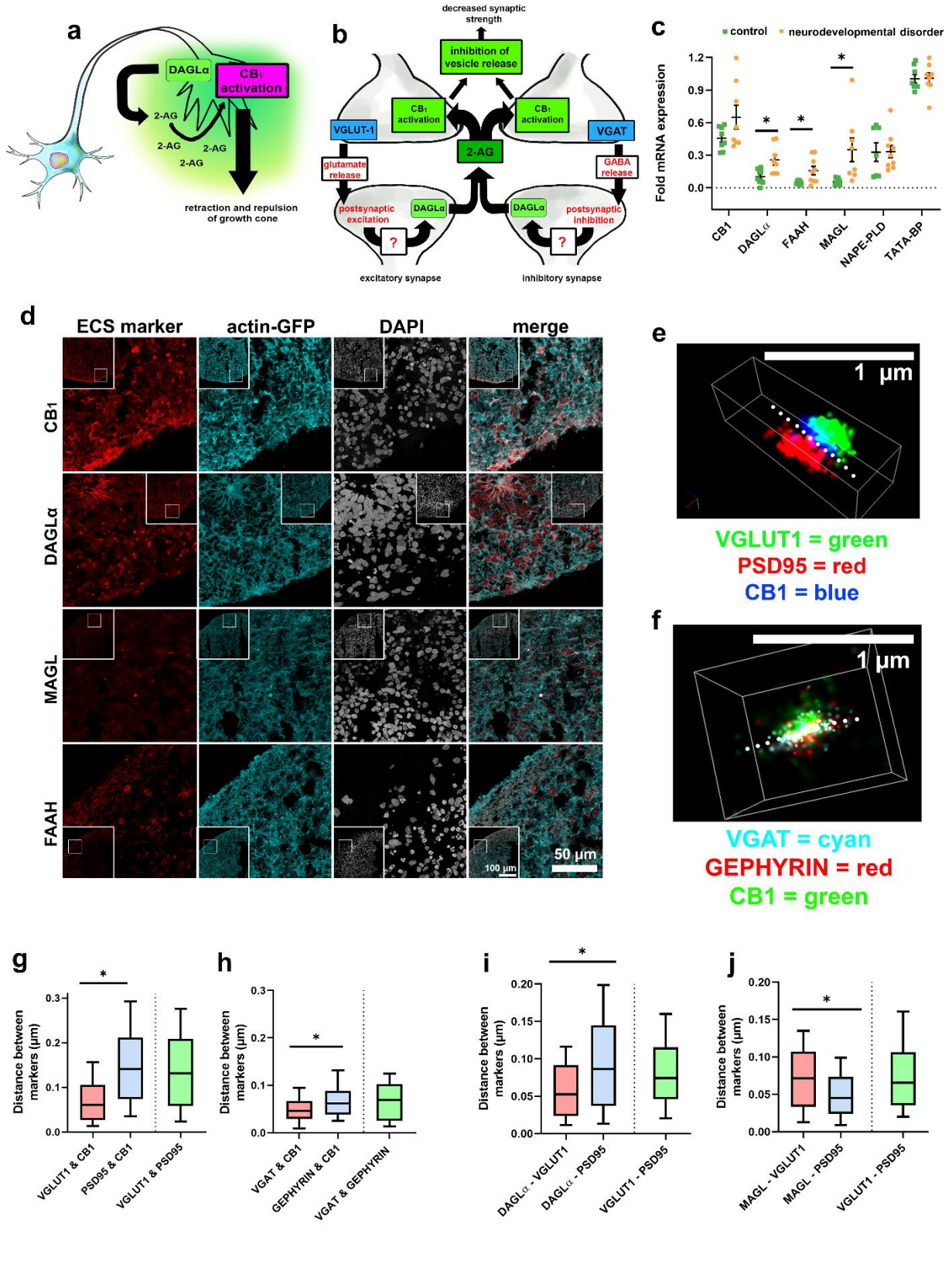
a
DAGLα
CB1 activation
2-AG
2-AG
2-AG
2-AG
retraction and repulsion of growth cone
b
decreased synaptic strength
inhibition of vesicle release
CB1 activation
CB1 activation
VGLUT-1
VGAT
2-AG
glutamate release
GABA release
postsynaptic excitation
DAGLα
DAGLα
postsynaptic inhibition
?
?
excitatory synapse
inhibitory synapse
c
control
neurodevelopmental disorder
Fold mRNA expression
1.2
0.9
0.6
0.3
0.0
*
*
*
CB1
DAGLα
FAAH
MAGL
NAPE-PLD
TATA-BP
d
ECS marker
actin-GFP
DAPI
merge
CB1
DAGLα
MAGL
FAAH
50 µm
100 µm
e
1 µm
VGLUT1 = green
PSD95 = red
CB1 = blue
f
1 µm
VGAT = cyan
GEPHYRIN = red
CB1 = green
g
Distance between markers (µm)
0.3
0.2
0.1
0.0
*
VGLUT1 & CB1
PSD95 & CB1
VGLUT1 & PSD95
h
Distance between markers (µm)
0.3
0.2
0.1
0.0
*
VGAT & CB1
GEPHYRIN & CB1
VGAT & GEPHYRIN
i
Distance between markers (µm)
0.20
0.15
0.10
0.05
0.00
*
DAGLα - VGLUT1
DAGLα - PSD95
VGLUT1 - PSD95
j
Distance between markers (µm)
0.20
0.15
0.10
0.05
0.00
*
MAGL - VGLUT1
MAGL - PSD95
VGLUT1 - PSD95

FIGURE 4.2 CB_1 antagonist SR141716A (SR) increases excitatory synaptogenesis in a cortical spheroid model of human brain development. (a) Work flow of synapse analysis. **(b)** Representative confocal images of cortical spheroids stained with excitatory presynaptic marker VGLUT1 and excitatory postsynaptic marker PSD95. **(c)** Representative confocal images of cortical spheroids stained with inhibitory presynaptic marker VGAT and inhibitory postsynaptic marker gephyrin. All cortical spheroids endogenously express GFP-linked β-actin (ACTIN-GFP). This was used as the internal control for synaptic area measurements. **(d)** Excitatory presynaptic (VGLUT1) and postsynaptic (PSD95) area after SR treatment. Both high and low doses of SR increased VGLUT1 area compared to vehicle control (0 vs 30 and 0 vs 300: p = 0.0001). SR increased PSD95 area in a dose dependent manner (30 vs 300: p = 0.0001). **(e)** Box plot of inhibitory presynaptic (VGAT) and postsynaptic (gephyrin) area after SR treatment. The low dose but not the high dose of SR increased VGAT area (0 vs 30: p = 0.0035). **(f)** SR increases excitatory synapse area in a dose dependent manner (30 vs 300: p = < 0.0001). SR also increased inhibitory synapse area when compared to control (0 vs 30: p = 0.0121, 0 vs 300: p = 0.0301) **(g)** SR increases the number of excitatory synapses in a dose dependent manner (30 vs 300: p = 0.0030) and increases the number of inhibitory synapses at the low dose when compared to vehicle control (0 vs 30: p = 0.0011). **(h)** SR increases the area of CB_1-positive excitatory synapses at the low dose when compared to vehicle control (0 vs 30: p = 0.0001) but has no effect on the ratio of CB_1-positive inhibitory synapses. **(i)** Cumulative distribution plot of individual excitatory synapse size after treatment with SR. Analyzed by Kolmogorov-Smirnov tests. Data from graphs d-h was analyzed by ordinary one-way ANOVA with multiple comparisons. Data represented as mean ± SEM. n= 90 areas analyzed per dose group. Significance (*****) defined as $p < 0.05$.

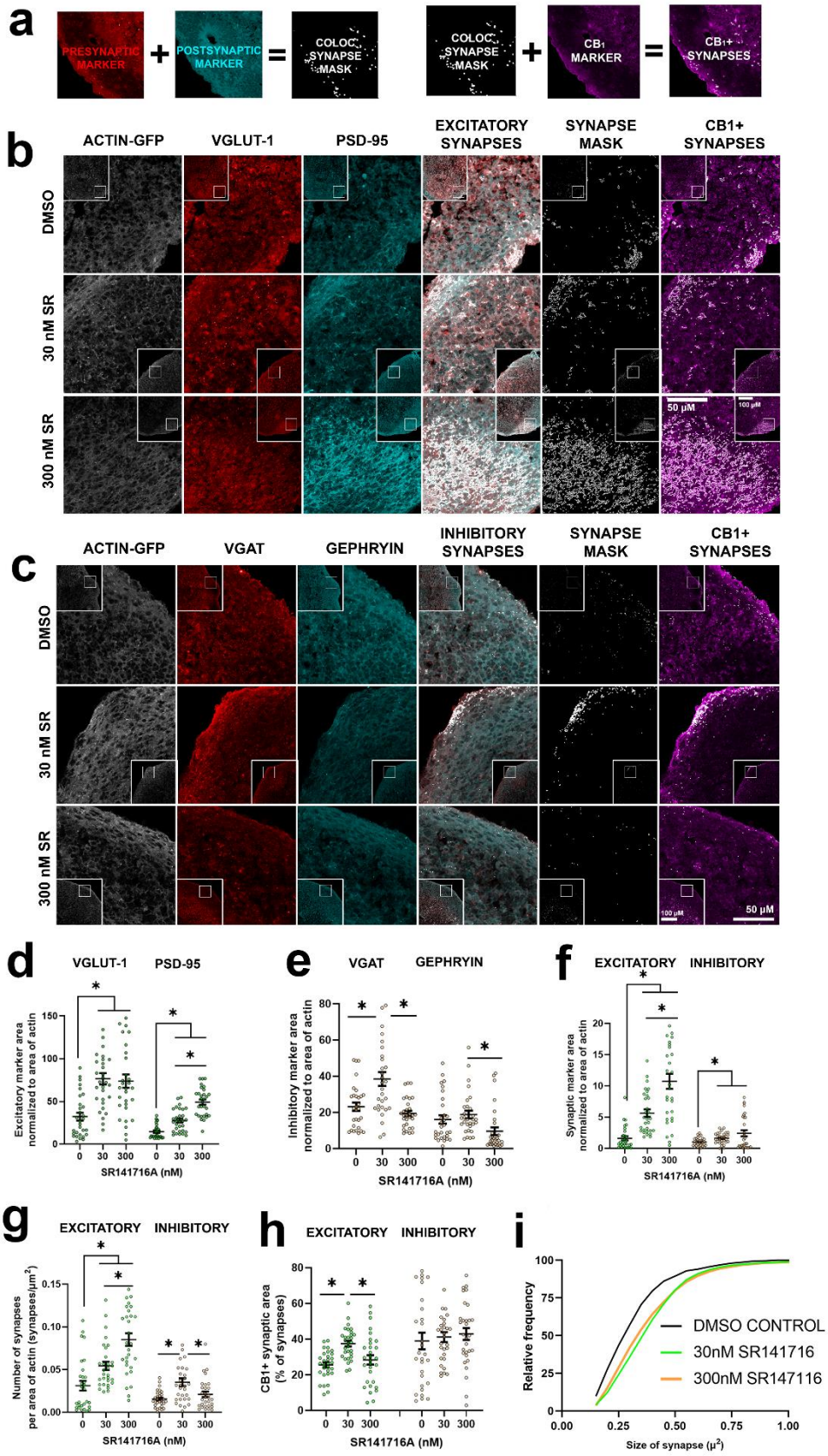
a
PRESYNAPTIC MARKER
POSTSYNAPTIC MARKER
COLOC SYNAPSE MASK
CB1 MARKER
CB1+ SYNAPSES
b
ACTIN-GFP
VGLUT-1
PSD-95
EXCITATORY SYNAPSES
SYNAPSE MASK
CB1+ SYNAPSES
DMSO
30 nM SR
300 nM SR
50 µM
100 µM
c
ACTIN-GFP
VGAT
GEPHRYIN
INHIBITORY SYNAPSES
SYNAPSE MASK
CB1+ SYNAPSES
DMSO
30 nM SR
300 nM SR
100 µM
50 µM
d
VGLUT-1
PSD-95
Excitatory marker area normalized to area of actin
SR141716A (nM)
e
VGAT
GEPHRYIN
Inhibitory marker area normalized to area of actin
SR141716A (nM)
f
EXCITATORY
INHIBITORY
Synaptic marker area normalized to area of actin
SR141716A (nM)
g
EXCITATORY
INHIBITORY
Number of synapses per area of actin (synapses/µm²)
SR141716A (nM)
h
EXCITATORY
INHIBITORY
CB1+ synaptic area (% of synapses)
SR141716A (nM)
i
Relative frequency
Size of synapse (µ²)
DMSO CONTROL
30nM SR141716
300nM SR147116

Figure 4.3 CB_1 selective antagonism by SR141716A in 90-day old cortical spheroids decreases activity of actin regulator GTPase RhoA (a) Representative confocal images of cyrosectioned cortical spheroids stained with Active RhoA, Total RhoA, and excitatory presynaptic marker VGLUT1. Activated RhoA was distinguished from total RhoA by an antibody bound to the GTP form of RhoA (activated). An antibody bound to the GDP form of RhoA distinguished the "total" RhoA. All cortical spheroids express endogenous GFP-linked β-actin (actin-GFP). **(b)** Shown are the normalized ratios of activated RhoA to total RhoA as measured by ratiometric image analysis. Treatment of cortical spheroids with 30 nM and 300 nM SR141716A decreased the relative intensity of gray values at sites colocalized with excitatory presynaptic marker VGLUT1 (0 nM vs 30 nM: $p > 0.001$, 0 nM vs 300 nM: $p > 0.001$). The significant decrease of gray value intensity indicates decreased RhoA activation in the dose groups when compared to the control group. Additionally, an increase in RhoA activity was seen in the 300 nM group (25-75% range: 0.465 - 1.11 a.u., median: 0.728 a.u. n = 57,577) when compared to the 30 nM group (25-75% range: 0.417 - 1.03 a.u., median: 0.670, n = 48,899) (30 nM vs 300 nM: $p > 0.001$). Significance determined by Kruskal-Wallis test with significance defined as $p < 0.05$. Control group (0 nM SR) had n = 43,862 VGLUT1-positive areas analyzed. 3 independent sets of 3 cortical spheroids were analyzed per treatment group for a total of 4-6 cortical spheroids analyzed. Normalized mean gray values are reported as relative intensity with arbitrary units (a.u.).

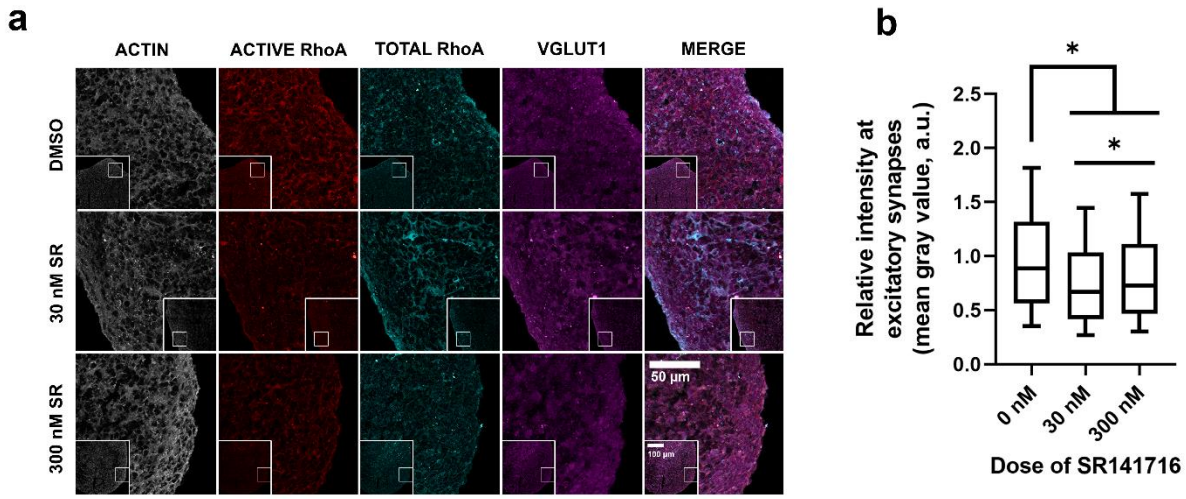
a
ACTIN
ACTIVE RhoA
TOTAL RhoA
VGLUT1
MERGE
DMSO
30 nM SR
300 nM SR
50 µm
100 µm
b
Relative intensity at excitatory synapses (mean gray value, a.u.)
2.5
2.0
1.5
1.0
0.5
0.0
*
*
0 nM
30 nM
300 nM
Dose of SR141716

FIGURE 4.4 SR141716A did not significantly increase WMFR or bursting frequency but increased variability (a) Schematic illustrating the process of cortical spheroid culture, dissociation, and plating. **(b)** Image of dissociated cortical spheroids on top of 16 micro electrodes. Image taken 19 days after dissociation. **(c)** Dissociated spheroids adjust to the MEA plate for 30 days. They are then treated with SR and recorded for 24 hours. Raster plots of extracellular activity are analyzed for spiking and bursting activity. **(d)** The weighted mean firing rate (WMFR) of the vehicle control significantly decreased by 50% after 15 hours (0 hr vs 15 hr: $p = 0.0423$, 0 hr vs 18 hr: $p = 0.0131$, 0 hr vs 21 hr $p = 0.0094$, 0 hr vs 24 hr $p = 0.0099$). There was no significant change to WMFR over 24 hours of SR treatment. **(e)** Bursting frequency was significantly reduced after 6 hours of vehicle treatment (0 hr vs 6 hr: $p = 0.0442$). **(f)** The average WMFR IQR of the control group over 24 hours was 39.3 ± 4.7 compared to 61± 4.6 in the 3 nM group, 124 ± 7.3 in the 30 nM group, and 87 ± 7.7 in the 300 nM group. SR treatment significantly increased the WMFR IQR when compared to vehicle treated controls (VEH vs 3 nM: $p = 0.026$, VEH vs 30 nM: $p < 0.001$, VEH vs 300 nM: $p = 0.001$) (Fig 4f). The variability of the 30 nM group was significantly higher than the 3 nM group (3 nM vs 30 nM: $p < 0.0001$) but the variability of the 300 nM group was significantly lower than the 30 nM group (30 nM vs 300 nM: $p = 0.0166$) (Fig 4f) **(g)** Bursting frequency IQR within the control group over 24 hours was 32.5 ± 3.5. SR increased the mean IQR to 110 ± 20 in the 3 nM group, 647 ± 88 in the 30 nM group, and 137 ± 27 in the 300 nM group. SR significantly increased bursting frequency variability (VEH vs 3 nM: $p = 0.0221$, VEH vs 30 nM: $p = 0.0005$, VEH vs 300 nM: $p = 0.0267$). Variability was greatest at 30 nM (3 nM vs 30 nM: $p = 0.0008$, 30 nM vs 300 nM: $p = 0.0009$). Effects in panels (d) and (e) were compared using one-way ANOVA with multiple comparisons. Effects in panels (f) and (g) were compared using Dunnett's T3 multiple

comparisons test. Data represented as mean ± SEM. Significance (*****) defined by $p < 0.05$. Schematics in panel (a) and (c) were created with BioRender (https://biorender.com/).

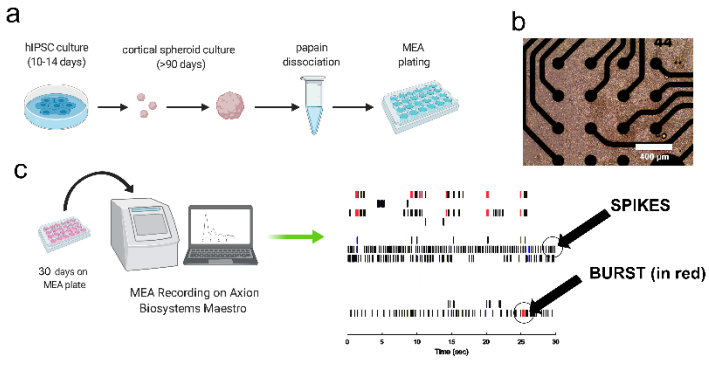
a
hIPSC culture (10-14 days)
cortical spheroid culture (>90 days)
papain dissociation
MEA plating
b
44
400 µm
c
30 days on MEA plate
MEA Recording on Axion Biosystems Maestro
SPIKES
BURST (in red)
Time (sec)

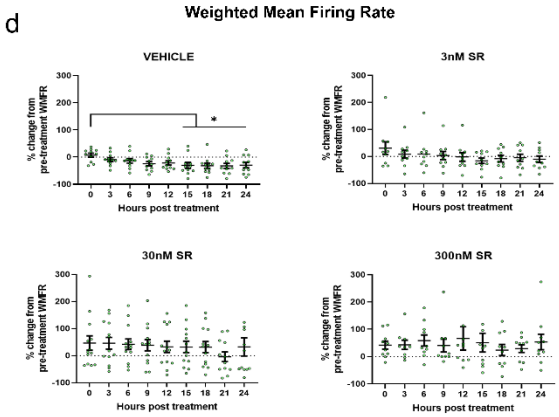
d
Weighted Mean Firing Rate
VEHICLE
3nM SR
30nM SR
300nM SR
% change from pre-treatment WMFR
Hours post treatment

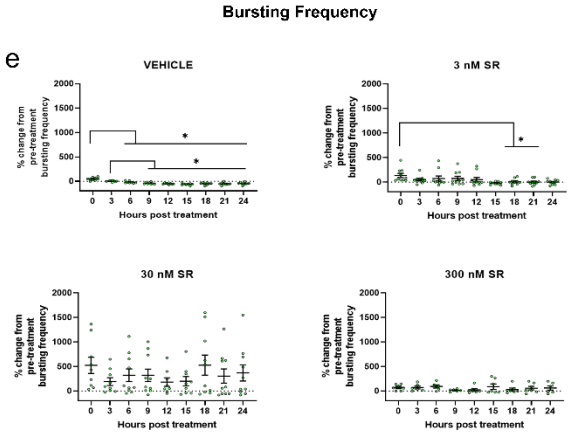
Bursting Frequency
e
VEHICLE
3 nM SR
30 nM SR
300 nM SR
% change from pre-treatment bursting frequency
Hours post treatment

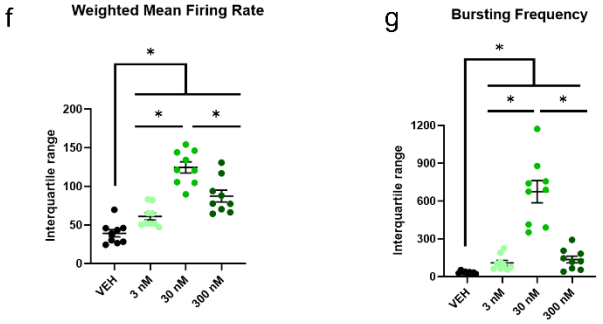
f
Weighted Mean Firing Rate
Interquartile range
VEH
3 nM
30 nM
300 nM
g
Bursting Frequency
Interquartile range
VEH
3 nM
30 nM
300 nM

Figure 4.5: DAGLα and MAGL area was increased in cortical spheroids derived from ASD patient lines. (**a**) Using IF image analysis, we found that DAGLα area significantly increased ($p > 0.001$) from 0.109 ± 0.01% in the control patient line to 0.795 ± 0.06% and 0.469 ± 0.05% in the ASD patient lines 1 and 2, respectively. (**b**) MAGL area significantly increased ($p > 0.001$) from 0.636 ± 0.06% in the control patient cell line to 1.34 ± 0.14% and 1.45 ± 0.05% in the ASD patient lines 1 and 2, respectively. In the third patient, DAGLα was significantly increased (mean: 0.216 ± 0.02%, CTRL PT vs ASD PT 3: $p > 0.001$) but MAGL was not significantly different from cortical spheroids derived from the control patient IPSCs (mean: 0.462 ± 0.04%). (**c**) Cyrosections of cortical spheroids derived from control and ASD patient IPSC lines. Spheroids were stained with DAGLα and DAPI. (**d**) Cyrosections of control and ASD patient cortical spheroids stained with MAGL and DAPI. 3 independent replicates of 90 day old cortical spheroids were analyzed for a total of 4-6 cortical spheroids evaluated per cell line. Data represented as mean ± SEM. Significance determined by ANOVA with multiple comparisons against a control. Significance defined as $p < 0.05$.

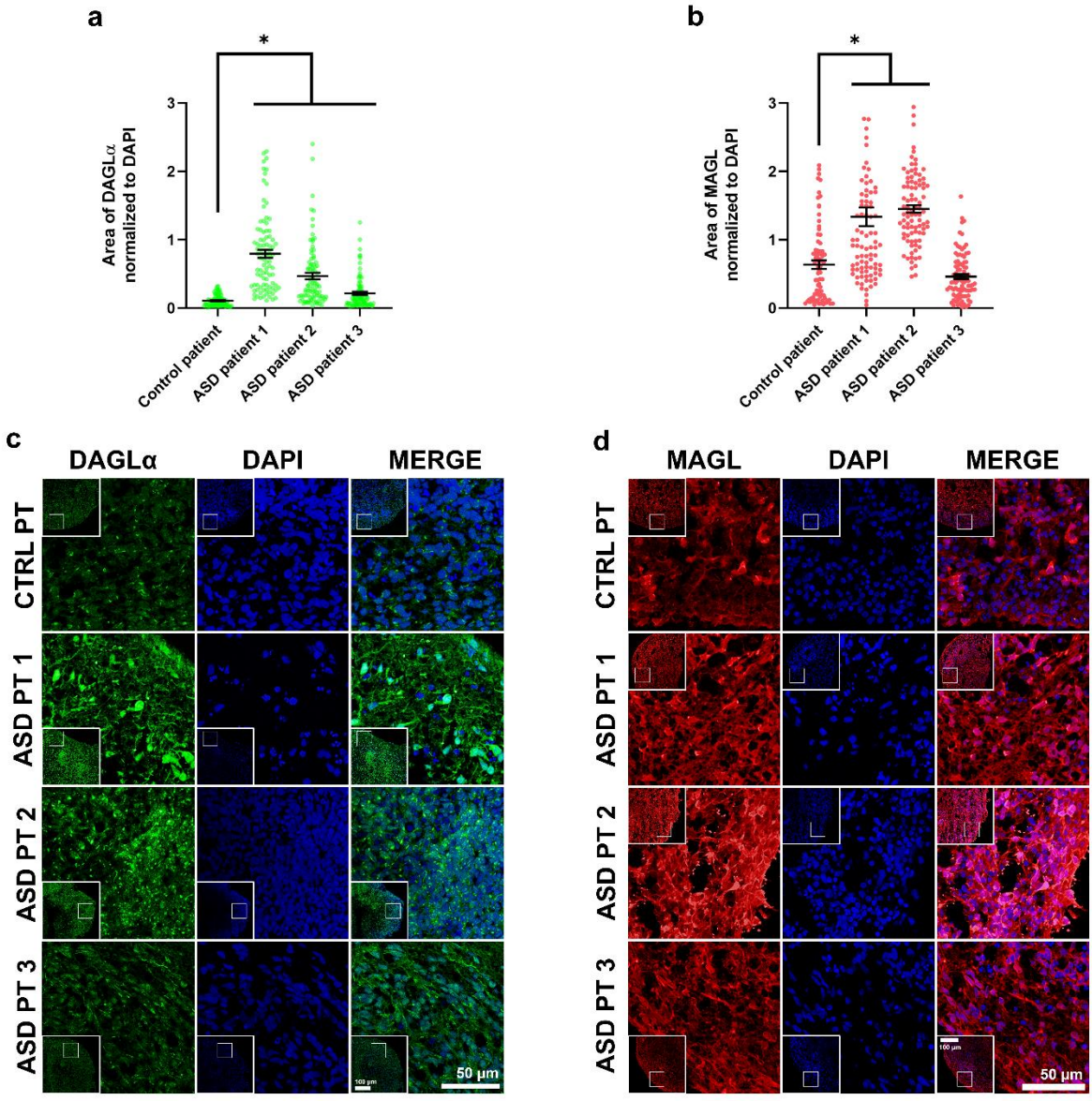
a
*
Area of DAGLα normalized to DAPI
3
2
1
0
Control patient
ASD patient 1
ASD patient 2
ASD patient 3
b
*
Area of MAGL normalized to DAPI
3
2
1
0
Control patient
ASD patient 1
ASD patient 2
ASD patient 3
c
DAGLα
DAPI
MERGE
CTRL PT
ASD PT 1
ASD PT 2
ASD PT 3
50 µm
d
MAGL
DAPI
MERGE
CTRL PT
ASD PT 1
ASD PT 2
ASD PT 3
50 µm

Figure 4.6: **(a)** Using STORM microscopy, we investigated CB_1 molecular count at excitatory and inhibitory synapses and found significantly higher CB_1 molecular count at excitatory synapses (530 ± 25 molecules of CB_1 per synapse) when compared to inhibitory synapse (262 ± 14 molecules of CB_1 per synapse) ($p < 0.001$, Welch's t-test). **(b)** CB_1 receptor count was positively associated with the molecular count of $_{posts1ynaptic}$ excitatory marker PSD95 ($p = 0.048$). **(c)** CB_1 receptor count was also positively associated with the molecular count of inhibitory synapse marker gephyrin ($p = 0.019$). **(d)** Presynaptic excitatory markerVGLUT1 displayed a nonsignificant relationship with CB_1. **(e)** Presynaptic inhibitory marker VGAT also displayed a nonsignificant relationship with CB_1. **(f and g)** Excitatory synapse markers VGLUT1 and PSD95, as well as inhibitory synapse markers VGAT and gephyrin, displayed positive relationships with one another suggesting synaptic scaling. All measures were taken in the zone of active synaptogenesis (100 µm from the exterior) in 90-day old cortical spheroids. A total of 111 excitatory synapses and 180 inhibitory synapses were measured for the molecular count. For panels b through g, significance was defined by slope deviation from zero via simple linear regression analysis. All values given as mean ± SEM.

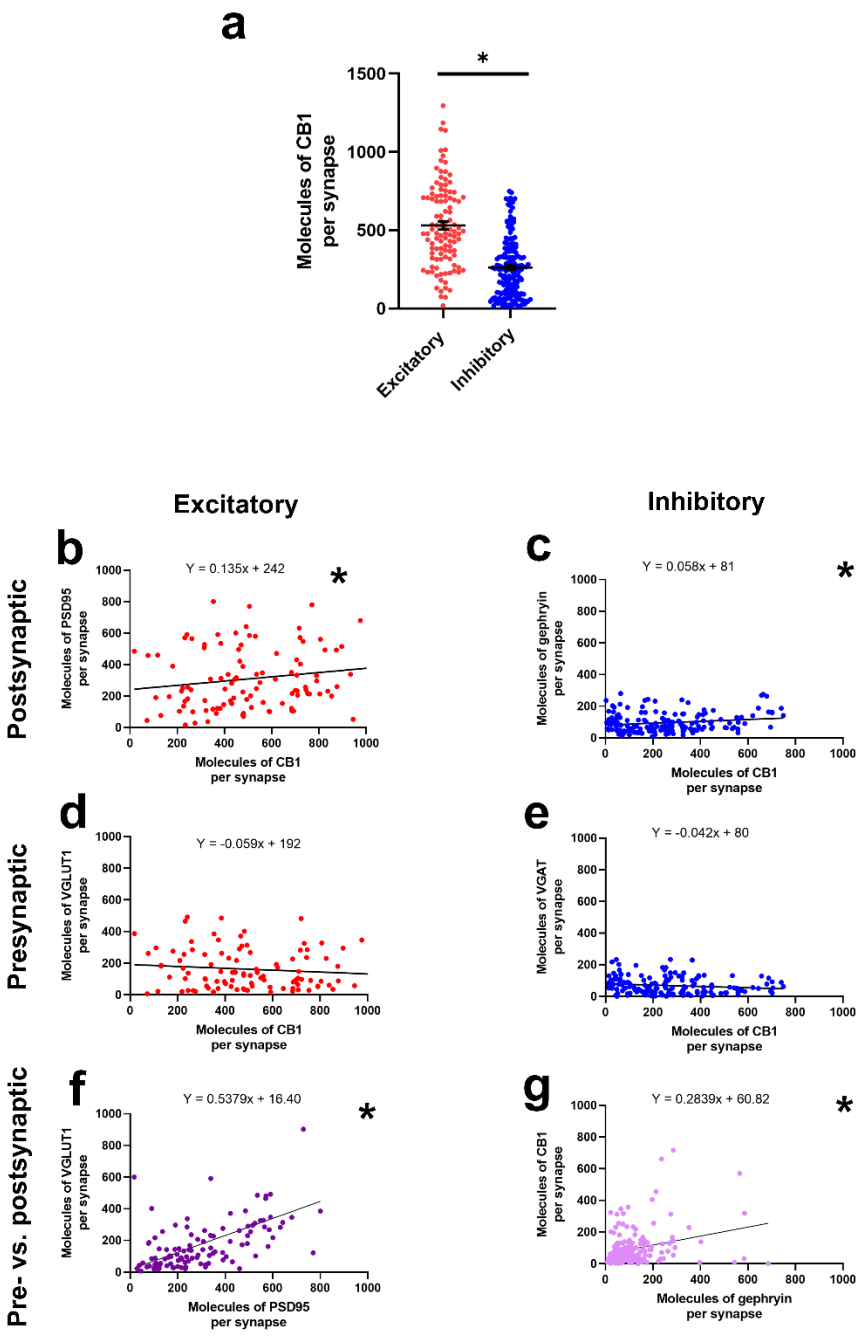
a
*
1500
1000
500
0
Molecules of CB1 per synapse
Excitatory
Inhibitory
Excitatory
Inhibitory
Postsynaptic
Presynaptic
Pre- vs. postsynaptic
b
Y = 0.135x + 242
*
Molecules of PSD95 per synapse
Molecules of CB1 per synapse
c
Y = 0.058x + 81
*
Molecules of gephryin per synapse
Molecules of CB1 per synapse
d
Y = -0.059x + 192
Molecules of VGLUT1 per synapse
Molecules of CB1 per synapse
e
Y = -0.042x + 80
Molecules of VGAT per synapse
Molecules of CB1 per synapse
f
Y = 0.5379x + 16.40
*
Molecules of VGLUT1 per synapse
Molecules of PSD95 per synapse
g
Y = 0.2839x + 60.82
*
Molecules of CB1 per synapse
Molecules of gephryin per synapse

Figure 4.7: Confocal images of 2 week old hIPSC-derived neurons expressing ECS constituents as well as neurite marker βIII-tubulin. Abundant cystolic CB_1, DAGLα, and MAGL was observed in the neurons at this timepoint with some localization of ECS constituents to neurite processes. Neurons were derived from a neurotypical control patient's IPSCs (ActB IPSCs) and have been gene edited via CRISPR-Cas9 technology to endogenously express GFP-tagged β-actin.

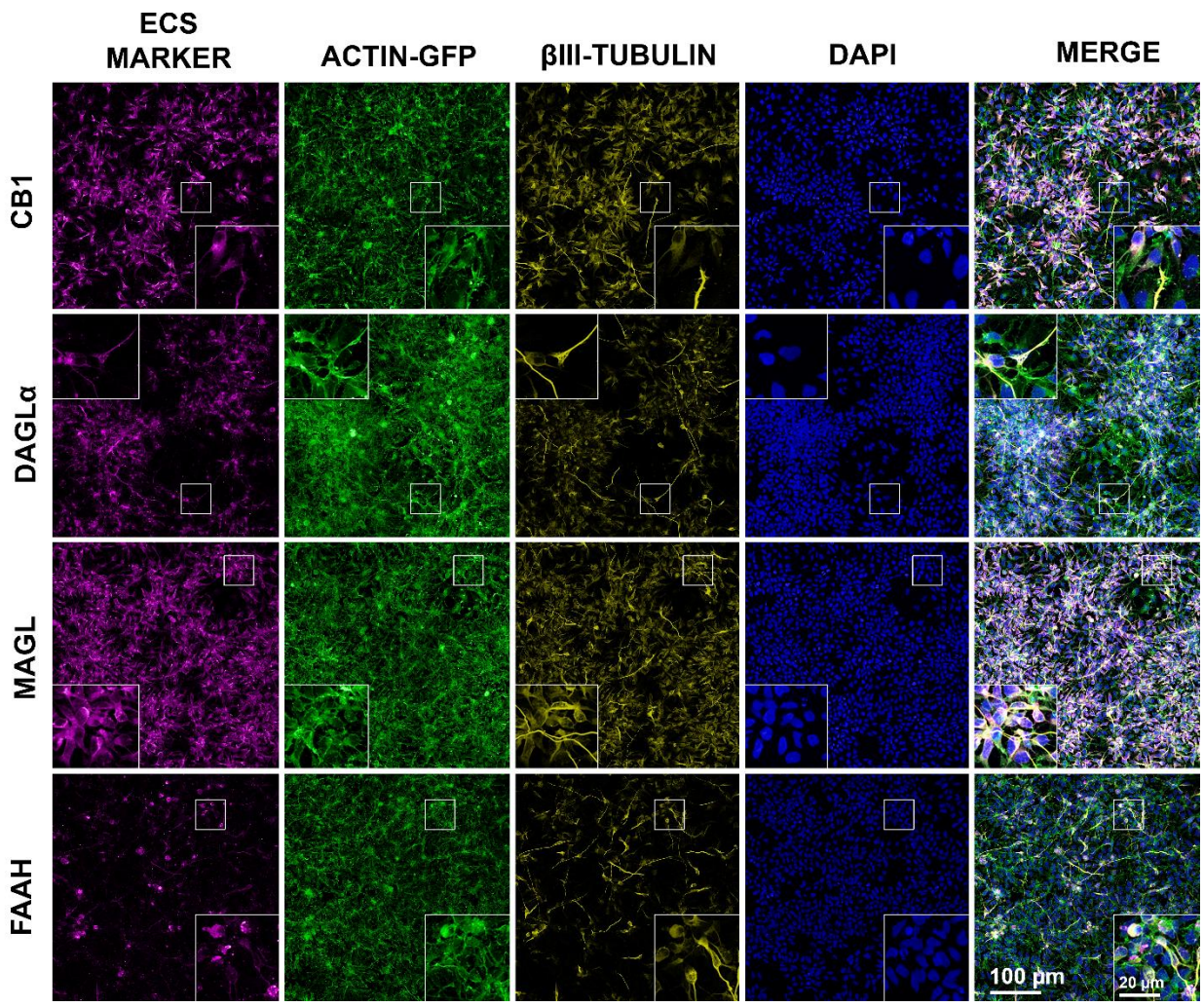
ECS MARKER
ACTIN-GFP
βIII-TUBULIN
DAPI
MERGE
CB1
DAGLα
MAGL
FAAH
100 μm
20 μm

Figure 4.8: We treated 24-hour old, iPSC-derived neurons with vehicle (DMSO), 2µM of CB_1 agonist WIN, or 2µM WIN + CB_1 antagonist/inverse agonist SR for 24 hours. We saw a significant reduction in neurite length after treatment with 2µM WIN compared to vehicle treatment (DMSO median = 0.693, WIN median = 0.484, DMSO vs WIN: $p < 0.001$, as shown by #). This effect of decreased neurite length was reversed with the addition of 3 nM – 30 nM SR (as shown by *, $p < 0.001$). However, we did not see a positive correlation between neurite length and higher doses of SR. The impact of SR treatment on neurite length was greatest at the 10 nM dose (WIN median = 0.484, WIN + 10 nM SR median = 0.796, WIN vs WIN + 10 nM SR: $p < 0.001$). SR at the higher concentrations of 100 nM and 300 nM still showed increased neurite length compared to WIN treated neurons (100 nM SR: $p = 0.011$, 300 nM SR: $p < 0.001$). This implies that SR efficacy is biphasic and distinct in excitatory and inhibitory cells (consistent with data shown in Figure 2). Data represented as box and whisker plots with a range of 10-90%. Significance determined by one-way ANOVA. n = 5000-12000 neurites per dose group analyzed.

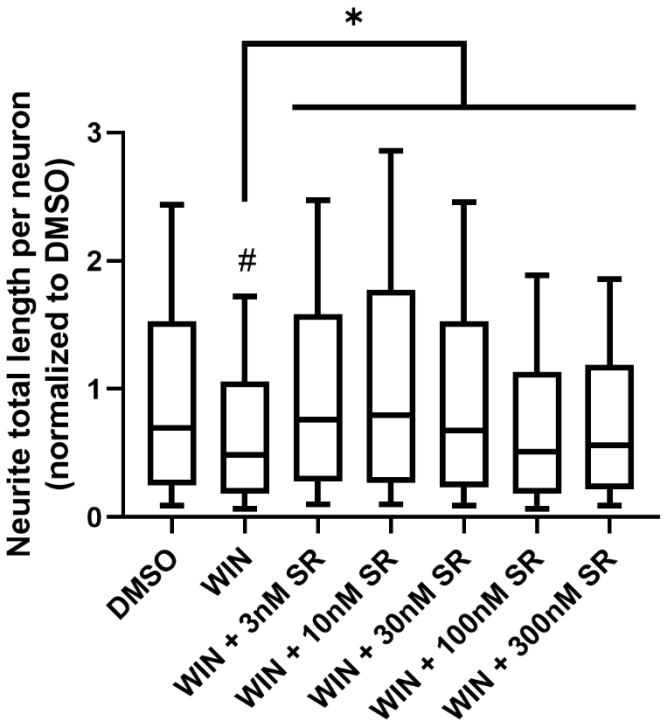
*
#
Neurite total length per neuron
(normalized to DMSO)
3
2
1
0
DMSO
WIN
WIN + 3nM SR
WIN + 10nM SR
WIN + 30nM SR
WIN + 100nM SR
WIN + 300nM SR

Table 1: Primers used for qRT-PCR.

Gene Target	Primer Sequence
CB1 Forward	GATGCGAAGGGATTGCCCC
CB1 Reverse	GATGGTGCGGAAGGTGGTAT
CB2 Forward	GTCCTGGGAGAGGACAGAAAAC
CB2 Reverse	GTCTAGAAGGCTTTGGGTTGTG
DAGLa Forward	GAATTCACAAGAGATGCTCCGC
DAGLa Reverse	TCCTCGATGGTGACTCCAGG
DAGLb Forward	AGGAACAACCAAGAGCCTGC
DAGLb Reverse	CAGCAGTCACCACCAATCCT
MAGL Forward	GAATGCAAACGCCAGCACAT
MAGL Reverse	TGGGACACAAAGATGAGGGC
FAAH Forward	CTTCACCTACAAGGGCCAGG
FAAH Reverse	TTCCATGGGTTCACGGTCTG
TATA-BP Forward	TTTGCAGTGACCCAGCATCA
TATA-BP Reverse	CCAGCACACTCTTCTCAGCA

Table 2: Antibodies used for confocal and STORM imaging.

PRIMARY ANTIBODIES

Dilution	Antibody name	Host	Manufacturer	Catalog number
1:1000	VGLUT-1	guinea pig	Synaptic Systems	135304
1:50	PSD-95	mouse	Santa Cruz Biotech	sc-32291
1:500	VGAT	guinea pig	Synaptic Systems	131004
1:500	Gephyrin	mouse	Abcam	ab32206
1:200	CB_1	rabbit	Custom	
1:200	DAGLα	goat	Abcam	ab81984
1:50	MAGL	rabbit	Sigma-Aldrich	ABN1000
1:50	FAAH	rabbit	ThermoFisher	PA5-32183
1:200	GTPase RhoA-GDP (total)	rabbit	Proteintech	10749-AP
1:500	GTPase RhoA-GTP (active)	mouse	ewEast Biosciences	26904

SECONDARY ANTIBODIES

Dilution	Antibody name	Host	Manufacturer	Catalog number
1:500	Atto488	Goat anti-rabbit IgG	Rockland Antibodies and Assays	611-152-1225
1:500	Alexa Fluor 647	Goat anti-guinea pig IgG	ThermoFisher	A-21450
1:500	Alexa Fluor 594	Goat anti-mouse IgG	ThermoFisher	A-11032
1:500	Alexa Fluor 594	Goat anti-rabbit IgG	ThermoFisher	A-11012
1:500	Alexa Fluor 405	Goat anti-mouse IgG	ThermoFisher	A-31553
1:500	Alexa Fluor 594	Donkey anti-goat IgG	ThermoFisher	A-11058

CHAPTER FIVE: Characterization of cortical spheroid activity by MEA

5.1 Introduction

Before one can manipulate a system, one must first understand what the system is and how that system functions at a basal level. Human iPSC-derived brain organoids and cortical spheroids are a relatively new technology and, as with any novel model system, there is a great deal of basic research which must be conducted to fully characterize and validate the system. Thus, we assessed how cortical spheroids respond to the excitatory neurotransmitter glutamate and the $GABA_A$ antagonist bicuculline in order to assess maturity. By 90 days of age, cortical spheroids model the mid-gestational fetal dorsal telencephalon, which implies that the primary excitatory and inhibitory neurotransmitters are glutamate and GABA, respectively [217]. Since GABA is initially an excitatory, depolarizing neurotransmitter during the first trimester of fetal development [218], it is important to demonstrate that GABA has switch to being hyperpolarizing and inhibitory in our model at 90 days. We hypothesize that cortical spheroid synapses are functional by 90 days of age and that glutamate will increase activity. Additionally, we hypothesized that cortical spheroids at 90 days of age have inhibitory GABA function, which we demonstrate through increased activity after the antagonism of $GABA_A$ receptors.

This section includes unpublished work which evaluates the effects of glutamate and bicuculline on neural activity in cortical spheroids. We have established glutamatergic signaling as excitatory and GABAergic signaling is inhibitory in our system, which is important for characterizing the maturity of our model [219]. Together, these results further confirm that cortical spheroids model the human brain during mid-fetal gestation.

5.2 Methods and materials

iPSC culture and cortical spheroid generation: Chapter 4

MEA recording and analysis: Chapter 4

Determination of glutamate effect in cortical spheroids: Determination of the EC50 of glutamate in this system took place prior to experimentation. A dose of 10nM was chosen as the EC50 dose. Glutamate was dissolved in MEA media and thus the vehicle control for this experiment was MEA media. A treatment volume of 1µL was used in all experiment replicates. The treatment recording was 15 minutes long and plates were allowed to stabilize for 5 minutes prior to the recording.

Determination of bicuculline EC50 in cortical spheroids: Bicuculline (30 mM) was dissolved in DMSO and underwent serial dilutions in MEA media. We used a range of doses, from 10 nM to 3 µM, to capture the EC50. This range of bicuculline doses was chosen based upon previous experiments and previous literature. Treatment recordings were 15 minutes long. Dosing did not

occur on a set time schedule, rather, activity was visually monitored and bicuculline doses were given once activity appeared to decrease or activity levels had not changed in 30 minutes.

Statistics All statistics were run in GraphPad Prism. Information about statistical tests used can be found in the figure legends. Figures represent the average ± SEM and data are reported as such. A p value of < 0.05 was considered statistically significant.

5.3 Results

Micro electrode array (**MEA**) systems measure the extracellular field potential of dissociated cortical spheroids. This extracellular field potential corresponds to multiple, local action potentials. Neural activity is reported as "spikes" which represent an increase in activity across a small area of multiple cells. Multiple spikes of 5 or more in quick succession (< 100 ms between spikes) are defined as "bursts" and represent rapid communication between populations of cells. Synchronous bursting between multiple electrodes is characteristic of mature communication patterns. Using this MEA system, we wanted to evaluate the effects of glutamate, an excitatory neurotransmitter, and bicuculline, a $GABA_A$ antagonist, in cortical spheroids derived from control patient IPSCs.

After determining an EC50 value for glutamate, we evaluated the effects of 10 nM glutamate in control patient-derived cortical spheroids (Figure 5.1). Glutamate significantly increased ($p = 0.022$) the bursting frequency of dissociated cortical spheroids. The bursting frequency of glutamate-treated wells increased by 56.39 ± 15.25% from their pre-treatment values, compared to the bursting frequency of vehicle-treated wells, which increased by 13.98 ± 9.09% compared to their pre-treatment values. Additionally, we performed a dose response using

$GABA_A$ antagonist bicuculline (Figure 5.2). We found that bicuculline increases bursting frequency in 90-day old dissociated cortical spheroids. The bursting frequency of the vehicle treated wells increased by 35.82 ± 10.82% compared to the pre-treatment baseline recording. At 300 nM bicuculline, bursting frequency increased by 141.76 ± 34.59%, and we observed a significant increase ($p = 0.0316$) in bursting frequency. A significant increase ($p = 0.0122$) in bursting frequency was also observed at 1 μM bicuculline, which increased by 215.70 ± 52.83% compared to pretreatment.

Together, these results further confirm the presence of alterable neurotransmitter systems in cortical spheroids, which recapitulate mid-fetal gestation. Importantly, cortical spheroids at 90 days old utilize GABA as an inhibitory neurotransmitter.

5.4 Discussion

Our research has provided a foundation for future pharmaceutical studies within cortical spheroids. Additionally, we have confirmed that cortical spheroids possess neural circuitry which behaves similarly to the mid-gestational, fetal brain using bicuculline and glutamate treatments. Our first experiment confirmed that glutamate is behaving as an excitatory, depolarizing neurotransmitter in our model (Figure 5.1). Glutamatergic signaling during development is necessary for appropriate proliferation, differentiation and migration of neurons [220]. Thus, it is important to demonstrate that cortical spheroids can actively respond to glutamate rather than passively produce it. Our second experiment, the bicuculline dose response, demonstrates that GABA signaling is inhibitory and functions to dampen glutamatergic signaling (Figure 5.2). Interestingly, some hypothesize that a delayed switch in GABA being depolarizing to

hyperpolarizing governs the disruption to neural circuit homeostasis in 22q11.2 deletion syndrome, which has high comorbidity with both schizophrenia and ASD [218]. Together, this data further builds upon the body of literature which states IPSC-derived cortical spheroids are reliable models of human neurodevelopment.

Figure 5.1 10 nM glutamate significantly increases the bursting frequency of dissociated cortical spheroids (p = 0.022, Welch's t-test). The bursting frequency of vehicle-treated wells increased by 13.98 ± 9.09% compared to their pre-treatment values. The bursting frequency of glutamate-treated wells increased by 56.39 ± 15.25% from their pre-treatment values. Experiment preformed in 3 separate replicates of dissociated cortical spheroids derived from a neurotypical patient. N = 21 vehicle-treated wells and 24 glutamate-treated wells. Values represented as mean ± SEM. Data normalized to pre-treatment bursting frequency.

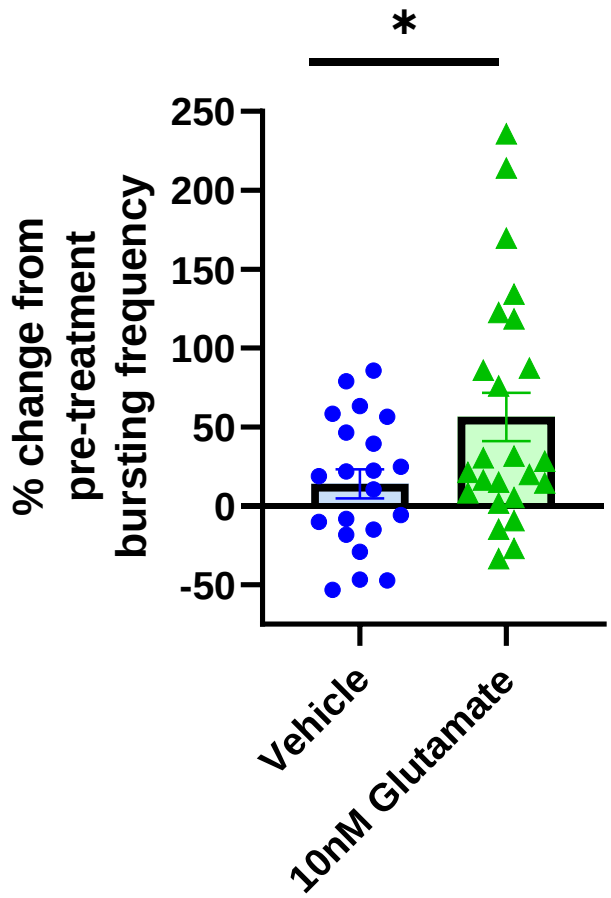

Figure 5.2: Bicuculline increases bursting frequency in 90-day old dissociated cortical spheroids. The bursting frequency of the vehicle treated wells increased by 35.82 ± 10.82% compared to the pre-treatment baseline recording. At 300 nM bicuculline, bursting frequency increased by 141.76 ± 34.59%, and we observed a significant increase ($p = 0.0316$) in bursting frequency. A significant increase ($p = 0.0122$) in bursting frequency was also observed at 1 µM bicuculline, which increased by 215.70 ± 52.83% compared to pretreatment. Experiment was performed in 3 separate replicates of dissociated cortical spheroids derived from a neurotypical patient. N = 35 wells per treatment group. Values represented as mean ± SEM. Data normalized to pre-treatment bursting frequency.

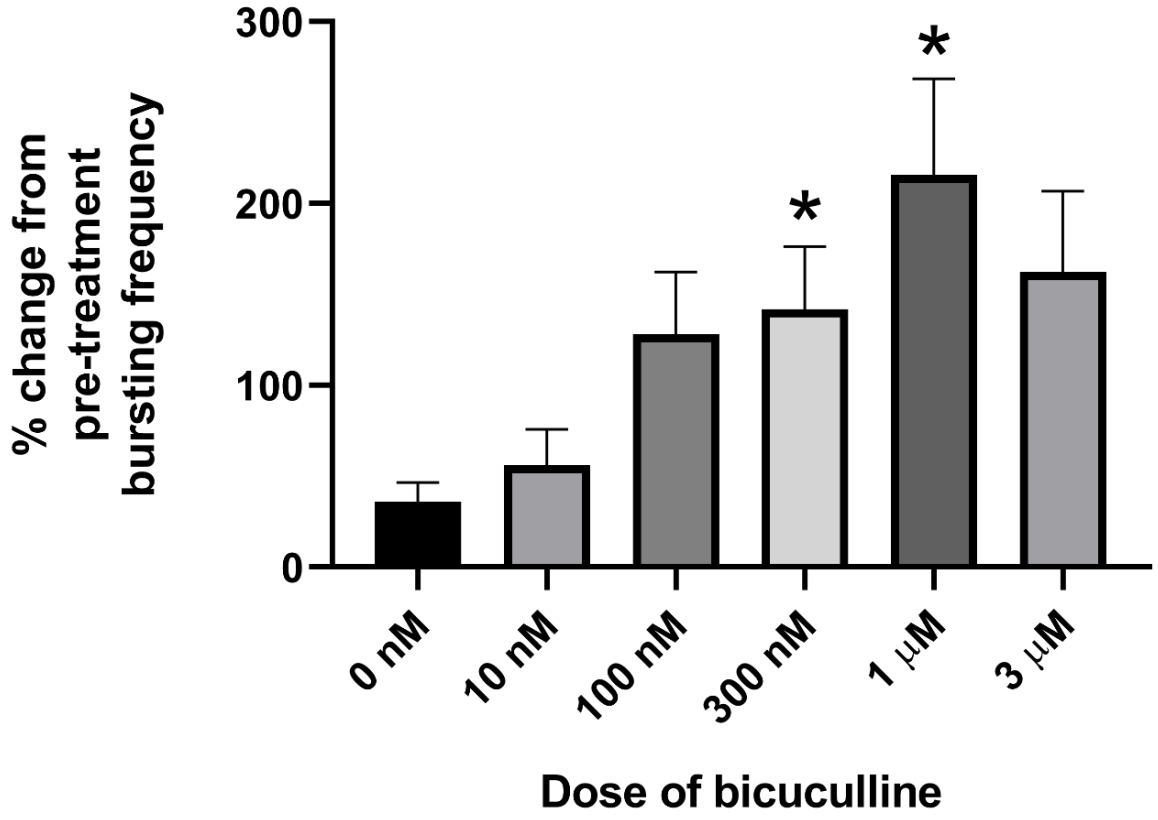

CHAPTER SIX: Differential temporal regulation of the ECS highlights functional distinctions between the fetal and adult brain

6.1 Fetal synaptogenesis is controlled by ECS mechanisms not observed in adult brains

The ECS is a complex modulatory system which has an established role in maintaining neural circuit homeostasis at both excitatory and inhibitory synapses in the adult brain. In the fetal brain, however, the ECS regulates multiple developmental processes, including the directionality of axonal projections and the initiation of synaptogenesis [24]. Before the mystery of the fetal ECS is further unraveled, we must first recognize that fetal brain is not a simple mirror of the adult brain. This may be difficult to reconcile because the adult brain has been explored in much greater detail than the fetal brain. Consequently, this makes it is easy for assumptions about the fetal ECS to be misleading. However, this problem is being addressed by organoid and spheroid models which are bridging the knowledge gap between fetal and adult brain function. Using a cortical spheroid model of neurodevelopment, this body of work expands upon the idea that the developmental endocannabinoid system is functionally distinct from the adult ECS and that the ECS plays a critical role in fetal synaptogenesis.

Cortical spheroids are a novel technology which have allowed us to model the fetal brain environment. Due to this novelty, we first wanted to investigate the presence of ECS components in cortical spheroids using confocal microscopy. We have demonstrated that CB_1, MAGL, DAGLα, and FAAH are all expressed in the cortical spheroid model (Chapters 4 and 5). This is

in line with recent research which has also reported ECS expression in human and mouse brain organoids [197], [199]. Interestingly, we found that cortical spheroids derived from ASD patients have increased mRNA and protein expression of MAGL and DAGLα (Figure 4.1 and Figure 4.5). Both MAGL and DAGLα are differentially regulated at the pre- and postsynapse during development, where they have opposite localizations compared to adult samples. Our finding was particularly intriguing in the context of previous studies which have found correlations between disrupted ECS tone and both environmental and genetic models of ASD [74]. For example, adult mice which lack fragile X mental retardation protein (FMRP, deleted in Fragile X Syndrome) have increased striatal DAGL and MAGL activity [201]. Additionally, acute pre-natal exposure to valproic acid induced greater hippocampal MAGL activity in adolescent rats [221]. Notably, CB_1 expression and function were unaffected in both studies. This is in line with our quantitative RT-PCR results, which indicated no significant differences between neurotypical and ASD-patient CB_1 mRNA levels (Figure 4.1). Further investigation of ECS dysfunction in ASD is certainly warranted. Building upon a theory of disrupted visual processing and preference in ASD, previous studies have found that *CNR1* single-nucleotide polymorphisms (SNPs) affect eye gaze duration and striatal responses to happy faces [78], [79].

Other ECS components, such as DAGLα and MAGL, were not analyzed. Thus, we first propose more studies at the clinical level to determine the frequency of DAGLα and MAGL polymorphisms in the ASD population. Secondly, considering the current deficiency of treatment options for core ASD features, pre-clinical and clinical research should focus on determining if the ECS can be targeted for the relief of language deficits and social anxiety. For this, we propose the investigation of MAGL inhibitors, which have been shown to facilitate cue-induced reward seeking [222], reduce inflammation [208], [223], and promote antinociception [208].

Lastly, we suggest pre-clinical investigation of upstream, neuroinflammatory pathways which could be altering ECS expression during development.

After determining the ECS is present in cortical spheroids, we wanted to ascertain the subcellular localization of ECS constituents using STORM microscopy. We first observed presynaptic localization of CB_1 at both excitatory and inhibitory synapses (Figure 4.1). This is in line with previous STORM observations of presynaptic CB_1 at GABAergic interneurons in hippocampal slices of adolescent mouse brains [224]. We additionally found that the number of CB_1 molecules has a direct relationship with the number of postsynaptic marker molecules at both excitatory and inhibitory synapses (Figure 4.5). This implies that fetal CB_1 partakes in synaptic scaling, which is a homeostatic type of synaptic plasticity by which synapses adjust their strength and size to stabilize firing activity [225]. This type of plasticity is an important feature of maturing, functional synapses [226]. We propose that as the postsynaptic area increases in size to accommodate greater activity, more CB_1 is recruited to the presynapse to regulate vesicular release. This is supported by our observation of significantly more CB_1 molecules at actively growing excitatory synapses compared to inhibitory synapses (Figure 4.6). Our finding of greater CB_1 tone at excitatory synapses is in contrast to a large body of research in juvenile/adult brains which indicates CB_1 is primarily located at inhibitory interneuron synapses in the neocortex [194], [227], [228]. However, as previously mentioned, the fetal ECS is not a mirror of the adult ECS. Studies have found high expression (> 50% of cells) of CB_1 in both excitatory and inhibitory cells of adolescent mice [58]. We believe that the higher molecular count at excitatory synapses may be a function of maturing and growing synapses (Figure 4.6). In addition to our CB_1 data, we observed that the 2-AG regulatory enzymes DAGLα and MAGL are expressed at the presynapse and postsynapse, respectively (Figure 4.1). This pattern of

expression is the opposite of what is observed in the adult brain but is similar to other findings in fetal murine models [20], [28], [47]. DAGLα and CB_1 co-expression in the growth cone of migrating glutamatergic neurons is likely important for tonic agonism of CB_1, which prevents premature initiation of synaptogenesis [47]. Similar to the neocortex, CB_1 in the fetal cerebellum has transient localizations and functions [229]. Notably, mossy fiber CB_1 activation inhibits granule cell excitation which suppresses progressive synaptic potentiation and slows maturation [229]. Thus, our observations are in line with the idea that divergent cellular and subcellular localization of the ECS occurs during fetal development and this divergent expression has functional implications for synapse generation and maintenance.

After determining basal characteristics of the ECS in cortical spheroids, we wanted to manipulate cortical spheroids derived from neurotypical patients with selective, CB_1 antagonist SR141716A. Our hypothesis was that CB_1 antagonism would disrupt synaptogenesis and recapitulate an unbalanced excitatory/inhibitory synapse phenotype. We observed increased excitatory and inhibitory synaptogenesis, increased variability in neural activity, and decreased RhoA activation after an acute treatment with SR141716A (SR, Figure 4.2 - 4.4). In conjunction with prior observations of CB_1 agonism causing neurite retraction via increased RhoA activation[184], we observed CB_1 antagonism increases synapse area via decreased RhoA activation (Figure 4.2-4.3). Together, this strongly suggests that CB_1 is a bidirectional, upstream regulator of neurite and synapse growth via RhoA. This is likely a unique, developmental function of CB_1. Our hypothesis of bidirectional neurite control via CB_1 is further supported by literature which describes increased dendritic spine density [188] and disorganized neuronal activity after treatment with SR [178]. Additionally, the AM-family of CB_1 antagonists reliably produces increases to total neurite length, the number of axon branches, and the number of

dendrites [24]. Comparatively, experiments with CB_1 agonists have less reliable effects on neurite growth direction, as both extension and retraction have been observed in primary neuronal culture [24]. This indicates that cell-specific and drug-specific mechanisms must be further evaluated in the context of CB_1-mediated neurite growth. Importantly, our high dose of SR (300 nM) increased excitatory synapse area but decreased inhibitory synapse area in comparison with the low dose of SR (30 nM) (Fig 4.2). This suggests that differential ECS regulation of excitatory and inhibitory synapses occurs during the initiation of synaptogenesis. While we have utilized SR in a proof-of-concept study design using neurotypical cortical spheroids, others have used mouse models of Fragile X syndrome to demonstrate SR ameliorates synaptic deficits [230], [231]. FMRP KO mice often show increased neuronal excitability that manifests in a brain-region and cell-type specific manner [232]. Using SR in FMRP KO mice, LTD at glutamatergic, hippocampal terminals was restored, synaptic morphology was improved, and cognitive deficits were mended [230], [231]. Thus, we propose that CB_1 negatively regulates neurite branching in fetal glutamatergic neurons, which aids in synchronizing early neural activity by decreasing the number of potential synaptic connections. While we must make equivalencies between adult and fetal models here, the evidence still stands that the ECS is an attractive target for pharmaceutical treatment of ASD. We again propose indirect targeting of CB_1 activity through MAGL and DAGL manipulation due to the substantial risks and impairments caused by direct CB_1 manipulation. For example, while patients who have impaired excitatory signaling may benefit from the glutamatergic targeting of CB_1 antagonist treatments, this treatment likely increases seizure susceptibility in a patient population which already possess epilepsy comorbidity[173]. Nonetheless, our evidence further establishes CB_1 as

a multimodal regulator of synaptogenesis and suggests that CB_1 function is necessary for the stabilization of neural activity in the fetal brain.

6.2 Future directions

The ECS regulates a diverse array of functions including vocal learning [233], memory [234], neural inflammation [235], sleep [236], social play [46], [237], pain perception [238], [239], and seizure susceptibility [25], [240]. Because of the high overlap between ECS functions and ASD comorbidities, the ECS represents a pharmaceutically targetable point of convergence for ASD. Core ASD symptoms such as communication dysfunction and behavioral inflexibility, as well as comorbid diagnoses such as social anxiety, seizures, and insomnia, can all potentially be targeted by a single, cannabinoid treatment. While the body of work which details the role of the fetal and adolescent ECS in the pathology of ASD is growing rapidly, there are still gaps in knowledge that must be addressed prior to pharmaceutical development. First, we lack understanding of the temporal dynamics of endocannabinoid signaling across human development. As previously mentioned, the adult brain has been well characterized but the characterization of the pre-pubertal and fetal ECS is comparatively lacking. Second, there is little understanding of the relationship between basal endocannabinoid signaling and cytoskeletal effects. We propose that the molecular mechanisms which underlie CB_1-mediated cytoskeletal motility and transport should be explored in greater detail, as this may unite multiple cellular signaling systems which go awry in neurodevelopmental disease. Finally, we lack understanding of the ECS in non-neuronal cell types such as astrocytes and microglia. Previous studies have found that the ECS is present in astroglia during early development [241], [242] and plays a role

in phagocytosis of new cells [243]. However, the exact role of the ECS in astroglia remains elusive. Thus, we propose further investigation of an astroglial ECS which mediates homeostatic, inflammation-dependent synapse pruning mechanisms during early development.

CB_1 is a mediator of growth cone directionality and is thus a mediator of axonal guidance [22], [24], [59]. The mechanisms behind CB_1-mediated axonal steering are unclear, however, several studies have tried to elucidate the role CB_1 plays. Evidence suggests CB_1 acts through the Rho-family of GTPases to modulate the cytoskeletal system before and during synaptogenesis [65], [184], [215]. Treatment with CB_1 agonists AEA and WIN55,212-2 rapidly increase GTP-bound, active RhoA in cortical neuron culture [65]. Increased RhoA activity causes cytoskeletal contraction, growth cone collapse, and growth cone repulsion through the activation of Rho-associated protein kinase (ROCK) and phosphorylation of myosin light chains [65], [244]. Interestingly, inhibition of ROCK not only nullifies CB_1 agonist-induced growth cone repulsion, it changes CB_1 activation into a chemoattraction event [65]. We have observed decreased RhoA activation in our cortical spheroids after treatment with CB_1 antagonist SR141716A (Figure 4.3), which is in line with previous observations that CB_1 agonism increases RhoA activity[184]. We suggest that CB_1 impacts cellular motility in a bidirectional manner through the cytoskeleton, with CB_1 antagonism increasing motility and CB_1 agonism decreasing motility. However, CB1 affects RhoA through an unknown cellular signaling cascade. Interestingly, CB_1 may be acting through non-canonical pathways to influence axonal pathfinding and synaptogenesis during development by utilizing heterotrimeric G_{12}/G_{13} proteins rather than the canonical $G_{i/o}$ pathway [184]. Rapid and reversible growth cone collapse brought on by CB_1 G_{12}/G_{13} activation works through Rho-GTPase and ROCK in a non-muscle myosin II dependent manner [184], which highlights the uniqueness of the fetal endocannabinoid system.

As previously mentioned, the expression of CB_1 in the human fetal brain peaks during mid-fetal gestation, coinciding with the onset of synaptogenesis (Figure 2.1). However, it is likely that the participation of CB_1 in synaptogenesis does not fully explain the peak expression levels of CB_1 in the fetal brain. Astrogliogenesis, or the generation and differentiation of glial cells and astrocytes, is also initiated during this period [64]. Astrocytes are a type of supporting cell in the brain and participate in synapse building through the "tripartite synapse" hypothesis, which declares synapses are composed of an astrocytic extension in addition to the pre- and postsynapse [56]. CB_1, which is present at both the presynapse and astrocytic protrusion, plays a role in directing astrocytic-mediated processes necessary for synapse maintenance [245]. For example, astrocytes spatially control endocannabinoid tone around the neuronal pre- and postsynapse of mature synapses [245]. In concordance with the current body of literature, we have observed abundant CB_1 expression in 1 week old iPSC-derived astrocytes (Fig 6.1) and potential astrocytic CB_1 at nascent synapses (Figure 5.4). Additionally, we have observed intense DAGLα expression localized to radial glia projections (Fig 6.2). DAGLα is reported to be expressed at low levels in radial glia [241] and higher levels in neural progenitor cells [242]. Further work is necessary to determine if DAGLα in cortical spheroids is being expressed in the radial glia or in early cortical progenitor neurons, which utilize the radial glia as scaffolding to migrate [246]. Thus, recent literature has shed light on the extensive developmental role of astrocytes in early synapse maintenance, with postulated roles in cell adhesion and synapse stabilization [56]. Interestingly, CB_1 activation has been shown to promote astrocyte differentiation and CB_1 KO is associated with impaired astrogliogenesis [247]. There are also behavioral outcomes linked to astrocytic endocannabinoid manipulation, with decreased endocannabinoid-mediated phagocytosis leading to increased astrocytic density and

demasculinized rodent play-behaviors [243]. These findings are particularly interesting in the context of immune-regulated neurodevelopment disorders.

While synaptic pathologies in neurodevelopmental disorders tend to be propagated by deficits in multiple synaptic regulatory pathways, the ECS plays an outsized role due to the global expression of CB_1[73]. Our body of work provides a framework for future studies of the endocannabinoid system in a cortical spheroid model. We have demonstrated that the ECS, specifically CB_1, MAGL, and DAGLα, is present in a cortical spheroid model of fetal brain development. We have also demonstrated that CB_1 can be antagonized to create a phenotype which displays increased excitatory synaptogenesis and increased variability of neural activity. Thus, we have established that cortical spheroids are an appropriate model for exploring the ECS in the context of neurotypical and neurodivergent fetal brain development. We speculate that the ECS plays a role in the synaptic pathology of neurodevelopmental disorders and we propose the utilization of CB_1 as a targetable receptor for therapeutics.

Figure 6.1 CB_1 is expressed in 1-week old, IPSC-derived astrocytes. CB_1 expression was ubiquitous throughout the cytosol and was not well localized. Astrocytes were cultured in a monolayer and derived from a neurotypical control patient's IPSCs (ActB IPSCs). This cell line has been gene edited via CRISPR-Cas9 technology to endogenously express GFP-tagged β-actin.

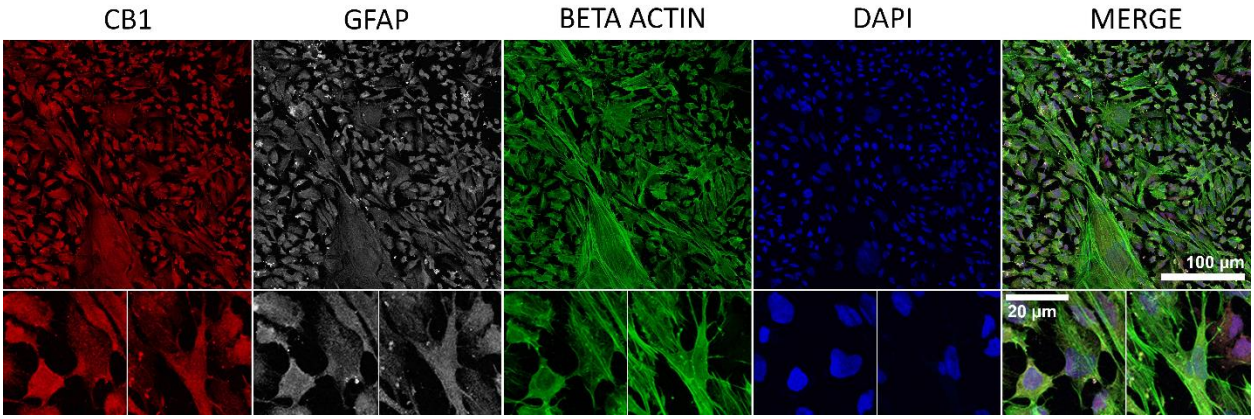

Figure 6.2 DAGLα localization suggests radial glia in cortical spheroids express DAGLα. Cryosections from both neurotypical and ASD-patient derived cortical spheroids possess radial glia with intense DAGLα staining. DAGLα expression projects outward, presumably along the scaffolding of the radial glia.

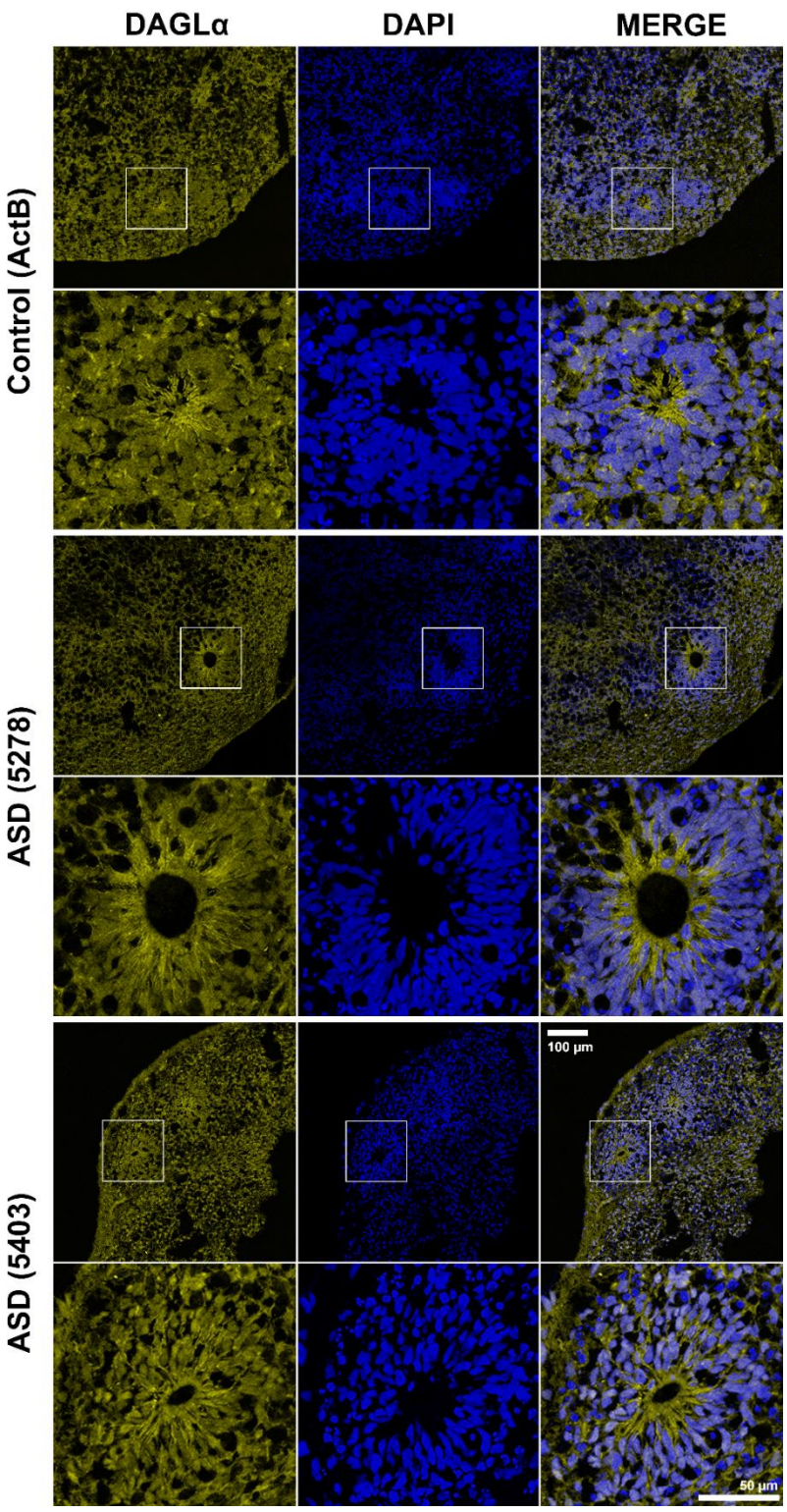

REFERENCES

[1] S. Pisanti and M. Bifulco, “Medical Cannabis: A plurimillennial history of an evergreen,” *Journal of Cellular Physiology*, vol. 234, no. 6. pp. 8342–8351, 2019.

[2] R. G. Pertwee, “Cannabinoid pharmacology: The first 66 years,” *British Journal of Pharmacology*, vol. 147, no. SUPPL. 1. Jan-2006.

[3] E. B. Russo, “Current therapeutic cannabis controversies and clinical trial design issues,” *Frontiers in Pharmacology*, vol. 7, no. SEP. p. 309, 2016.

[4] M. A. Crocq, “History of cannabis and the endocannabinoid system,” *Dialogues Clin. Neurosci.*, vol. 22, no. 3, pp. 223–228, Sep. 2020.

[5] M. Booth, *Cannabis: A history*. New York: Picador, 2005.

[6] M. Frankhauser, “History of Cannabis in western medicine,” in *Cannabis and Cannabinoids: Pharmacology, Toxicology, and Therapeutic Potential*, F. Grotenherman and E. Russo, Eds. New York, 2002, pp. 37–49.

[7] W. B. O’Shaughnessy, “On the preparations of the Indian Hemp, or Gunjah.,” *Trans. Med. Phys. Soc. Bengal*, vol. 8, no. 1838–1840, pp. 421–461, 1839.

[8] D. M. Lambert and C. J. Fowler, “The endocannabinoid system: Drug targets, lead compounds, and potential therapeutic applications,” *Journal of Medicinal Chemistry*, vol. 48, no. 16. pp. 5059–5087, 2005.

[9] R. Mechoulam, L. O. Hanuš, R. Pertwee, and A. C. Howlett, “Early phytocannabinoid chemistry to endocannabinoids and beyond,” *Nature Reviews Neuroscience*, vol. 15, no.

11. pp. 757–764, 2014.

[10] R. Mechoulam and Y. Gaoni, “A Total Synthesis of dl-Δ1-Tetrahydrocannabinol, the Active Constituent of Hashish,” *J. Am. Chem. Soc.*, vol. 87, no. 14, pp. 3273–3275, Jul. 1965.

[11] M. A. ElSohly and D. Slade, “Chemical constituents of marijuana: The complex mixture of natural cannabinoids,” in *Life Sciences*, 2005, vol. 78, no. 5, pp. 539–548.

[12] L. S. Melvin, G. M. Milne, M. R. Johnson, B. Subramaniam, G. H. Wilken, and A. C. Howlett, “Structure-activity relationships for cannabinoid receptor-binding and analgesic activity: studies of bicyclic cannabinoid analogs.,” *Mol. Pharmacol.*, vol. 44, no. 5, 1993.

[13] A. C. Howlett, “Cannabinoid Receptor Signaling,” in *Cannabinoids. Handbook of Experimental Pharmacology.*, 168th ed., R. G. Pertwee, Ed. Springer-Verlag, 2005, pp. 53–79.

[14] L. A. Matsuda, S. J. Lolait, M. J. Brownstein, A. C. Young, and T. I. Bonner, “Structure of a cannabinoid receptor and functional expression of the cloned cDNA,” *Nature*, vol. 346, no. 6284, pp. 561–564, 1990.

[15] S. Munro, K. L. Thomas, and M. Abu-Shaar, “Molecular characterization of a peripheral receptor for cannabinoids,” *Nature*, vol. 365, no. 6441, pp. 61–65, 1993.

[16] W. A. Devane *et al.*, “Isolation and structure of a brain constituent that binds to the cannabinoid receptor,” *Science (80-.).*, vol. 258, no. 5090, pp. 1946–1949, 1992.

[17] R. Mechoulam *et al.*, “Identification of an endogenous 2-monoglyceride, present in canine gut, that binds to cannabinoid receptors,” *Biochem. Pharmacol.*, vol. 50, no. 1, pp. 83–90, Jun. 1995.

[18] R. G. Pertwee, “The pharmacology of cannabinoid receptors and their ligands: An

overview," *International Journal of Obesity*, vol. 30, no. 1. Nature Publishing Group, pp. S13–S18, 29-Mar-2006.

[19] A. C. Howlett, "International Union of Pharmacology. XXVII. Classification of Cannabinoid Receptors," *Pharmacol. Rev.*, 2002.

[20] V. Di Marzo, "Endocannabinoid signaling in the brain: Biosynthetic mechanisms in the limelight," *Nat. Neurosci.*, vol. 14, no. 1, pp. 9–15, Jan. 2011.

[21] L. D. Schurman, D. Lu, D. A. Kendall, A. C. Howlett, and A. H. Lichtman, "Molecular mechanism and cannabinoid pharmacology," in *Handbook of Experimental Pharmacology*, vol. 258, Springer, 2020, pp. 323–353.

[22] S. Watson, D. Chambers, C. Hobbs, P. Doherty, and A. Graham, "The endocannabinoid receptor, CB1, is required for normal axonal growth and fasciculation," *Mol. Cell. Neurosci.*, vol. 38, no. 1, pp. 89–97, May 2008.

[23] T. Harkany, K. Mackie, and P. Doherty, "Wiring and firing neuronal networks: endocannabinoids take center stage," *Current Opinion in Neurobiology*, vol. 18, no. 3. pp. 338–345, Jun-2008.

[24] A.-L. L. Gaffuri, D. Ladarre, and Z. Lenkei, "Type-1 Cannabinoid Receptor Signaling in Neuronal Development," *Pharmacology*, vol. 90, no. 1–2, pp. 19–39, Aug. 2012.

[25] J. Díaz-Alonso *et al.*, "Loss of Cannabinoid CB1 Receptors Induces Cortical Migration Malformations and Increases Seizure Susceptibility," *Cereb. Cortex*, vol. 27, no. 11, pp. 5303–5317, Nov. 2017.

[26] T. L. Clarke, R. L. Johnson, J. J. Simone, and R. L. Carlone, "The endocannabinoid system and invertebrate neurodevelopment and regeneration," *International Journal of Molecular Sciences*, vol. 22, no. 4. pp. 1–24, 2021.

[27] M. R. Elphick, “The evolution and comparative neurobiology of endocannabinoid signalling,” *Philosophical Transactions of the Royal Society B: Biological Sciences*, vol. 367, no. 1607. pp. 3201–3215, 2012.

[28] T. Bisogno *et al.*, “Cloning of the first sn1-DAG lipases points to the spatial and temporal regulation of endocannabinoid signaling in the brain,” *J. Cell Biol.*, vol. 163, no. 3, pp. 463–468, Nov. 2003.

[29] J. M. McPartland, I. Matias, V. Di Marzo, and M. Glass, “Evolutionary origins of the endocannabinoid system,” *Gene*, vol. 370, no. 1–2, pp. 64–74, 2006.

[30] L. De Petrocellis, D. Melck, T. Bisogno, A. Milone, and V. Di Marzo, “Finding of the endocannabinoid signalling system in Hydra, a very primitive organism: Possible role in the feeding response,” *Neuroscience*, vol. 92, no. 1, pp. 377–387, 1999.

[31] C. Galles *et al.*, “Endocannabinoids in Caenorhabditis elegans are essential for the mobilization of cholesterol from internal reserves,” *Sci. Rep.*, vol. 8, no. 1, 2018.

[32] M. Valenti *et al.*, “The endocannabinoid system in the brain of Carassius auratus and its possible role in the control of food intake,” *J. Neurochem.*, vol. 95, no. 3, pp. 662–672, Nov. 2005.

[33] K. Soderstrom, Q. Tian, M. Valenti, and V. Di Di Marzo, “Endocannabinoids link feeding state and auditory perception-related gene expression,” *J. Neurosci.*, 2004.

[34] T. C. Kirkham, C. M. Williams, F. Fezza, and V. Di Marzo, “Endocannabinoid levels in rat limbic forebrain and hypothalamus in relation to fasting, feeding and satiation: Stimulation of eating by 2-arachidonoyl glycerol,” *Br. J. Pharmacol.*, vol. 136, no. 4, pp. 550–557, 2002.

[35] K. Soderstrom, Q. Tian, M. Valenti, and V. Di Di Marzo, “Endocannabinoids link feeding

state and auditory perception-related gene expression," *J. Neurosci.*, vol. 24, no. 44, pp. 10013–10021, Nov. 2004.

[36] M. Pucci *et al.*, "On the role of central type-1 Cannabinoid receptor gene regulation in food intake and eating behaviors," *Int. J. Mol. Sci.*, vol. 22, no. 1, pp. 1–16, 2021.

[37] J. Sandry, D. Trafimow, M. J. Marks, and S. Rice, "Adaptive Memory: Evaluating Alternative Forms of Fitness-Relevant Processing in the Survival Processing Paradigm," *PLoS One*, vol. 8, no. 4, p. 60868, Apr. 2013.

[38] S. Vaseghi, M. Nasehi, and M.-R. Zarrindast, "How do stupendous cannabinoids modulate memory processing via affecting neurotransmitter systems?," *Neurosci. Biobehav. Rev.*, vol. 120, pp. 173–221, 2021.

[39] S. M. Augustin and D. M. Lovinger, "Functional Relevance of Endocannabinoid-Dependent Synaptic Plasticity in the Central Nervous System," *ACS Chemical Neuroscience*, vol. 9, no. 9. American Chemical Society, pp. 2146–2161, 19-Sep-2018.

[40] T. J. Ryan and S. G. N. Grant, "The origin and evolution of synapses," *Nature Reviews Neuroscience*, vol. 10, no. 10. pp. 701–712, Oct-2009.

[41] Q. Li and B. D. Burrell, "Associative, bidirectional changes in neural signaling utilizing NMDA receptor- and endocannabinoid-dependent mechanisms," *Learn. Mem.*, vol. 18, no. 9, pp. 545–553, 2011.

[42] H. Sunada *et al.*, "Pharmacological effects of cannabinoids on learning and memory in Lymnaea," 2017.

[43] J. Acosta Urquidi and R. Chase, "The effects of Δ9 tetrahydrocannabinol on action potentials in the mollusc Aplysia," *Can. J. Physiol. Pharmacol.*, vol. 53, no. 5, pp. 793–798, 1975.

[44] K. Soderstrom and F. Johnson, “Cannabinoid exposure alters learning of zebra finch vocal patterns,” *Dev. Brain Res.*, vol. 142, no. 2, pp. 215–217, May 2003.

[45] Y. Litvin, A. Phan, M. N. Hill, D. W. Pfaff, and B. S. McEwen, “CB1 receptor signaling regulates social anxiety and memory,” *Genes Brain Behav.*, 2013.

[46] A. Manduca *et al.*, “Interacting Cannabinoid and Opioid Receptors in the Nucleus Accumbens Core Control Adolescent Social Play,” *Front. Behav. Neurosci.*, 2016.

[47] M. Maccarrone, M. Guzmán, K. Mackie, P. Doherty, and T. Harkany, “Programming of neural cells by (endo)cannabinoids: from physiological rules to emerging therapies,” *Nat. Publ. Gr.*, 2014.

[48] J. G. Scotchie, R. F. Savaris, C. E. Martin, and S. L. Young, “Endocannabinoid regulation in human endometrium across the menstrual cycle,” *Reprod. Sci.*, vol. 22, no. 1, pp. 113–123, Jan. 2015.

[49] S. Chaudhury, V. Sharma, V. Kumar, T. C. Nag, and S. Wadhwa, “Activity-dependent synaptic plasticity modulates the critical phase of brain development,” *Brain and Development*, vol. 38, no. 4. Elsevier B.V., pp. 355–363, 01-Apr-2016.

[50] K. Soderstrom and F. Johnson, “Zebra finch CB1 cannabinoid receptor: Pharmacology and in vivo and in vitro effects of activation,” *J. Pharmacol. Exp. Ther.*, vol. 297, no. 1, pp. 189–197, 2001.

[51] K. Soderstrom, M. Leid, F. L. Moore, and T. F. Murray, “Behavioral, pharmacological, and molecular characterization of an amphibian cannabinoid receptor,” *J. Neurochem.*, 2000.

[52] A. Biegon and I. A. Kerman, “Autoradiographic study of pre- and postnatal distribution of cannabinoid receptors in human Brain,” *Neuroimage*, vol. 14, no. 6, pp. 1463–1468, 2001.

[53] X. Wang, D. Dow-Edwards, E. Keller, and Y. L. Hurd, “Preferential limbic expression of the cannabinoid receptor mRNA in the human fetal brain,” *Neuroscience*, vol. 118, no. 3, pp. 681–694, 2003.

[54] S. Mato, E. Del Olmo, and A. Pazos, “Ontogenetic development of cannabinoid receptor expression and signal transduction functionality in the human brain,” *Eur. J. Neurosci.*, vol. 17, no. 9, pp. 1747–1754, May 2003.

[55] H. C. Meyer, F. S. Lee, and D. G. Gee, “The Role of the Endocannabinoid System and Genetic Variation in Adolescent Brain Development,” *Neuropsychopharmacology*, vol. 43, no. 1. Nature Publishing Group, pp. 21–33, 01-Jan-2018.

[56] I. Farhy-Tselnicker and N. J. Allen, “Astrocytes, neurons, synapses: A tripartite view on cortical circuit development,” *Neural Development*, vol. 13, no. 1. 2018.

[57] X. Wang, D. Dow-Edwards, E. Keller, and Y. L. Hurd, “Preferential limbic expression of the cannabinoid receptor mRNA in the human fetal brain,” *Neuroscience*, vol. 118, no. 3, pp. 681–694, May 2003.

[58] E. L. Hill *et al.*, “Functional CB1 receptors are broadly expressed in neocortical GABAergic and glutamatergic neurons,” *J. Neurophysiol.*, vol. 97, pp. 2580–2589, 2007.

[59] C. S. Wu *et al.*, “Requirement of cannabinoid CB1 receptors in cortical pyramidal neurons for appropriate development of corticothalamic and thalamocortical projections,” *Eur. J. Neurosci.*, vol. 32, no. 5, pp. 693–706, Sep. 2010.

[60] J. Mulder *et al.*, “Endocannabinoid signaling controls pyramidal cell specification and long-range axon patterning,” *Proc. Natl. Acad. Sci.*, vol. 105, no. 25, pp. 8760–8765, Jun. 2008.

[61] D. Van Vactor, “Adhesion and signalling in axonal fasciculation,” *Curr. Opin. Neurobiol.*,

vol. 8, no. 1, pp. 80–86, 1998.

[62] V. De Giacomo, S. Ruehle, | Beat Lutz, | Martin Häring, and F. Remmers, “Cell type-specific genetic reconstitution of CB1 receptor subsets to assess their role in exploratory behaviour, sociability, and memory,” *Eur J Neurosci*, vol. 00, pp. 1–13, 2021.

[63] M. J. Oudin, C. Hobbs, and P. Doherty, “DAGL-dependent endocannabinoid signalling: roles in axonal pathfinding, synaptic plasticity and adult neurogenesis,” *Eur. J. Neurosci.*, vol. 34, no. 10, pp. 1634–1646, Nov. 2011.

[64] J. C. C. Silbereis, S. Pochareddy, Y. Zhu, M. Li, and N. Sestan, “The Cellular and Molecular Landscapes of the Developing Human Central Nervous System,” *Neuron*, vol. 89, no. 2, pp. 248–268, Jan. 2016.

[65] P. Berghuis *et al.*, “Hardwiring the brain: endocannabinoids shape neuronal connectivity.,” *Science*, vol. 316, no. 5828, pp. 1212–6, May 2007.

[66] J. Pevsner *et al.*, “Specificity and regulation of a synaptic vesicle docking complex,” *Neuron*, vol. 13, no. 2, pp. 353–361, 1994.

[67] X. Zhao and A. Bhattacharyya, “Human Models Are Needed for Studying Human Neurodevelopmental Disorders,” *American Journal of Human Genetics*, vol. 103, no. 6. Cell Press, pp. 829–857, 06-Dec-2018.

[68] A. Papariello and K. Newell-Litwa, “Human-Derived Brain Models: Windows into Neuropsychiatric Disorders and Drug Therapies,” *Assay and Drug Development Technologies*, vol. 18, no. 2. pp. 79–88, 2020.

[69] C. W. Habela, H. Song, and G.-L. Ming, “Modeling synaptogenesis in schizophrenia and autism using human iPSC derived neurons.,” *Mol. Cell. Neurosci.*, vol. 73, pp. 52–62, 2016.

[70] C. A. Trujillo *et al.*, “Complex Oscillatory Waves Emerging from Cortical Organoids Model Early Human Brain Network Development,” *Cell Stem Cell*, 2019.

[71] K. E. Sanchack and C. A. Thomas, “Autism spectrum disorder: Primary care principles,” *Am. Fam. Physician*, 2016.

[72] J. J. Hutsler and H. Zhang, “Increased dendritic spine densities on cortical projection neurons in autism spectrum disorders.,” *Brain Res.*, vol. 1309, pp. 83–94, Jan. 2010.

[73] R. Gao and P. Penzes, “Common Mechanisms of Excitatory and Inhibitory Imbalance in Schizophrenia and Autism Spectrum Disorders,” *Curr. Mol. Med.*, vol. 15, no. 2, pp. 146–167, Mar. 2015.

[74] E. Zamberletti, M. Gabaglio, and D. Parolaro, “The endocannabinoid system and autism spectrum disorders: Insights from animal models,” *International Journal of Molecular Sciences*, vol. 18, no. 9. MDPI AG, 07-Sep-2017.

[75] C. Compagnucci *et al.*, “Type-1 (CB1) Cannabinoid Receptor Promotes Neuronal Differentiation and Maturation of Neural Stem Cells,” *PLoS One*, vol. 8, no. 1, p. 54271, 2013.

[76] M. L. Yeh and E. S. Levine, “Perspectives on the Role of Endocannabinoids in Autism Spectrum Disorders.,” *OBM Neurobiol.*, vol. 1, no. 2, 2017.

[77] A. Aran *et al.*, “Lower circulating endocannabinoid levels in children with autism spectrum disorder.,” *Mol. Autism*, vol. 10, p. 2, 2019.

[78] B. Chakrabarti, L. Kent, J. Suckling, E. Bullmore, and S. Baron-Cohen, “Variations in the human cannabinoid receptor (CNR1) gene modulate striatal responses to happy faces,” *Eur. J. Neurosci.*, vol. 23, no. 7, pp. 1944–1948, Apr. 2006.

[79] B. Chakrabarti and S. Baron-Cohen, “Variation in the human cannabinoid receptor CNR1

gene modulates gaze duration for happy faces," 2011.

[80] R. G. Pertwee *et al.*, "International Union of Basic and Clinical Pharmacology. LXXIX. Cannabinoid Receptors and Their Ligands: Beyond CB1 and CB2," *Pharmacol. Rev.*, 2010.

[81] "Medicines for Treating Autism's Core Symptoms | Autism Speaks." [Online]. Available: https://www.autismspeaks.org/medicines-treating-autisms-core-symptoms. [Accessed: 27-May-2021].

[82] C. L. Gooch, E. Pracht, and A. R. Borenstein, "The burden of neurological disease in the United States: A summary report and call to action," *Annals of Neurology*, vol. 81, no. 4. John Wiley and Sons Inc., pp. 479–484, 01-Apr-2017.

[83] S. L. Colby and J. M. Ortman, "Projections of the Size and Composition of the U.S. Population: 2014 to 2060," *Program*, 2014.

[84] J. A. Fisher, M. D. Cottingham, and C. A. Kalbaugh, "Peering into the pharmaceutical 'pipeline': Investigational drugs, clinical trials, and industry priorities," *Soc. Sci. Med.*, vol. 131, pp. 322–330, Apr. 2015.

[85] Q. Liu *et al.*, "Effect of potent γ-secretase modulator in human neurons derived from multiple presenilin 1-induced pluripotent stem cell mutant carriers," *JAMA Neurol.*, vol. 71, no. 12, pp. 1481–1489, Dec. 2014.

[86] Y. Pei *et al.*, "Comparative neurotoxicity screening in human iPSC-derived neural stem cells, neurons and astrocytes," *Brain Res.*, vol. 1638, pp. 57–73, May 2016.

[87] S. R. Chaplan, W. A. Eckert III, and N. I. Carruthers, *Drug Discovery and Development for Pain*. 2010.

[88] E. Wilson, T. Rudisill, B. Kirk, C. Johnson, P. Kemper, and K. Newell-Litwa,

"Cytoskeletal regulation of synaptogenesis in a model of human fetal brain development," *J. Neurosci. Res.*, 2020.

[89] J. Nagy *et al.*, "Altered neurite morphology and cholinergic function of induced pluripotent stem cell-derived neurons from a patient with Kleefstra syndrome and autism," *Transl. Psychiatry*, vol. 7, no. 7, p. e1179, Jul. 2017.

[90] Y. Sun *et al.*, "A deleterious Nav1.1 mutation selectively impairs telencephalic inhibitory neurons derived from Dravet Syndrome patients," *Elife*, vol. 5, no. 2016JULY, Jul. 2016.

[91] H. Darville *et al.*, "Human Pluripotent Stem Cell-derived Cortical Neurons for High Throughput Medication Screening in Autism: A Proof of Concept Study in SHANK3 Haploinsufficiency Syndrome," *EBioMedicine*, vol. 9, pp. 293–305, Jul. 2016.

[92] F. Liao and D. M. Holtzman, "Human Neurons Derived From Induced Pluripotent Stem Cells as a New Platform for Preclinical Drug Screening and Development," *JAMA Neurol.*, vol. 71, no. 12, p. 1475, Dec. 2014.

[93] D. Prilutsky, N. P. Palmer, N. Smedemark-Margulies, T. M. Schlaeger, D. M. Margulies, and I. S. Kohane, "IPSC-derived neurons as a higher-throughput readout for autism: Promises and pitfalls," *Trends in Molecular Medicine*, vol. 20, no. 2. Trends Mol Med, pp. 91–104, Feb-2014.

[94] C. Arber, C. Lovejoy, and S. Wray, "Stem cell models of Alzheimer's disease: progress and challenges," *Alzheimers. Res. Ther.*, vol. 9, no. 1, p. 42, Dec. 2017.

[95] A. Serrano-Pozo, M. P. Frosch, E. Masliah, and B. T. Hyman, "Neuropathological alterations in Alzheimer disease.," *Cold Spring Harb. Perspect. Med.*, vol. 1, no. 1, p. a006189, Sep. 2011.

[96] J. G. Richards *et al.*, "PS2APP transgenic mice, coexpressing hPS2mut and hAPPswe,

show age-related cognitive deficits associated with discrete brain amyloid deposition and inflammation.," *J. Neurosci.*, vol. 23, no. 26, pp. 8989–9003, Oct. 2003.

[97] C. Sturchler-Pierrat *et al.*, "Two amyloid precursor protein transgenic mouse models with Alzheimer disease-like pathology.," *Proc. Natl. Acad. Sci. U. S. A.*, vol. 94, no. 24, pp. 13287–92, Nov. 1997.

[98] J. Götz, F. Chen, J. van Dorpe, and R. M. Nitsch, "Formation of neurofibrillary tangles in P301l tau transgenic mice induced by Abeta 42 fibrils.," *Science*, vol. 293, no. 5534, pp. 1491–5, Aug. 2001.

[99] B. Roberts *et al.*, "Systematic gene tagging using CRISPR/Cas9 in human stem cells to illuminate cell organization.," *Mol. Biol. Cell*, vol. 28, no. 21, pp. 2854–2874, Oct. 2017.

[100] X. Zhang, Y. Li, H. Xu, and Y. Zhang, "The gamma-secretase complex: from structure to function," *Front. Cell. Neurosci.*, vol. 8, p. 427, Dec. 2014.

[101] D. Scheuner *et al.*, "Secreted amyloid β–protein similar to that in the senile plaques of Alzheimer's disease is increased in vivo by the presenilin 1 and 2 and APP mutations linked to familial Alzheimer's disease," *Nat. Med.*, vol. 2, no. 8, pp. 864–870, Aug. 1996.

[102] T. Yagi *et al.*, "Modeling familial Alzheimer's disease with induced pluripotent stem cells," *Hum. Mol. Genet.*, vol. 20, no. 23, pp. 4530–4539, Dec. 2011.

[103] N. Yahata *et al.*, "Anti-Aβ Drug Screening Platform Using Human iPS Cell-Derived Neurons for the Treatment of Alzheimer's Disease," *PLoS One*, vol. 6, no. 9, p. e25788, Sep. 2011.

[104] A. K. Ghosh, S. Gemma, and J. Tang, "β-Secretase as a therapeutic target for Alzheimer's disease," *Neurotherapeutics*, vol. 5, no. 3, pp. 399–408, Jul. 2008.

[105] M. A. Israel *et al.*, "Probing sporadic and familial Alzheimer's disease using induced

pluripotent stem cells.," *Nature*, vol. 482, no. 7384, pp. 216–20, Feb. 2012.

[106] D. Kumar, A. Ganeshpurkar, D. Kumar, G. Modi, S. K. Gupta, and S. K. Singh, "Secretase inhibitors for the treatment of Alzheimer's disease: Long road ahead," *Eur. J. Med. Chem.*, vol. 148, pp. 436–452, Mar. 2018.

[107] T. Kondo *et al.*, "iPSC-Based Compound Screening and In Vitro Trials Identify a Synergistic Anti-amyloid β Combination for Alzheimer's Disease," *Cell Rep.*, vol. 21, no. 8, pp. 2304–2312, Nov. 2017.

[108] S. Sances *et al.*, "Human iPSC-Derived Endothelial Cells and Microengineered Organ-Chip Enhance Neuronal Development," *Stem Cell Reports*, vol. 10, no. 4, pp. 1222–1236, Apr. 2018.

[109] A. A. Mansour *et al.*, "An in vivo model of functional and vascularized human brain organoids," *Nat. Biotechnol.*, vol. 36, no. 5, pp. 432–441, Apr. 2018.

[110] F. Maiullari *et al.*, "A multi-cellular 3D bioprinting approach for vascularized heart tissue engineering based on HUVECs and iPSC-derived cardiomyocytes," *Sci. Rep.*, vol. 8, no. 1, p. 13532, Dec. 2018.

[111] A. Nakajima *et al.*, "Nobiletin, a citrus flavonoid that improves memory impairment, rescues bulbectomy-induced cholinergic neurodegeneration in mice.," *J. Pharmacol. Sci.*, vol. 105, no. 1, pp. 122–6, Sep. 2007.

[112] A. Nakajima *et al.*, "Nobiletin, a citrus flavonoid, ameliorates cognitive impairment, oxidative burden, and hyperphosphorylation of tau in senescence-accelerated mouse," *Behav. Brain Res.*, vol. 250, pp. 351–360, Aug. 2013.

[113] J. Kimura *et al.*, "Nobiletin Reduces Intracellular and Extracellular β-Amyloid in iPS Cell-Derived Alzheimer's Disease Model Neurons," *Biol. Pharm. Bull.*, vol. 41, no. 4, pp.

451–457, 2018.

[114] R. Balez *et al.*, “Neuroprotective effects of apigenin against inflammation, neuronal excitability and apoptosis in an induced pluripotent stem cell model of Alzheimer’s disease,” *Sci. Rep.*, vol. 6, no. 1, p. 31450, Nov. 2016.

[115] S. H. Choi, Y. H. Kim, C. D’Avanzo, J. Aronson, R. E. Tanzi, and D. Y. Kim, “Recapitulating amyloid β and tau pathology in human neural cell culture models: clinical implications.,” *US Neurol.*, vol. 11, no. 2, pp. 102–105, 2015.

[116] S. H. Choi, Y. H. Kim, L. Quinti, R. E. Tanzi, and D. Y. Kim, “3D culture models of Alzheimer’s disease: A road map to a ‘cure-in-a-dish,’” *Mol. Neurodegener.*, 2016.

[117] A. Kremer, “GSK3 and Alzheimer’s disease: facts and fiction…,” *Front. Mol. Neurosci.*, vol. 4, p. 17, Aug. 2011.

[118] C. Gonzalez, E. Armijo, J. Bravo-Alegria, A. Becerra-Calixto, C. E. Mays, and C. Soto, “Modeling amyloid beta and tau pathology in human cerebral organoids,” *Mol. Psychiatry*, vol. 23, no. 12, pp. 2363–2374, Dec. 2018.

[119] M. Goedert, F. Clavaguera, and M. Tolnay, “The propagation of prion-like protein inclusions in neurodegenerative diseases,” *Trends Neurosci.*, vol. 33, no. 7, pp. 317–325, Jul. 2010.

[120] F. Birey *et al.*, “Assembly of functionally integrated human forebrain spheroids,” *Nature*, vol. 545, no. 7652, pp. 54–59, Apr. 2017.

[121] E. S. Wilson and K. Newell-Litwa, “Stem cell models of human synapse development and degeneration,” *Mol. Biol. Cell*, vol. 29, no. 24, pp. 2913–2921, Nov. 2018.

[122] Y. Xiang *et al.*, “Fusion of Regionally Specified hPSC-Derived Organoids Models Human Brain Development and Interneuron Migration,” *Cell Stem Cell*, vol. 21, no. 3, pp. 383-

398.e7, Sep. 2017.

[123] J. Baio, “Prevalence of autism spectrum disorder among children aged 8 years - autism and developmental disabilities monitoring network, 11 sites, United States, 2010.,” *MMWR. Surveill. Summ.*, 2014.

[124] A. V. S. Buescher, Z. Cidav, M. Knapp, and D. S. Mandell, “Costs of autism spectrum disorders in the United Kingdom and the United States,” *JAMA Pediatr.*, 2014.

[125] T. A. Lavelle, M. C. Weinstein, J. P. Newhouse, K. Munir, K. A. Kuhlthau, and L. A. Prosser, “Economic Burden of Childhood Autism Spectrum Disorders,” *Pediatrics*, 2014.

[126] G. Tang *et al.*, “Loss of mTOR-Dependent Macroautophagy Causes Autistic-like Synaptic Pruning Deficits,” *Neuron*, vol. 83, no. 5, pp. 1131–1143, Sep. 2014.

[127] J. J. Hutsler and H. Zhang, “Increased dendritic spine densities on cortical projection neurons in autism spectrum disorders,” *Brain Res.*, 2010.

[128] S. A. Irwin, “Dendritic Spine Structural Anomalies in Fragile-X Mental Retardation Syndrome,” *Cereb. Cortex*, 2000.

[129] H.-T. Chao, H. Y. Zoghbi, and C. Rosenmund, “MeCP2 Controls Excitatory Synaptic Strength by Regulating Glutamatergic Synapse Number,” *Neuron*, vol. 56, no. 1, pp. 58–65, Oct. 2007.

[130] D. Ebrahimi-Fakhari and M. Sahin, “Autism and the synapse: Emerging mechanisms and mechanism-based therapies,” *Current Opinion in Neurology*. 2015.

[131] D. Kumari, M. Swaroop, N. Southall, W. Huang, W. Zheng, and K. Usdin, “High-Throughput Screening to Identify Compounds That Increase Fragile X Mental Retardation Protein Expression in Neural Stem Cells Differentiated From Fragile X Syndrome Patient-Derived Induced Pluripotent Stem Cells,” *Stem Cells Transl. Med.*, 2015.

[132] W. Guo *et al.*, “Inhibition of GSK3 improves hippocampus-dependent learning and rescues neurogenesis in a mouse model of fragile X syndrome,” *Hum. Mol. Genet.*, vol. 21, no. 3, pp. 681–691, Feb. 2012.

[133] M. Kaufmann *et al.*, “High-Throughput Screening Using iPSC-Derived Neuronal Progenitors to Identify Compounds Counteracting Epigenetic Gene Silencing in Fragile X Syndrome,” *J. Biomol. Screen.*, vol. 20, no. 9, pp. 1101–1111, Oct. 2015.

[134] C. S. Leblond *et al.*, “Meta-analysis of SHANK Mutations in Autism Spectrum Disorders: A Gradient of Severity in Cognitive Impairments,” *PLoS Genet.*, vol. 10, no. 9, p. e1004580, Sep. 2014.

[135] T. M. Boeckers, J. Bockmann, M. R. Kreutz, and E. D. Gundelfinger, “ProSAP/Shank proteins - a family of higher order organizing molecules of the postsynaptic density with an emerging role in human neurological disease,” *J. Neurochem.*, vol. 81, no. 5, pp. 903–910, May 2002.

[136] R. R. Shah and A. P. Bird, “MeCP2 mutations: progress towards understanding and treating Rett syndrome.,” *Genome Med.*, vol. 9, no. 1, p. 17, 2017.

[137] M. C. N. Marchetto *et al.*, “A Model for Neural Development and Treatment of Rett Syndrome Using Human Induced Pluripotent Stem Cells,” *Cell*, vol. 143, no. 4, pp. 527–539, Nov. 2010.

[138] G. Pini *et al.*, “Illness Severity, Social and Cognitive Ability, and EEG Analysis of Ten Patients with Rett Syndrome Treated with Mecasermin (Recombinant Human IGF-1),” *Autism Res. Treat.*, 2016.

[139] C. Vahdatpour, A. H. Dyer, and D. Tropea, “Insulin-Like Growth Factor 1 and Related Compounds in the Treatment of Childhood-Onset Neurodevelopmental Disorders.,”

Front. Neurosci., vol. 10, p. 450, 2016.

[140] M. J. *et al.*, "FOXG1-Dependent Dysregulation of GABA/Glutamate Neuron Differentiation in Autism Spectrum Disorders," *Cell*. 2015.

[141] C. Wang *et al.*, "Scalable Production of iPSC-Derived Human Neurons to Identify Tau-Lowering Compounds by High-Content Screening," *Stem Cell Reports*, vol. 9, no. 4, pp. 1221–1233, Oct. 2017.

[142] N. Mellios *et al.*, "MeCP2-regulated miRNAs control early human neurogenesis through differential effects on ERK and AKT signaling," *Mol. Psychiatry*, vol. 23, no. 4, pp. 1051–1065, Apr. 2018.

[143] K.-H. Chang *et al.*, "Modeling Alzheimer's Disease by Induced Pluripotent Stem Cells Carrying APP D678H Mutation," *Mol. Neurobiol.*, pp. 1–12, Sep. 2018.

[144] N. M. Radio, "Neurite Outgrowth Assessment Using High Content Analysis Methodology," Humana Press, 2012, pp. 247–260.

[145] O. Sirenko, J. Hesley, I. Rusyn, and E. F. Cromwell, "High-Content High-Throughput Assays for Characterizing the Viability and Morphology of Human iPSC-Derived Neuronal Cultures," *Assay Drug Dev. Technol.*, vol. 12, no. 9–10, pp. 536–547, Dec. 2014.

[146] S. P. Sherman and A. G. Bang, "High-throughput screen for compounds that modulate neurite growth of human induced pluripotent stem cell-derived neurons.," *Dis. Model. Mech.*, vol. 11, no. 2, p. dmm031906, Feb. 2018.

[147] T. J. F. Nieland *et al.*, "High content image analysis identifies novel regulators of synaptogenesis in a high-throughput RNAi screen of primary neurons.," *PLoS One*, vol. 9, no. 3, p. e91744, 2014.

[148] L. J. Harbom, T. L. Rudisill, N. Michel, K. A. Litwa, M. P. Beenhakker, and M. J. McConnell, “The effect of rho kinase inhibition on morphological and electrophysiological maturity in iPSC-derived neurons,” *Cell Tissue Res.*, Nov. 2018.

[149] R. M. Koffie, B. T. Hyman, and T. L. Spires-Jones, “Alzheimer’s disease: synapses gone cold.”

[150] M. C. Marchetto *et al.*, “Altered proliferation and networks in neural cells derived from idiopathic autistic individuals,” *Mol. Psychiatry*, vol. 22, no. 6, pp. 820–835, Jun. 2017.

[151] C. Wing, M. Komatsu, S. M. Delaney, M. Krause, H. E. Wheeler, and M. E. Dolan, “Application of stem cell derived neuronal cells to evaluate neurotoxic chemotherapy,” *Stem Cell Res.*, vol. 22, pp. 79–88, Jul. 2017.

[152] M. Niedringhaus *et al.*, “Transferable neuronal mini-cultures to accelerate screening in primary and induced pluripotent stem cell-derived neurons,” *Sci. Rep.*, vol. 5, no. 1, p. 8353, Jul. 2015.

[153] S. Knight *et al.*, “Enabling 1536-Well High-Throughput Cell-Based Screening through the Application of Novel Centrifugal Plate Washing,” *SLAS Discov. Adv. Life Sci. R&D*, vol. 22, no. 6, pp. 732–742, Jul. 2017.

[154] L. G. J. Tertoolen, S. R. Braam, B. J. van Meer, R. Passier, and C. L. Mummery, “Interpretation of field potentials measured on a multi electrode array in pharmacological toxicity screening on primary and human pluripotent stem cell-derived cardiomyocytes,” *Biochem. Biophys. Res. Commun.*, vol. 497, no. 4, pp. 1135–1141, Mar. 2018.

[155] A. M. Pasca *et al.*, “Functional cortical neurons and astrocytes from human pluripotent stem cells in 3D culture,” *Nat Methods*, 2015.

[156] Y. Zhang *et al.*, “Rapid single-step induction of functional neurons from human

pluripotent stem cells.," *Neuron*, vol. 78, no. 5, pp. 785–98, Jun. 2013.

[157] M. Garita-Hernandez *et al.*, "Optogenetic Light Sensors in Human Retinal Organoids," *Front. Neurosci.*, vol. 12, p. 789, Nov. 2018.

[158] Y. Takarae and J. Sweeney, "Neural Hyperexcitability in Autism Spectrum Disorders," *Brain Sci.*, vol. 7, no. 12, p. 129, Oct. 2017.

[159] A. M. Tidball and J. M. Parent, "Concise Review: Exciting Cells: Modeling Genetic Epilepsies with Patient-Derived Induced Pluripotent Stem Cells.," *Stem Cells*, vol. 34, no. 1, pp. 27–33, Jan. 2016.

[160] A. Odawara, H. Katoh, N. Matsuda, and I. Suzuki, "Physiological maturation and drug responses of human induced pluripotent stem cell-derived cortical neuronal networks in long-term culture," *Sci. Rep.*, vol. 6, no. 1, pp. 1–14, May 2016.

[161] M. A. Busche and A. Konnerth, "Impairments of neural circuit function in Alzheimer's disease.," *Philos. Trans. R. Soc. Lond. B. Biol. Sci.*, vol. 371, no. 1700, 2016.

[162] H. Amin, A. Maccione, F. Marinaro, S. Zordan, T. Nieus, and L. Berdondini, "Electrical Responses and Spontaneous Activity of Human iPS-Derived Neuronal Networks Characterized for 3-month Culture with 4096-Electrode Arrays," *Front. Neurosci.*, vol. 10, p. 121, Mar. 2016.

[163] Y.-T. Lin *et al.*, "APOE4 Causes Widespread Molecular and Cellular Alterations Associated with Alzheimer's Disease Phenotypes in Human iPSC-Derived Brain Cell Types," *Neuron*, vol. 98, no. 6, pp. 1141-1154.e7, Jun. 2018.

[164] C. Madore *et al.*, "Neuroinflammation in Autism: Plausible Role of Maternal Inflammation, Dietary Omega 3, and Microbiota.," *Neural Plast.*, vol. 2016, p. 3597209, 2016.

[165] T. Zhou *et al.*, "High-Content Screening in hPSC-Neural Progenitors Identifies Drug Candidates that Inhibit Zika Virus Infection in Fetal-like Organoids and Adult Brain.," *Cell Stem Cell*, vol. 21, no. 2, pp. 274-283.e5, Aug. 2017.

[166] C. C. Miranda, T. G. Fernandes, M. M. Diogo, and J. M. S. Cabral, "Towards Multi-Organoid Systems for Drug Screening Applications.," *Bioeng. (Basel, Switzerland)*, vol. 5, no. 3, Jun. 2018.

[167] M. J. Oudin, S. Gajendra, G. Williams, C. Hobbs, G. Lalli, and P. Doherty, "Endocannabinoids Regulate the Migration of Subventricular Zone-Derived Neuroblasts in the Postnatal Brain," *J. Neurosci.*, vol. 31, no. 11, pp. 4000–4011, Mar. 2011.

[168] T. Harkany, E. Keimpema, K. Barabás, and J. Mulder, "Endocannabinoid functions controlling neuronal specification during brain development," *Mol. Cell. Endocrinol.*, 2008.

[169] C. C. Garner, R. G. Zhai, E. D. Gundelfinger, and N. E. Ziv, "Molecular mechanisms of CNS synaptogenesis," *Trends in Neurosciences*, vol. 25, no. 5. Elsevier Current Trends, pp. 243–250, 01-May-2002.

[170] A. Shcheglovitov *et al.*, "SHANK3 and IGF1 restore synaptic deficits in neurons from 22q13 deletion syndrome patients," *Nature*, vol. 503, no. 7475, pp. 267–271, Nov. 2013.

[171] J. Stiles and T. L. Jernigan, "The basics of brain development.," *Neuropsychol. Rev.*, vol. 20, no. 4, pp. 327–48, Dec. 2010.

[172] C. L. Gatto and K. Broadie, "Genetic controls balancing excitatory and inhibitory synaptogenesis in neurodevelopmental disorder models.," *Front. Synaptic Neurosci.*, vol. 2, p. 4, 2010.

[173] Y. Bozzi, G. Provenzano, and S. Casarosa, "Neurobiological bases of autism-epilepsy

comorbidity: a focus on excitation/inhibition imbalance.," *Eur. J. Neurosci.*, vol. 47, no. 6, pp. 534–548, 2018.

[174] K. Brennand *et al.*, "Phenotypic differences in hiPSC NPCs derived from patients with schizophrenia.," *Mol. Psychiatry*, vol. 20, no. 3, pp. 361–8, Mar. 2015.

[175] S. Tordjman *et al.*, "Animal models relevant to schizophrenia and autism: Validity and limitations," *Behavior Genetics*. 2007.

[176] R. M. Marton and S. P. Pașca, "Organoid and Assembloid Technologies for Investigating Cellular Crosstalk in Human Brain Development and Disease," *Trends in Cell Biology*, vol. 30, no. 2. Elsevier Ltd, pp. 133–143, 01-Feb-2020.

[177] E. Wilson, W. Knudson, and K. Newell-Litwa, "Hyaluronan regulates synapse formation and function in developing neural networks," *Sci. Rep.*, vol. 10, no. 1, Dec. 2020.

[178] R. Piet *et al.*, "State-dependent, bidirectional modulation of neural network activity by endocannabinoids," *J. Neurosci.*, 2011.

[179] J. L. Blankman, G. M. Simon, and B. F. Cravatt, "A Comprehensive Profile of Brain Enzymes that Hydrolyze the Endocannabinoid 2-Arachidonoylglycerol," *Chem. Biol.*, vol. 14, no. 12, pp. 1347–1356, Dec. 2007.

[180] E. Keimpema *et al.*, "Differential subcellular recruitment of monoacylglycerol lipase generates spatial specificity of 2-arachidonoyl glycerol signaling during axonal pathfinding," *J. Neurosci.*, vol. 30, no. 42, pp. 13992–14007, Oct. 2010.

[181] E. Keimpema *et al.*, "Diacylglycerol lipase a manipulation reveals developmental roles for intercellular endocannabinoid signaling," *Sci. Rep.*, vol. 3, no. 1, pp. 1–9, Jun. 2013.

[182] P. Berghuis *et al.*, "Endocannabinoids regulate interneuron migration and morphogenesis by transactivating the TrkB receptor," *Proc. Natl. Acad. Sci. U. S. A.*, 2005.

[183] C. Shum *et al.*, “Δ9-tetrahydrocannabinol and 2-AG decreases neurite outgrowth and differentially affects ERK1/2 and Akt signaling in hiPSC-derived cortical neurons,” *Mol. Cell. Neurosci.*, vol. 103, Mar. 2020.

[184] A. B. Roland *et al.*, “Cannabinoid-induced actomyosin contractility shapes neuronal morphology and growth,” *Elife*, vol. 3, Sep. 2014.

[185] G. Tortoriello *et al.*, “Miswiring the brain: Δ9-tetrahydrocannabinol disrupts cortical development by inducing an SCG10/stathmin-2 degradation pathway.,” *EMBO J.*, vol. 33, no. 7, pp. 668–85, Apr. 2014.

[186] G. Zuccarini *et al.*, “Interference with the cannabinoid receptor CB1R results in miswiring of GnRH3 and AgRP1 axons in zebrafish embryos,” *Int. J. Mol. Sci.*, vol. 21, no. 1, Jan. 2020.

[187] K. Soderstrom and Q. Tian, “CB1 cannabinoid receptor activation dose dependently modulates neuronal activity within caudal but not rostral song control regions of adult zebra finch telencephalon,” *Psychopharmacology (Berl).*, 2008.

[188] T. L. Holland and K. Soderstrom, “Chronic CB1 cannabinoid receptor antagonism persistently increases dendritic spine densities in brain regions important to zebra finch vocal learning and production in an antidepressant-sensitive manner,” *Brain Res.*, 2017.

[189] A. C. Howlett and M. E. Abood, “CB1 and CB2 Receptor Pharmacology,” in *Advances in Pharmacology*, 2017.

[190] G. A. Cabral, E. S. Raborn, L. Griffin, J. Dennis, and F. Marciano-Cabral, “CB 2 receptors in the brain: Role in central immune function,” *British Journal of Pharmacology*, vol. 153, no. 2. Wiley-Blackwell, pp. 240–251, Jan-2008.

[191] B. Chakrabarti, A. Persico, N. Battista, and M. Maccarrone, “Endocannabinoid Signaling

in Autism," *Neurotherapeutics*, vol. 12, pp. 837–847, 2015.

[192] L. Cristino, R. Imperatore, and V. Di Marzo, "Techniques for the Cellular and Subcellular Localization of Endocannabinoid Receptors and Enzymes in the Mammalian Brain," *Methods Enzymol.*, vol. 593, pp. 61–98, Jan. 2017.

[193] M. R. Domenici *et al.*, "Cannabinoid receptor type 1 located on presynaptic terminals of principal neurons in the forebrain controls glutamatergic synaptic transmission," *J. Neurosci.*, 2006.

[194] I. Katona *et al.*, "Presynaptically located CB1 cannabinoid receptors regulate GABA release from axon terminals of specific hippocampal interneurons," *J. Neurosci.*, 1999.

[195] M. London, I. Segev, J. C. Magee, and E. P. Cook, "Synaptic scaling in vitro and in vivo (multiple letters)," *Nature Neuroscience*, vol. 4, no. 9. Nature Publishing Group, pp. 853–855, 2001.

[196] M. Fagiolini and J. J. Leblanc, "Autism: A critical period disorder?," *Neural Plasticity*. 2011.

[197] J. Paraíso-Luna *et al.*, "Endocannabinoid signalling in stem cells and cerebral organoids drives differentiation to deep layer projection neurons via CB1 receptors," *Development*, vol. 147, no. 24, p. dev192161, Dec. 2020.

[198] C. Guimas Almeida *et al.*, "hiPSC-Based Model of Prenatal Exposure to Cannabinoids: Effect on Neuronal Differentiation," *Front. Mol. Neurosci.*, vol. 13, Jul. 2020.

[199] Z. Ao *et al.*, "One-Stop Microfluidic Assembly of Human Brain Organoids to Model Prenatal Cannabis Exposure," *Anal. Chem.*, vol. 92, no. 6, pp. 4630–4638, Mar. 2020.

[200] K. R. Skelton, A. A. Hecht, and S. E. Benjamin-Neelon, "Recreational cannabis legalization in the US and maternal use during the preconception, prenatal, and

postpartum periods," *Int. J. Environ. Res. Public Health*, vol. 17, no. 3, Feb. 2020.

[201] M. MacCarrone *et al.*, "Abnormal mGlu 5 receptor/endocannabinoid coupling in mice lacking FMRP and BC1 RNA," *Neuropsychopharmacology*, vol. 35, no. 7, pp. 1500–1509, 2010.

[202] H. J. Kang *et al.*, "Spatio-temporal transcriptome of the human brain," *Nature*, 2011.

[203] M. B. Johnson *et al.*, "Functional and Evolutionary Insights into Human Brain Development through Global Transcriptome Analysis," *Neuron*, 2009.

[204] S. T. Schafer *et al.*, "Pathological priming causes developmental gene network heterochronicity in autistic subject-derived neurons," *Nat. Neurosci.*, 2019.

[205] I. Jenniches *et al.*, "Anxiety, Stress, and Fear Response in Mice with Reduced Endocannabinoid Levels," *Biol. Psychiatry*, vol. 79, no. 10, pp. 858–868, May 2016.

[206] D. Ogasawara *et al.*, "Rapid and profound rewiring of brain lipid signaling networks by acute diacylglycerol lipase inhibition," *Proc. Natl. Acad. Sci. U. S. A.*, 2016.

[207] G. Bedse, M. N. Hill, and S. Patel, "Review 2-Arachidonoylglycerol Modulation of Anxiety and Stress Adaptation: From Grass Roots to Novel Therapeutics," 2020.

[208] G. Griebel *et al.*, "Selective blockade of the hydrolysis of the endocannabinoid 2-arachidonoylglycerol impairs learning and memory performance while producing antinociceptive activity in rodents," *Sci. Rep.*, 2015.

[209] M. Lafourcade, I. Elezgarai, S. Mato, Y. Bakiri, and P. Grandes, "Molecular Components and Functions of the Endocannabinoid System in Mouse Prefrontal Cortex," *PLoS One*, vol. 2, no. 8, p. 709, 2007.

[210] T. M. M. Saez, M. P. Aronne, L. Caltana, and A. H. Brusco, "Prenatal exposure to the CB $_1$ and CB $_2$ cannabinoid receptor agonist WIN 55,212-2 alters migration of early-born

glutamatergic neurons and GABAergic interneurons in the rat cerebral cortex," *J. Neurochem.*, vol. 129, no. 4, pp. 637–648, May 2014.

[211] S. H. Lee, C. Földy, and I. Soltesz, "Distinct endocannabinoid control of GABA release at perisomatic and dendritic synapses in the hippocampus," *J. Neurosci.*, vol. 30, no. 23, pp. 7993–8000, Jun. 2010.

[212] P. J. Uhlhaas and W. Singer, "Abnormal neural oscillations and synchrony in schizophrenia," *Nature Reviews Neuroscience*, vol. 11, no. 2. Nature Publishing Group, pp. 100–113, Feb-2010.

[213] I. Dinstein *et al.*, "Disrupted Neural Synchronization in Toddlers with Autism," *Neuron*, vol. 70, no. 6, pp. 1218–1225, Jun. 2011.

[214] T. Klausberger, "GABAergic interneurons targeting dendrites of pyramidal cells in the CA1 area of the hippocampus," *Eur. J. Neurosci.*, vol. 30, no. 6, pp. 947–957, Sep. 2009.

[215] C. Njoo, N. Agarwal, B. Lutz, and R. Kuner, "The Cannabinoid Receptor CB1 Interacts with the WAVE1 Complex and Plays a Role in Actin Dynamics and Structural Plasticity in Neurons," *PLoS Biol.*, vol. 13, no. 10, pp. 1–36, Oct. 2015.

[216] I. Katona and T. F. Freund, "Endocannabinoid signaling as a synaptic circuit breaker in neurological disease," *Nature Medicine*. 2008.

[217] A. M. Paşca *et al.*, "Functional cortical neurons and astrocytes from human pluripotent stem cells in 3D culture," *Nat. Methods*, vol. 12, no. 7, pp. 671–8, May 2015.

[218] H. Amin, F. Marinaro, D. D. P. Tonelli, and L. Berdondini, "Developmental excitatory-to-inhibitory GABA-polarity switch is disrupted in 22q11.2 deletion syndrome: A potential target for clinical therapeutics," *Sci. Rep.*, vol. 7, no. 1, pp. 1–18, Dec. 2017.

[219] D. D. Wang and A. R. Kriegstein, "Defining the role of GABA in cortical development,"

in *Journal of Physiology*, 2009, vol. 587, no. 9, pp. 1873–1879.

[220] R. Luján, R. Shigemoto, and G. López-Bendito, "Glutamate and GABA receptor signalling in the developing brain," *Neuroscience*, vol. 130, no. 3. Pergamon, pp. 567–580, 01-Jan-2005.

[221] D. M. Kerr, L. Downey, M. Conboy, D. P. Finn, and M. Roche, "Alterations in the endocannabinoid system in the rat valproic acid model of autism," *Behav. Brain Res.*, vol. 249, pp. 124–132, Jul. 2013.

[222] M. Feja *et al.*, "The novel MAGL inhibitor MJN110 enhances responding to reward-predictive incentive cues by activation of CB1 receptors," *Neuropharmacology*, vol. 162, p. 107814, Jan. 2020.

[223] J. R. Piro *et al.*, "Inhibition of 2-AG hydrolysis differentially regulates blood brain barrier permeability after injury," *J. Neuroinflammation*, vol. 15, no. 1, pp. 1–15, May 2018.

[224] B. Dudok *et al.*, "Cell-specific STORM super-resolution imaging reveals nanoscale organization of cannabinoid signaling.," *Nat. Neurosci.*, vol. 18, no. 1, pp. 75–86, Jan. 2015.

[225] G. G. Turrigiano, "The Self-Tuning Neuron: Synaptic Scaling of Excitatory Synapses," *Cell*, vol. 135, no. 3. Elsevier B.V., pp. 422–435, 31-Oct-2008.

[226] T. C. Moulin, D. Rayêe, M. J. Williams, and H. B. Schiöth, "The synaptic scaling literature: A systematic review of methodologies and quality of reporting," *Frontiers in Cellular Neuroscience*, vol. 14. Frontiers Media S.A., pp. 1–10, 16-Jun-2020.

[227] S. M. Eggan and D. A. Lewis, "Immunocytochemical distribution of the cannabinoid CB1 receptor in the primate neocortex: A regional and laminar analysis," *Cereb. Cortex*, vol. 17, no. 1, pp. 175–191, 2007.

[228] G. Marsicano and B. Lutz, “Expression of the cannabinoid receptor CB1 in distinct neuronal subpopulations in the adult mouse forebrain,” *Eur. J. Neurosci.*, vol. 11, no. 12, pp. 4213–4225, Dec. 1999.

[229] J. L. Barnes, C. Mohr, C. R. Ritchey, C. M. Erikson, H. Shiina, and D. J. Rossi, “Developmentally transient cb1rs on cerebellar afferents suppress afferent input, downstream synaptic excitation, and signaling to migrating neurons,” *J. Neurosci.*, vol. 40, no. 32, pp. 6133–6145, Aug. 2020.

[230] A. Busquets-Garcia *et al.*, “Targeting the endocannabinoid system in the treatment of fragile X syndrome,” *Nat. Med.*, 2013.

[231] M. Gomis-González, C. Matute, R. Maldonado, S. Mato, and A. Ozaita, “Possible therapeutic doses of cannabinoid type 1 receptor antagonist reverses key alterations in fragile X syndrome mouse model,” *Genes (Basel).*, vol. 7, no. 9, Sep. 2016.

[232] A. Contractor, V. A. Klyachko, and C. Portera-Cailliau, “Altered Neuronal and Circuit Excitability in Fragile X Syndrome,” *Neuron*, vol. 87, no. 4. Cell Press, pp. 699–715, 19-Aug-2015.

[233] K. Soderstrom and M. T. Gilbert, “Cannabinoid mitigation of neuronal morphological change important to development and learning: Insight from a zebra finch model of psychopharmacology,” in *Life Sciences*, 2013, vol. 92, no. 8–9, pp. 467–475.

[234] G. Marsicano and P. Lafenêtre, “Roles of the Endocannabinoid system in learning and memory,” *Current Topics in Behavioral Neurosciences*, vol. 1. Springer Verlag, pp. 201–230, 2009.

[235] M. S. Crowe, S. R. Nass, K. M. Gabella, and S. G. Kinsey, “The endocannabinoid system modulates stress, emotionality, and inflammation,” *Brain, Behavior, and Immunity*. 2014.

[236] O. Prospéro-García, O. Amancio-Belmont, A. L. Becerril Meléndez, A. E. Ruiz-Contreras, and M. Méndez-Díaz, "Endocannabinoids and sleep," *Neuroscience and Biobehavioral Reviews*, vol. 71. Elsevier Ltd, pp. 671–679, 01-Dec-2016.

[237] J. W. VanRyzin *et al.*, "Microglial Phagocytosis of Newborn Cells Is Induced by Endocannabinoids and Sculpts Sex Differences in Juvenile Rat Social Play," *Neuron*, vol. 102, no. 2, pp. 435-449.e6, Apr. 2019.

[238] S. G. Woodhams, D. R. Sagar, J. J. Burston, and V. Chapman, "The role of the endocannabinoid system in pain," *Handb. Exp. Pharmacol.*, vol. 227, pp. 119–143, 2015.

[239] D. R. Smith, C. M. Stanley, T. Foss, R. G. Boles, and K. McKernan, "Rare genetic variants in the endocannabinoid system genes CNR1 and DAGLA are associated with neurological phenotypes in humans.," *PLoS One*, vol. 12, no. 11, p. e0187926, 2017.

[240] D. García-Rincón *et al.*, "Contribution of altered endocannabinoid system to overactive mTORC1 signaling in focal cortical dysplasia," *Front. Pharmacol.*, vol. 9, no. JAN, 2019.

[241] P. M. Turunen, L. M. Louhivuori, V. Louhivuori, J. P. Kukkonen, and K. E. Åkerman, "Endocannabinoid Signaling in Embryonic Neuronal Motility and Cell–Cell Contact – Role of mGluR5 and TRPC3 Channels," *Neuroscience*, vol. 375, pp. 135–148, Apr. 2018.

[242] I. Galve-Roperh, V. Chiurchiù, J. Díaz-Alonso, M. Bari, M. Guzmán, and M. Maccarrone, "Cannabinoid receptor signaling in progenitor/stem cell proliferation and differentiation," *Progress in Lipid Research*, vol. 52, no. 4. pp. 633–650, 2013.

[243] J. W. VanRyzin *et al.*, "Microglial Phagocytosis of Newborn Cells Is Induced by Endocannabinoids and Sculpts Sex Differences in Juvenile Rat Social Play," *Neuron*, vol. 102, no. 2, pp. 435-449.e6, Apr. 2019.

[244] J. G. Duman, S. Mulherkar, Y. K. Tu, J. X. Cheng, and K. F. Tolias, "Mechanisms for

spatiotemporal regulation of Rho-GTPase signaling at synapses," *Neuroscience Letters*, vol. 601. Elsevier Ireland Ltd, pp. 4–10, 05-May-2015.

[245] M. Navarrete, A. Díez, and A. Araque, "Astrocytes in endocannabinoid signalling," *Philosophical Transactions of the Royal Society B: Biological Sciences*, vol. 369, no. 1654. Royal Society of London, 19-Oct-2014.

[246] M. Turrero García and C. C. Harwell, "Radial glia in the ventral telencephalon.," *FEBS Lett.*, vol. 591, no. 24, pp. 3942–3959, 2017.

[247] T. Aguado *et al.*, "The endocannabinoid system promotes astroglial differentiation by acting on neural progenitor cells," *J. Neurosci.*, vol. 26, no. 5, pp. 1551–1561, Feb. 2006.